AD-A053 358 LOUISIANA STATE UNIV BATON ROUGE COASTAL STUDIES INST F/G 8/8
A NUMERICAL STUDY OF CURRENTS, WATER SURFACE ELEVATIONS, AND EN--ETC(U)
FEB 78 W E HART N00014-75-C-0192
UNCLASSIFIED TR-250 NL

1 OF 2
AD
A053358

DISCLAIMER NOTICE

THIS DOCUMENT IS BEST QUALITY PRACTICABLE. THE COPY FURNISHED TO DDC CONTAINED A SIGNIFICANT NUMBER OF PAGES WHICH DO NOT REPRODUCE LEGIBLY.

Coastal Studies Institute
Center for Wetland Resources
Louisiana State University
Baton Rouge, Louisiana 70803

Technical Report No. 250

A NUMERICAL STUDY OF CURRENTS, WATER SURFACE ELEVATIONS, AND ENERGY DISSIPATION IN CHANDELEUR-BRETON SOUND, LOUISIANA

By William E. Hart

February 1978

ABSTRACT

Numerical methods in the form of a digital computer model were used to simulate and study the tide- and wind-induced circulation in Chandeleur-Breton Sounds, which form a bar-built estuary southeast of New Orleans, Louisiana. The model output agreed very well with current observations taken over a 6-month period at 5 widely spaced stations in and around the estuary. The responses of the model estuary to average, tropic, and equatorial tides were studied in detail. It was found that the estuary exhibits low current speeds, on the order of 10-20 cm/sec, except in some of the shallow entrances through the Chandeleur Island chain, where speed reaches 50-60 cm/sec for short periods. Surface elevations were found to have an average tide range of 60 cm at the northwestern end of the estuary and to increase in range to 90 cm during tropic tides. The range in the southern part of the estuary was about 15 cm less at all times. It was also shown that the estuary responds directly to an applied wind force and that the expected set-up of the surface is in the downwind direction. The current field is only slightly affected by representative local winds (order of 10 percent). The input to the estuary comes primarily from its northern and southern entrances. These entering tidal wave forms were simulated by two Kelvin waves, which had a resultant form that was found to be in close agreement with the computer model. Furthermore, it was shown that total energy in the estuary is relatively low and that kinetic energy is typically only one-sixth of the potential energy during the tidal cycle. Only about 25 percent of the energy advected into the Sound is dissipated by bottom friction, but the time-averaged energy balance is dominated by the dissipation term. The unsteady energy content term $\langle \partial E / \partial t \rangle$ is about 25 percent of the advective and dissipative terms in the time (tidal) average.

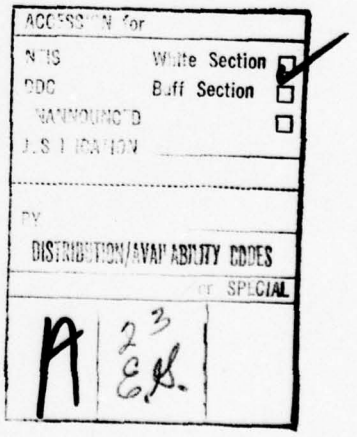

ACKNOWLEDGMENTS

This research was performed under a contract between the Geography Programs, Office of Naval Research, Arlington, Virginia 22217, and the Coastal Studies Institute, Louisiana State University, and served as partial fulfillment of the Ph.D. degree in the Department of Marine Sciences, LSU. The support of the U.S. Naval Oceanographic Office is gratefully acknowledged. We are indebted to Gerry Dunn and Carla Richardson for cartography and typing.

CONTENTS

LIST OF FIGURES

LIST OF TABLES

INTRODUCTION

The primary objective of this study was to use numerical methods in the form of a digital computer model to simulate tide- and wind-induced circulation in the Chandeleur-Breton Sounds estuary and from this information to draw conclusions about the physics which control the estuary. It was also intended that the model be easily adaptable for use by other investigators in studies of other applicable areas. Both objectives were met.

To accomplish the latter, the model was programmed in such a way that any investigator could use and/or modify it to suit his own purpose without the usual requirement of mastery of computer programming and, as is often necessary, a complete systems analysis and reprogramming effort. Basically, the model was formulated with a main computing scheme program and a number of subroutines, each of which isolates the treatment of the parameters that usually vary from one study to another. By this means changes are made easily, and concern about their impact on other parts of the model is eliminated.

The computer model was also formulated so that other investigators could control the use or non-use of several terms that apply to the basic equations. These terms are convective inertia, Coriolis, bottom friction, and wind stress. Their use is governed by an input card requiring only a one (1) for "use" or a zero (0) for "omit." One card's inputs are also used to control wind speed, direction, and start and stop times, as well as spatial grid size and time step increment size.

The main problem, reaching the point of being able to draw meaningful conclusions about the estuary's controlling physics and in a general sense describing the characteristics of the surface elevation, current flow field, energy balance, and possibly applicable theoretical wave forms, required numerical analysis for practical reasons. The area is simply too large to cover adequately with any program of comprehensive data collection and analysis, and fortunately there were just enough data available for use in verifying a numerical model.

A model developed by Leendertse (1967) was modified for this study. The modified model was first tested for computational accuracy and stability. This procedure is of prime importance in selecting one model over another. The test involved input cyclic sine curve tidal data so that it was known that the model output should repeat itself at cyclic intervals. It did, with surface elevations within about 1.5 to 2 percent and current velocities within 10 to 20 percent of full-scale values.

The foregoing test is basically a verification of the numerical method used to represent the hydrodynamic differential equations. The model was then tested against real data as verification of the theoretical assumption and formulation.

The test data were currents observed and recorded at 14 widely separated (spatially and temporally) stations in the estuary. The data were taken in 1968 by the National Ocean Survey ships Marmer and Ferrel. The model was run with input predicted tidal data for the periods of data collection, and the output was compared with that at each point and at combinations of points. The test or comparison was quite favorable and is described in the body of the report.

The effect of the individual terms mentioned previously was determined by running the model alternately with and without each term in succession. The effect is in terms of both magnitude and spatial orientation and is also described in the body of the paper.

The model was then run with input predicted tidal data that represented average, tropic, and equatorial tidal conditions. In this way, the study provided information on the average, high, and low energy conditions that could be expected during a tidal cycle.

Plotted output of the surface elevation and current flow fields under these conditions served as the basis for a descriptive analysis and characterization of the estuary. This description was aided by use of co-range and co-tidal diagrams that were made from the model data.

Generally, tides at the northern end of the estuary led those in the south by about 1 hour. Tidal ranges were also greatest in the north and northwest. The range in the north during tropic tides was over 90 cm and during average tidal periods was about 65 cm. At all times the range in the north was 10 to 15 cm greater than in the south.

The current flow field diagrams showed essentially two systems entering the estuary, one from the north and one from the south, and converging at about the center. This circumstance and the co-range and co-tidal lines suggested two Kelvin waves. Theoretical wave forms and currents were computed for two waves of this nature that started at each end with representative wave amplitudes. The ordinate values from each wave were added until a suitable time lag was determined for each wave, so that the resultant wave came closest to simulating that shown by the model to be in effect. The comparison was very good, considering the highly idealized theoretical wave forms, lack of applied frictional effects, and a straight channel assumption (which is not the case in the estuary). In fact, it is a fair assumption that these wave forms do exist in the estuary.

Total energy and energy flux were also computed from the output of the model data. Comparison was made between the computed energy flux for the estuary and the net sum of the energy input through all entrances, minus the energy dissipated by frictional velocity. The energy study showed good overall diurnal balance; an excess of energy entered on the incoming tides but was dissipated by friction on the outflowing tides. Total energy peaked about 1 hour after high tide, similarly was at a minimum about 1 hour after low tide, and was a rather symmetrical function about these times. Total energy was found to be primarily a function of potential energy. Kinetic energy, however, was twice the potential energy at the mid-tide maximum current flow periods, and, although the current speeds are generally small, frictional energy dissipation was sufficient to maintain the energy balance.

BACKGROUND

The Chandeleur-Breton Sounds estuary was studied because the area is of great environmental and commercial value and study of its physical and dynamic characteristics should add important information to the growing body of knowledge concerning the hydrodynamics of bar-built estuaries.

The estuary is located east-southeast of New Orleans (Fig. 1). Obviously there is considerable commercial interest in the area from the aspect of fisheries and shellfish industries. Numerous oyster beds are to be found in the region. The current flow field is certainly of importance to these interests because any bed area is affected by the flow over it, in terms of both potential nutrient and pollutant transport and also the potential high- and low-energy areas. The latter is most important in bed maintenance and small-boat operations. The oil industry has invested heavily in the area, both in offshore drilling platforms and pipelines and in efforts to maintain the environmental protection of this natural-resource area. There are several oil pipelines, in fact, that run the length of the estuary. Movement of these lines and possible eventual rupture and oil spills can be effected by local currents. Certainly the covering and uncovering of bottom structures, activities that are important in maintenance, are affected to some degree by local currents.

Pollution control is not only important but also topical and expensive in terms of ability to maintain it. For example, in 1970 there was an oil spill from one of the platforms southeast of Breton Island. Many months and much effort were spent in controlling the spill, and a major aspect was the use of a line of barges to form a net to somewhat retard the flow and aid in the effort to limit the surface flow of the spilling oil. Again, flow field information was important in this application.

Recreational and small-boat interests in the area are also quite important, as are, obviously, those of the larger commercial shipping forms. It can be seen from Figure 1 that the Mississippi River Gulf Outlet Channel is dredged across the area. Silting in the channel can be a maintenance problem, and knowledge of the current flow field is of direct applicability.

Physically, the study area is an approximately 80-km x 100-km, relatively flat bottomed, shallow (about 3-6 meters), bar-built estuary. Most study effort has gone into drowned coastal plain estuaries, e.g., Pritchard (1952, 1956). Fjord-type estuaries have also been studied, e.g., by McAlister et al. (1959). Very little, however, has been done on the bar-built estuary; the exceptions are a study by Dyer and Ramamoorthy (1969) and another, of local interest, on Caminada Bay, southwest of New Orleans, by Kjerfve (1973). Very little data (enough, however, for testing a numerical model) were available on the Chandeleur-Breton Sounds estuary. Current data used in the study are discussed later. Salinities and general information on current flow were found in Murray et al. (1970), Murray (1972), and Barrett (1971).

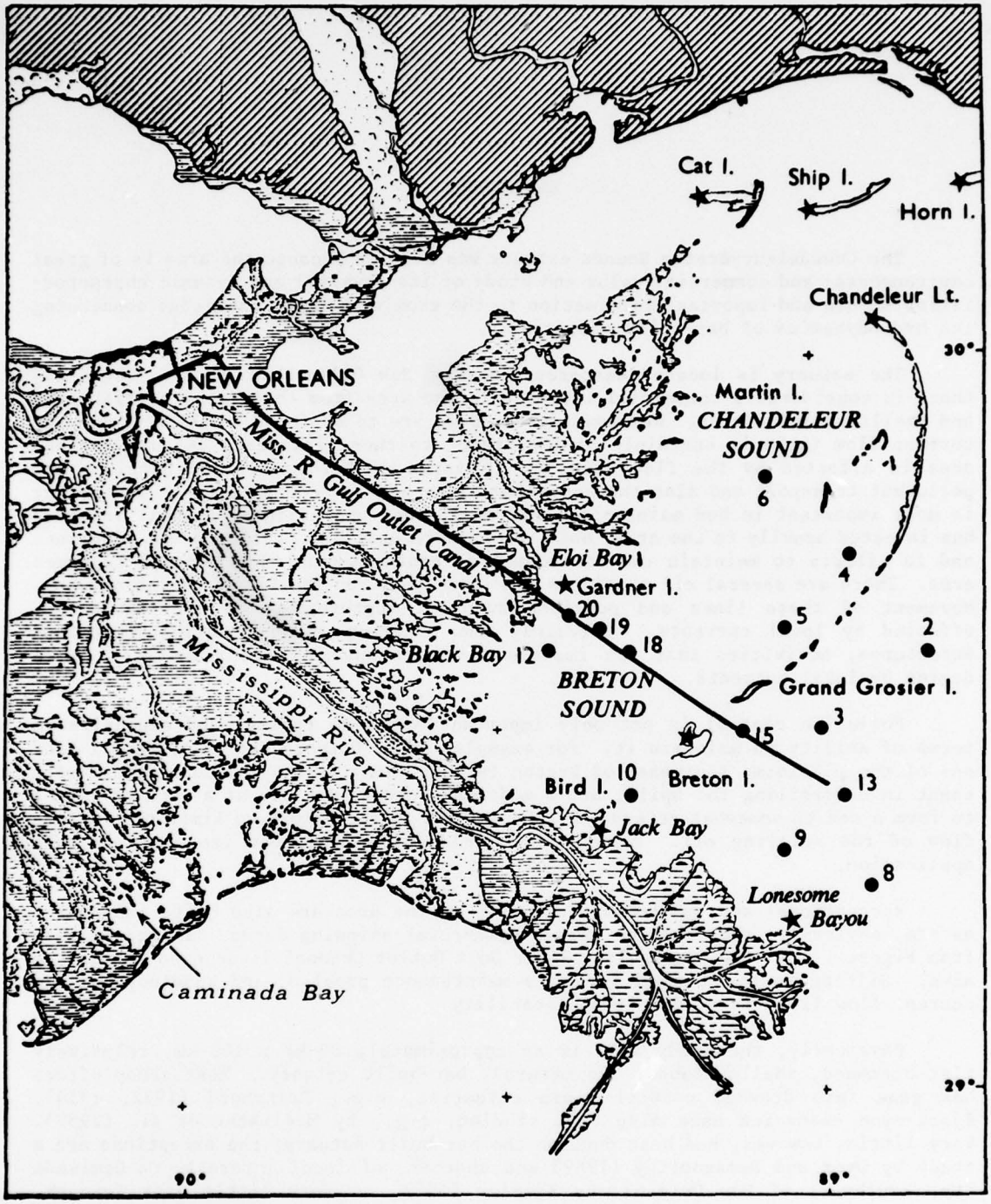

Figure 1. Chandeleur-Breton Sound location map.

The study was intended to provide much more information than was previously available on the area, and this objective was achieved.

BASIC THEORY AND FORMULATION

Before any numerical model is used, the theory, assumptions, and formulation should be reviewed. Such a review provides the assurance that the results are what they are represented to be and gives some framework to the capabilities and limitations of the model for its intended use.

Several authors developed the basic differential equations that describe long-period gravity waves in shallow waters. Those most closely followed in this presentation are Dronkers (1964) and Leendertse (1967). Both authors carried the development through to the finite-difference method of solving the differential equations. The former provided excellent reference to other comparable methods, and the latter developed the specific model that was modified, expanded, and used in this study. Others who have provided similar treatment but generally are limited to specific models are Reid and Bodine (1968). Youkey (1968), Mungall and Matthews (1970), Masch (1970), Abbott and Marshall (1970), Gunaratnam and Perkins (1970), and Hacker et al. (1971).

Differential Equations

The basic equations for the flow of long-period gravity waves are developed from Eulerian equations of motion and continuity at a position (x, y, z) in a Cartesian coordinate system. The x, y plane is mean sea level (MSL), and both the z axis and the coordinate of the free surface ζ are positive upward. Thus at the free surface $z = \zeta$. The three components of the velocity vector are u, v, and w in the x, y, and z directions.

The equations of motion (neglecting the direct tide generating forces) are:

$$\left.\begin{aligned} \frac{du}{dt} &= -\frac{1}{\rho}\frac{\partial P}{\partial x} + fv + \frac{1}{\rho}\frac{\partial F_x}{\partial z} \\ \frac{dv}{dt} &= -\frac{1}{\rho}\frac{\partial P}{\partial y} - fu + \frac{1}{\rho}\frac{\partial F_y}{\partial z} \\ \frac{dw}{dt} &= -\frac{1}{\rho}\frac{\partial P}{\partial z} - g + \frac{1}{\rho}\frac{\partial F_z}{\partial z} \end{aligned}\right\} \qquad (1)$$

where

ρ = water density
P = pressure
g = gravity acceleration
f = Coriolis parameter = $2\omega \sin \phi$
F_x, F_y, and F_z = the frictional forces

and the continuity equation is

$$\frac{\partial u}{\partial x} + \frac{\partial v}{\partial y} + \frac{\partial w}{\partial z} = 0 \tag{2}$$

When considering long-period gravity waves, it may be assumed that the vertical acceleration of water particles is negligible in comparison with the gravity term.

Integrating the hydrostatic equation from an arbitrary level to the surface and then differentiating P in the horizontal directions and using the Leibnitz Rule, we see that

$$\frac{\partial P}{\partial x} = g \int_z^{\zeta} \frac{\partial \rho}{\partial x}\, dz + g\rho_s \frac{\partial \zeta}{\partial x} + \frac{\partial P_o}{\partial x}$$

$$\frac{\partial P}{\partial y} = g \int_z^{\zeta} \frac{\partial \rho}{\partial y}\, dz + g\rho_s \frac{\partial \zeta}{\partial y} + \frac{\partial P_o}{\partial y} \tag{3}$$

where ρ_s is the density at the surface. Under average conditions $\partial P_o/\partial x$, $\partial P_o/\partial y$ can be safely neglected because their value of $\sim 10^{-4}$ dynes/cm^3 is somewhat less than the barotropic pressure gradient of $\sim 10^{-3}$ dynes/cm^3.

Data shown in Murray et al. (1970) and Barrett (1971) indicate that the baroclinic pressure gradient terms are about 1/10 the value of the barotropic terms and can probably be neglected for average conditions over the interior of the sound.

With these assumptions (1) becomes

$$\left.\begin{aligned} \frac{du}{dt} &= -g\frac{\rho_s}{\rho}\frac{\partial \zeta}{\partial x} + fv + \frac{1}{\rho}\frac{\partial F_x}{\partial z} \\ \frac{dv}{dt} &= -g\frac{\rho_s}{\rho}\frac{\partial \zeta}{\partial y} - fu + \frac{1}{\rho}\frac{\partial F_y}{\partial z} \end{aligned}\right\} \tag{4}$$

where it can be assumed that $\rho_s/\rho \simeq 1$.

At this point we account for the fact that there are gradients in the horizontal velocities as a function of depth, vertical density-salinity gradients, and bottom friction. Murray et al.(1970) showed severe departures of the density and speed from their vertical averages to be restricted to thin layers (~ 0.5 m) near the surface and bottom.

Thus it is reasonable to introduce vertically averaged velocity components:

$$\left.\begin{aligned} U &= \frac{1}{(h+\zeta)} \int_{-h}^{\zeta} u\,dz \\ V &= \frac{1}{(h+\zeta)} \int_{-h}^{\zeta} v\,dz \end{aligned}\right\} \tag{5}$$

The foregoing means that the numerical model should be able to give good average values suitable for a general characterization of the sound's surface elevation, current flow field, energy balance, and wave form. The model, however, may not be accurate at a given vertical level, especially near the surface, where salinities and velocities differ considerably from the average. This is, of course, the assumption that makes a two-dimensional model from a three-dimensional situation.

Rearranging (5) as follows, we have a volume transport function:

$$\left.\begin{aligned} U(h+\zeta) &= \int_{-h}^{\zeta} u\,dz \\ V(h+\zeta) &= \int_{-h}^{\zeta} v\,dz \end{aligned}\right\} \tag{6}$$

Integrating (4) from the bottom to the surface we have:

$$\int_{-h}^{\zeta} \frac{\partial u}{\partial t}\,dz + \int_{-h}^{\zeta} \vec{V} \cdot \nabla u\,dz = \int_{-h}^{\zeta} -g \frac{\partial \zeta}{\partial x}\,dz + f \int_{-h}^{\zeta} v\,dz + \frac{1}{\rho} \int_{-h}^{\zeta} \frac{\partial F_x}{\partial z}\,dz \tag{7}$$

with a similar development in the y direction.

Dividing each term in (7) by $(h+\zeta)$ and substituting (6) into the resulting integrals and integrating, we have:

$$\frac{\partial U}{\partial t} + \overline{u \frac{\partial u}{\partial x}} + \overline{v \frac{\partial u}{\partial y}} = -g \frac{\partial \zeta}{\partial x} + fV + (F_{sx} - F_{bx})/\rho(h+\zeta)$$

and similarly for the y direction:

$$\frac{\partial V}{\partial t} + \overline{u \frac{\partial v}{\partial x}} + \overline{v \frac{\partial v}{\partial y}} = -g \frac{\partial \zeta}{\partial y} - fU + (F_{sy} - F_{by})/\rho(h+\zeta) \tag{8}$$

where

F_s = surface, or wind friction force

F_b = bottom friction force

the overbar represents the vertical average of the respective cross-product.

Expanding $u = U + u'$ and $v = V + v'$, where the primed speeds are deviations, from the vertical averages, we see that

$$\overline{u \frac{\partial u}{\partial x}} = U \frac{\partial U}{\partial x} + \overline{u' \frac{\partial u'}{\partial x}}$$

with similar relations for the other three field accelerations. Assuming correlations between the vertical speed deviations and their horizontal gradients are small compared to the cross-product of the mean flow, (8) becomes

$$\begin{aligned} \frac{\partial U}{\partial t} + U \frac{\partial U}{\partial x} + V \frac{\partial U}{\partial y} &= - g \frac{\partial \zeta}{\partial x} + fV + (F_{sx} - F_{bx})/\rho\,(h+\zeta) \\ \frac{\partial V}{\partial t} + U \frac{\partial V}{\partial x} + V \frac{\partial V}{\partial y} &= - g \frac{\partial \zeta}{\partial y} - fU + (F_{sy} - F_{by})/\,\rho(h+\zeta) \end{aligned} \tag{9}$$

The empirical friction terms commonly used to represent bottom friction and wind stress are found in numerous texts, e.g., those of Dronkers (1964) and Leendertse (1967). It can be easily shown that the usual quadratic bottom stress law becomes:

$$\left.\begin{aligned} \frac{F_{bx}}{\rho(h+\zeta)} &= \frac{g\,U(U^2 + V^2)^{\frac{1}{2}}}{C^2\,(h+\zeta)} \\ \frac{F_{by}}{\rho(h+\zeta)} &= \frac{g\,V(U^2 + V^2)^{\frac{1}{2}}}{C^2\,(h+\zeta)} \end{aligned}\right\} \tag{10}$$

where C is the common Chezy friction factor. Similarly, from Dronkers (1964) the wind friction terms are

$$\begin{aligned} \frac{F_{sx}}{\rho(h+\zeta)} = W_x &= \frac{\rho_a \gamma^2 U_{10}^{\,2} \sin \alpha}{\rho\,(h+\zeta)} \\ \frac{F_{sy}}{\rho\,(h+\zeta)} = W_y &= \frac{\rho_a \gamma^2 U_{10}^{\,2} \cos \alpha}{\rho\,(h+\zeta)} \end{aligned} \tag{11}$$

where

$\rho_a \approx 1.25 \times 10^{-3}$ is the density of air (gm/cm^3)

α = the wind azimuth from north as used in the model

U_{10} = the wind speed at a standard anemometer height of 10 meters as used in the model

$\gamma^2 \approx 2.6 \times 10^{-3}$

In this study, however, γ^2 was determined from wind-speed-dependent formulation as developed by Wu (1969), where

for $U_{10} \geq 15$ meters/second

$$\gamma^2 = 2.6 \times 10^{-3}$$

and for $U_{10} < 15$ meters/second

$$\gamma^2 = 5 \times 10^{-4} (U_{10})^{\frac{1}{2}}$$

Thus (11) becomes

$$\left.\begin{aligned} W_x &= \frac{\rho_a}{\rho} \frac{\gamma^2 U_{10}^2 \sin \alpha}{(h + \zeta)} \\ W_y &= \frac{\rho_a}{\rho} \frac{\gamma^2 U_{10}^2 \cos \alpha}{(h + \zeta)} \end{aligned}\right\} \tag{12}$$

where γ^2 is now the wind friction factor from Wu (1969).

The basic continuity equation, repeated here,

$$\frac{\partial u}{\partial x} + \frac{\partial v}{\partial y} + \frac{\partial w}{\partial z} = 0 \tag{2}$$

is developed with the same assumptions to arrive at the vertically integrated continuity equation

$$\frac{\partial}{\partial x} \int_{-h}^{\zeta} u dz + \frac{\partial}{\partial y} \int_{-h}^{\zeta} v dz + \frac{\partial \zeta}{\partial t} = 0 \tag{13}$$

Using (6), this becomes the continuity equation used in the model calculations

$$\frac{\partial}{\partial x} U(h + \zeta) + \frac{\partial}{\partial y} V(h + \zeta) + \frac{\partial \zeta}{\partial t} = 0 \tag{14}$$

with no assumption of vertical homogeneity or the magnitude of $\partial w/\partial z$ with respect to $\partial u/\partial x$.

Substituting (11) and (12) in (9) likewise yields the equations of motion applicable to the study:

$$\frac{\partial U}{\partial t} = - U \frac{\partial U}{\partial x} - V \frac{\partial U}{\partial y} - g \frac{\partial \zeta}{\partial x} + fV - \frac{gU(U^2 + V^2)^{\frac{1}{2}}}{C^2 (h + \zeta)} + \frac{\rho_a \gamma^2 U_{10}{}^2 \sin \alpha}{\rho(h + \zeta)}$$

$$\frac{\partial V}{\partial t} = - U \frac{\partial V}{\partial x} - V \frac{\partial V}{\partial y} - g \frac{\partial \zeta}{\partial y} - fU - \frac{gV(U^2 + V^2)^{\frac{1}{2}}}{C^2 (h + \zeta)} + \frac{\rho_a \gamma^2 U_{10}{}^2 \cos \alpha}{\rho(h + \zeta)} \qquad (15)$$

Finite-Difference Methods

In this method finite-difference equations are made to represent the partial differential hydrodynamic tidal equations. The three major problems are to devise finite-difference equations which will:

1. Converge to the differential solution when the spatial and temporal increments go to zero.

2. Remain stable throughout the solution, i.e., not be subject to distorted solutions with unrealistic answers as a result of exponentially expanding the effect of small computational round-off errors.

3. Be economical in terms of computer time versus versatility in the number of parameters that can be considered in the problem.

Finite-differnce theory, development, and application to problems are covered extensively in the literature, e.g., Forsythe and Wasow (1960), Bramble (1966), Van der Houwen (1968), von Rosenberg (1969), etc. Dronkers (1964) gives a detailed example of the explicit system used by Hansen and then by Reid and Bodine.

All the systems are built from various methods of applying the basic first and second (if necessary) derivatives in finite-difference form. The basics stem from considering a continuous function u(x), with two values separated by a differential distance dx. Then

$$u(x + dx) = u(x) + \frac{du}{dx}(x) \cdot dx$$

But when discrete differences Δx are used, the left and right sides are not exactly equal. The exact relation using Δx is then a Taylor series:

$$u(x + \Delta x) = U(x) + \frac{du}{dx}(x) \cdot \Delta x + \frac{d^2u}{dx^2}(x) \cdot \frac{(\Delta x)^2}{2!} + \frac{d^3u}{dx^3}(x) \cdot \frac{(\Delta x)^3}{3!} +$$

When considering equally spaced points the series may be written as follows for points:

$$x_{i+1} = x_i + \Delta x$$

and

$$x_{i-1} = x_i - \Delta x$$

$$u_{i+1} = u_i + \left(\frac{du}{dx}\right)_i x + \left(\frac{d^2u}{dx^2}\right)_i \frac{x^2}{2} + \left(\frac{d^3u}{dx^3}\right)\frac{\Delta x^3}{6} + \ldots \quad (16)$$

$$u_{i-1} = u_i - \left(\frac{du}{dx}\right)_i \Delta x + \left(\frac{d^2u}{dx^2}\right)_i \frac{\Delta x^2}{2} - \left(\frac{d^3u}{dx^3}\right)\frac{\Delta x^3}{6} + \ldots \quad (17)$$

The first derivative is found by rearranging (16):

$$\left(\frac{du}{dx}\right)_i = \frac{u_{i+1} - u_i}{\Delta x} - \left(\frac{d^2u}{dx^2}\right)_i \frac{\Delta x}{2} - \ldots \quad (18)$$

The second derivative is found by adding (16) and (17) and rearranging but will not be recorded here because it is not used in the tidal equations (14) and (15).

The error in using (18) is in the order of the first term that is truncated from the series. In this case the second term is truncated (containing x), therefore the analog is referred to as only first-order correct. A better analog is found by subtracting (17) from (16) and rearranging:

$$\left(\frac{du}{dx}\right)_i = \frac{u_{i+1} - u_{i-1}}{2\Delta x} - \left(\frac{d^3u}{dx^3}\right)_i \frac{\Delta x^2}{6} - \ldots \quad (19)$$

This analog is second-order correct and is centered on the point x_i. Both are conditions that contribute to convergence. In the solutions devised by various investigators already cited, this analog is used in both space and time by centering on even, odd, and half values (either plus or minus) of i.

The next question, of stability, according to most authors is difficult to define. An example illustrating the idea (Forsythe and Wasow, 1960) is as follows:

Original differential equation: $\frac{\partial^2 u}{\partial x^2} - \frac{\partial^2 u}{\partial t^2} = 0$

Finite-difference form: $u(x,t+k) = 2u(x,t) - u(x,t-k)$
$+\lambda^2 [U(x-h,t) - 2U(x,t) + U(x-h,t)]$ (20)

where $\lambda = k/h = 2$

$U(x,0) = f(x)$

$\frac{u(x,k) - u(x,0)}{k} = g(x)$

Then, if only one round-off error is introduced, i.e., $u(0,k) = \epsilon$, instead of zero, such that

$$f(x) = 0 \qquad f(x) = \begin{cases} 0 \text{ for } x \neq 0 \\ \epsilon/k \text{ for } x = 0 \end{cases} \qquad (21)$$

then the growth of the error of substituting (21) into (20) can be seen from a table given in Dahlquist (1954):

t									
5K	256	-1536	4432	-7920	9541	-7920	4432	-1536	256
4K	0	64	-288	616	-780	616	-288	64	0
3K	0	0	16	-48	67	-48	16	0	0
2K	0	0	0	4	-6	4	0	0	0
K	0	0	0	0	1	0	0	0	0
0	0	0	0	0	0	0	0	0	0
x	-4h	-3h	-2h	-h	0	h	2h	3h	4h

It can be shown from a numerical analysis of the differential tidal equations that stability in some schemes can be assured if the time and distance increments stay within certain relative limits. In the Reid and Bodine (1968) model followed by Hacker et al. (1971), as with Hansen's model (Youkey, 1968), this criterion is

$$\frac{\Delta S}{\Delta t} \geq \sqrt{\frac{gh_{max}}{2}} \qquad (22)$$

where

ΔS = grid spacing
Δt = time increment
g = gravity acceleration
h = depth

Sobey (1970) compared the stability of four systems, those of Heaps, Reid and Bodine, Abbott, and Leendertse. Because the latter two schemes are implicit, they are shown to be stable under all $\Delta S/\Delta t$ conditions.

This factor is most significant in making the decision of which finite-difference system to use. The Reid and Bodine system is good, but for the Chandeleur-Breton estuary the stability requires the following:

Assume size 20 x 50 miles @ 1-mile grid = 1000 points
Assume maximum depth h = 12 meters, 1 mile = 1600 meters

From (22) $\quad \Delta t \leq \Delta S/(gh/2)^{\frac{1}{2}}$
$\leq 1600/(10 \times 6)^{\frac{1}{2}}$
$\leq$ 200 seconds

where ΔS, Δt, g, and h are defined above. Thus about a 3- to 3½-minute time step is allowed.

For the effect of an hour's change in tidal input, the program will have to cycle 17 to 20 times, and for 1000 computational points over a 21- or 24-hour tidal period this seems to require an excessive amount of computer time. The tradeoff, however, is that the implicit scheme of Leendertse, for example, requires more computational steps at each point than does the explicit scheme of Reid and Bodine. The latter is not a serious problem for a large digital computer.

The question of economical computer utilization is a moot point. It is solved most simply in most cases by fully utilizing the computer available to the investigator, and each computer has varying characteristics, such as total memory capacity. Briefly, therefore, the computational method selected for use and consequently the number of options open to the scheme may, in fact, be dictated by the limitations of the computer.

Implicit numerical schemes require more computer memory than explicit numerical schemes but are more versatile and overall require less computer time to arrive at the same areal system solutions.

The author fortunately had access to a UNIVAC 1108, which in terms of computer memory capacity and computing speed presented no limitations to any of the planned capabilities of the modified Leendertse scheme selected for a computer model of an estuary.

COMPUTATIONAL MODEL

General Description

The finite-difference computational scheme developed to model the surface and current flow fields of the Chandeleur-Breton Sounds estuary is basically that scheme developed and discussed by Leendertse (1967). Wherever possible, the coding in the author's modified program was exactly the same as that used by Leendertse so that interested investigators might make easy reference and comparison. Major revisions were made, however, in the organizational logic.

The shear length of finite-difference equations and a listing of the modified program make inclusion of it in this report impractical. However, a brief description and comparison of Leendertse's program and the modified model are warranted.

The model, as diagrammed in Figure 2, is arranged so that there is a main body program and 15 subroutines, the last of which is a plotter routine. This arrangement allows one to easily find and modify any part of the program without unwittingly affecting another part. This is often a major problem to an investigator who is attempting to modify an existing program to suit his needs, which of course is the common case, since no computer program can be used without some modification on such problems as modeling similar but uniquely differing estuaries.

As shown in Figure 2, the primary blocks and subdivisions function as follows, and the following definitions are understood:

SEP = surface elevation (from Leendertse's original symbol for zeta prime)
UP = east-west velocity component
VP = north-south velocity component (similarly from Leendertse) for U and V prime

First time step:

Section 100 - Implicit computation for SEP and UP
Section 200 - Explicit computation for SEP and VP

Second time step:

Section 300 - Implicit computation for SEP and VP
Section 400 - Explicit computation for UP

Upon completion of the second time step computations, the resultant values for both time steps are averaged [in the output subroutine (PRINT)] for each grid point, a procedure that gives, in essence, a time-centered finite-difference approximation to the appropriate grid-point-centered values.

COMPUTATIONAL MODEL

Main Program

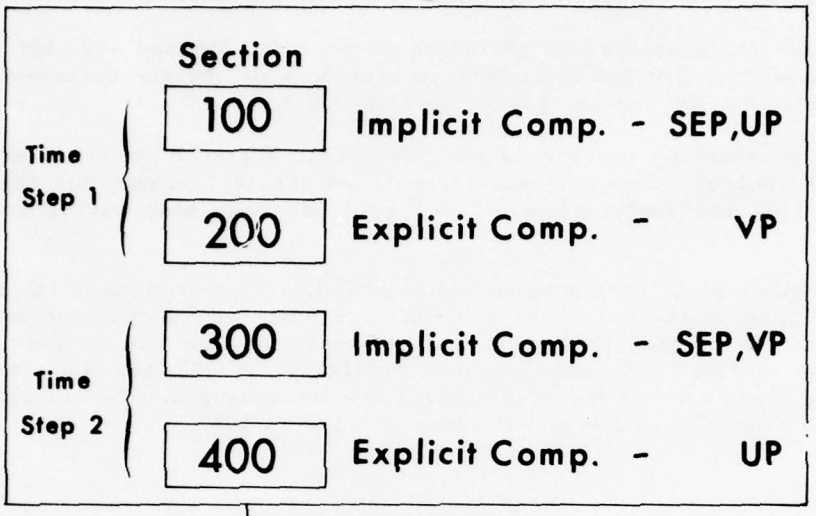

Subroutines

1	INPUT	Calls Input Subroutines
2	KURIH	Reads in Tidal Data at Known Points
3	DIVE	Reads in Locations of Land (0) & Water (1)
4	FIND	Locates, Codes, & Counts Water Sections
5	DEPTH	Reads in Water Depths
6	CHEZY	Reads in Chezy Coefficients
7	WIND	Wind Stress Routine
8	INVAL	Writes Out Initial Values
9	PRINT	Main Printout, Print, or Plot Routine
10	OPEN	Computes Open Bound Water Levels
11	STEADY	Computes Steady Flow Boundary Velocity
12	OVFLO	Computes Overflow Boundary Velocity
13	OVFLD	Sets Overflow Threshold Evaluation (D)
14	PLOTM	Prepares Data for Plotter Routine
15	MAINP	Main Plotter Routine

Figure 2. Identification of main units in the model computer program.

The computing sequence is as follows:

In section 100, values (SEP and UP) are computed for every grid point on a row from left to right (west to east), row after row, from bottom to top (south to north). In section 200, the value of VP is computed for every grid point on a column from south to north, column after column, from west to east.

Similar computations are performed in sections 300 and 400, but SEP and VP are done in section 300 and UP is done in section 400, whereas the sequence is per column in section 300 and per row in section 400.

This alternating routine is most important inasmuch as it is actually the factor that controls computing stability in an implicit scheme and thereby frees the model from the restrictions of the grid and time step ratio, as discussed earlier.

To further facilitate program modification, all program steps (there are more than 1000 lines in the main body program) are numbered in consecutive order and according to the section they are in. The steps are also exactly the same in the comparative sections 100 and 300 and similarly in 200 and 400, except that appropriate U and V terms and step numbers are interchanged. For example, step 103 compares to step 303, and step 203 compares to step 403.

Capabilities and Options

Input

Model adaptability per easily varied input parameters. Other than major sections of input tide, depth, boundary condition indicators, and friction factors (all of which will be discussed), the input variables that allow the model to be adapted to another estuarine environment are all listed prominently in the first few steps of the program. In each case the change is only that of a numerical constant.

For example, one-number changes are possible for the following:

1. The number of time steps for which one wants to run the program
2. The grid spacing
3. The time step span (number of hours, minutes, or seconds)
4. Mid-latitude of the area (necessary only for Coriolis terms)
5. Several maximum dimension values
6. Control for output: listing (0), printing (1), or both (2)
7. If wind is to be considered, the time step on which it is to begin and the ending step, as well as the velocity and direction

From that point on, since the constants are given variable names, the program uses the new values and the investigator need not trouble himself with tracing through the whole program for other steps where the constant is used in computation. Subroutines are called in automatically and where applicable by the main body program.

Boundary condition options. The computational model's first subroutine has two prime functions. It calls in the input data subroutines in the proper sequential order, and it starts the computations by calling in a few data cards

that provide output area identity (in this case, Chandeleur-Breton Sounds) and control numbers for each boundary point. These numbers allow four options to each coordinate direction of each boundary point:

0 if closed (solid boundary)
1 if open (tidal input)
2 if steady flow (stream input)
3 if overflow (marsh flooding)

Both the steady flow and overflow subroutines are additions to Leendertse's program but will not be discussed because they were not used in this study.

In addition to the boundary condition numbers, a group of data cards are read in with blanks (0s) or ones (1s) for every point in the computational matrix. A blank indicates a dry-land point or a boundary point where input values are known. The 1s mean the model will compute all required values for that grid point. It is this simple arrangement that allows an investigator to easily vary the size and configuration of the area that he intends to model. For example, the model may be run with a group of points representing an obstruction entered as 0s. A second run with the 0s changed to 1s will show the effect of removing the obstruction. The points used in the computational grid can be seen in Figure 5.

Depths. Depths at each grid point are brought into the program via the subroutine DEPTH. Within the routine and before entering the main-body program for computations, the depths are converted (in this case) to meters (the basic unit used in the computations, although output is in centimeter units). Conversion at this point is only a matter of changing the constant, thus allowing two things:

1. Depths can be entered in whatever units are convenient
2. The investigator need not search further to verify the effect of a unit change on computations

Chezy friction factors. The Chezy friction factors are entered in a manner similar to that of the depths, via subroutine CHEZY, per Leendertse (1967). Considerable discussion is given by Leendertse (1967) and Dronkers (1964) to correct empirical formulation for this value. It is a depth- and roughness-dependent formula with empirical constants. The correctness of choice, of course, is determined by the output of the model. Several formulae, all giving about the same results for the Chezy friction factor (C), were tested.

The following formula was used in the model:

$$C = 16.3 \ln (100\ h/d)$$

where

d = 5 = bottom roughness in centimeters
h = depth in meters

Tides. Tidal heights at all open boundary grid points are determined in a subroutine called OPEN. The inputs to this routine, however, are the tidal heights, which are brought into the program through the subroutine KURIH. The latter is based on that of Leendertse (1967).

The KURIH routine is designed to read in tidal heights for each time step for each point or tidal station in or near the model area for which the values are known. For the Chandeleur-Breton area it was most convenient to read in values from six tide stations. They will be identified in a later section. It is

possible, of course, that tidal constituents could be read in for various stations (if available or known), and the routine could be reprogrammed to compute tidal elevations for the required stations and time increments. The routine OPEN only requires getting values as stored by KURIH, not having any part in their creation. In the Chandeleur-Breton area, not enough of the station constituents were available, ergo the decision to read in values at half-hour intervals for all stations.

The OPEN subroutine is the one routine in the program that must be styled for the project area. Essentially, this routine sets up extrapolation and interpolation formulae to create tidal heights at each open boundary grid point on the basis of the values at known points as established in KURIH. The present configuration for the Chandeleur-Breton area shows several examples of linear interpolation that could be followed easily, but any degree of sophistication is possible. In any case, the programming requirement is quite elementary and should not present a problem to another investigator.

Winds. Leendertse's (1967) model did not include wind input, but he did discuss it as an option. The modified computational model does include wind.

The basic wind theory and formulation (12) are adapted from that of Wu (1969) and are identified in the subroutine WIND. As mentioned earlier, the only program inputs required are the wind speed and direction and times to start and stop the wind. The model is presently set up to accept input wind speeds in miles per hour, the common unit of measurement in climatological records. The program converts to meters per second for computations.

Originally the model lacked stability when winds were entered or stopped suddenly but was stable if winds were entered at the first time step and allowed to remain until the end of the run. This instability was eliminated by incorporating a simple linear ramping routine in the wind subroutine that allowed winds to be entered or stopped at any given time.

Basically, the model monitors the time steps, and when it reaches four half time steps preceding the given start or stop time step it begins to enter or end the wind at each of the next four half time steps in cumulative increments of the full U_{10} value. Because a half time step is 0.5 hour, it takes two time steps or 2 hours to fully ramp the wind in and out of the program. This, in fact, would not be too far from natural conditions, the exception being the sudden passage of a weather front.

Computational term options. For analytical purposes one may run the model with or without any combination of the four following terms: (1) Convective inertia (or non-linear acceleration terms), (2) Coriolis terms, (3) bottom friction, and (4) wind forces. Control of these options is quite simple. The first four input data card variables listed in the main body of the program require only a value of one (1) if the term is to be used or a zero (0) if it is to be omitted. The investigator need not trace the terms through the main-body formulation (which, as mentioned earlier, is over 1000 lines) inasmuch as the programming operates on these original control numbers and will automatically include or delete the terms wherever they appear.

Data

Observed field data--currents. The observed current and tidal data used in this study to evaluate the validity of the model are located at the positions shown in Figure 1.

Most of the data was collected and made available by elements of the former U.S. Coast & Geodetic Survey, now referred to as National Ocean Survey (NOS).

The current data at the locations shown were obtained during their Mississippi River Gulf Outlet survey, ergo the concentration in that area. Although the data are limited, they are the result of a major collection effort in the estuary and show clearly the value of a good computer model simulation.

The data were taken by two ships (USC&GS Ferrel and USC&GS Marmer) over a period of 6 months in 1968. Both Geodyne and Roberts meters were used, and where possible one meter was suspended at a depth of 4.5 meters and another at 9.0 meters. An index to the data is shown in Table 1. All current data include direction in degrees and speed in knots. Roberts meter data were in the form of graphical plots from hourly observations of both direction and speed. Geodyne meter data were in the form of an IBM listing for observations at roughly 10-minute time increments.

The 4.5-meter and 9.0-meter currents at a given point generally agreed in direction with speed within 5 cm/sec (0.1 knot). This agreement, of course, is quite supportive of the assumption that a vertically averaged current vector adequately represents the current field, as is done by the computational model.

Detailed inspection of the data revealed several facts:

1. It may be noted from Table 1 that data were not observed simultaneously at all fourteen stations but simultaneous observations were taken in groups of about three stations at a time.

2. Fortunately, the simultaneous observations were taken at stations differing widely in position, and each group happened to cover a different period in the monthly tidal cycle. This situation will be amplified in a later section, but essentially it offered the means by which the computational model could be given a rather comprehensive verification.

3. Unfortunately, the data, as will be shown later, were not of high quality. The readings appeared ragged and not representative of a smoothly flowing and progressively changing current. This circumstance, of course, raises considerable speculation as to the detailed quantitative accuracy of the computational model when comparisons are made for a given point and time.

Tides. Tidal heights used to pulse or drive the model as input to the open bounds were predicted tides, derived directly from the Tide Tables (U.S. Coast and Geodetic Survey, 1968).

Predicted tides were used because sufficient observed data were not available for the period during which all the current data were observed. The Corps of Engineers, New Orleans District, was able, however, to supply a limited amount of observed data for 1970 for a station at Gardner Island. Comparison with predicted values indicated that the correlation was quite good.

Proceeding, then, on the assumption that the predicted tides were representative of the area, the moon's ephemeris data were correlated with that of the tide table for a year's period. In conformance with the foregoing, semi-monthly tides occurred near new or full moon but always near maximum declination. Apogee and perigee were not consistently effective.

The monthly greatest daily range difference, however, always occurred near

Table 1

USC&GS Current Data

Station No.	Depth (m)	Survey Dates (1968) Start	End	Tides	Meter	Ship
2	4.5	9-04	10-03	E	G	F
3	4.5	9-20	10-07	E	G	F
4	3.0	4-09	4-08	T	G	M
5	1.8	9-18	9-26	E	R	F
6	2.7	7-27	8-14	A	G	F
8	4.5 & 9.0	8-16	9-03	A	G	F
9	4.5	7-25	7-28	A	G	F
10	4.5	4-28	5-06	T	G	M
12	1.05	8-07	8-24	A	R	F
13	4.5 & 9.0	9-17	10-03	E	R	F
15	4.5	7-27	8-05	A	G	F
15	4.5	8-26	9-01	A	G	F
18	4.5 & 9.0	8-21	9-07	A	R	F
19	4.5 & 9.0	8-21	9-10	A	R	F
20	4.5	4-19	5-05	T	G	M&F

Note: G = Geodyne meter; R = Roberts meter; F = USC&GS Ferrel; M = USC&GS Marmer; E = Equatorial; T = Tropic; A = Average

maximum southern declination, which of course is about the same angular distance below the equator as the latitude of the Louisiana coast is north of the equator. Briefly, maximum angular eccentricity was achieved.

The maximum daily range difference throughout the year (1968) occurred about 10-13 June, when the moon was full, at perigee, and near maximum southern declination.

Lowest tides always occurred when the moon was at about zero declination (on the equator).

In order to represent the model area during periods of minimum, average, and maximum daily tidal range, the tide tables were scanned for data covering the periods of current observations and for the significant periods of equatorial, average, and tropic tides, respectively. As it happened, current observations were taken at several stations simultaneously at each of these significant range periods. The effects will be pointed out in a later section.

The computational model was driven by predicted tidal heights, at 0.5-hour intervals, from the six stations listed in Table 2. The table also shows their relative phase lag. Input tides will be listed as they apply to later sections of the study.

Wind. Observed wind data were not available for the period during which the NOS (USC&GS) ships Marmer and Ferrel recorded current data. Therefore, repre-

Table 2
Tidal Base Stations

Station	Latitude	Longitude	Time		Height		Range Diurnal (m)	MTL Above MLW (m)
			High Water h m	High Water h m	High Water (m)	High Water (m)		
Cat Island	30°14'	89°10'	-0 44	+0 07	+0.12	0.0	0.52	0.24
Ship Island	30°13'	88°59'	-0 42	-0 30	+0.12	0.0	0.52	0.24
Horn Island	30°13'	88°29'	-0 31	-0 53	+0.12	0.0	0.52	0.24
Chandeleur Light	30°03'	88°52'	-0 39	-0 21	-0.03	0.0	0.36	0.18
Breton Island	29°30'	89°10'	-0 21	-0 15	0.0	0.0	0.40	0.21
Jack Bay	29°22'	89°21'	+0 12	+0 30	-0.03	0.0	0.36	0.18
Lonesome Bayou	29°14'	89°03'	-2 35	-2 47	-0.06	0.0	0.33	0.10

NOTE: Time and height relative to Pensacola (TM 90°).

sentative wind conditions were obtained from climatological data.

The actual figures used were the approximate average monthly wind speed and direction. It should be noted, however, that wind speeds are not high in the New Orleans area, averaging only about 2 or 3 meters per second. Noting the criteria and formulation of Wu (1969) as presented earlier, one would expect little effect from these low-velocity winds. To emphasize the effect, therefore, the model was run with 10 m/sec winds. The effect will be discussed in a later section.

Depth. The water depths at each grid point were scaled from large-scale charts applicable to the pre-Camille conditions of 1968. The charts were USC&GS-1267, -1268, -1270, and -1271. A small-scale representation is shown in Figure 3.

The rather uniform depths should be noted, since the model water surface elevation and currents will be shown to have distinct patterns that are not readily indicated by the hydrography. Points to note are the following: Basically the whole estuary inside the island arc is rather flat, the channel depth being about 5 to 6 meters. There is a smooth, uniform gradient to the marsh side (west) but a relatively abrupt rise to the island arc (east). Three channel scours exist, one on each side of Breton Island and one outside (north of) Chandeleur Island. Outside the island arc the bottom drops off rather uniformly to about 45 meters in the southeastern corner of the model area.

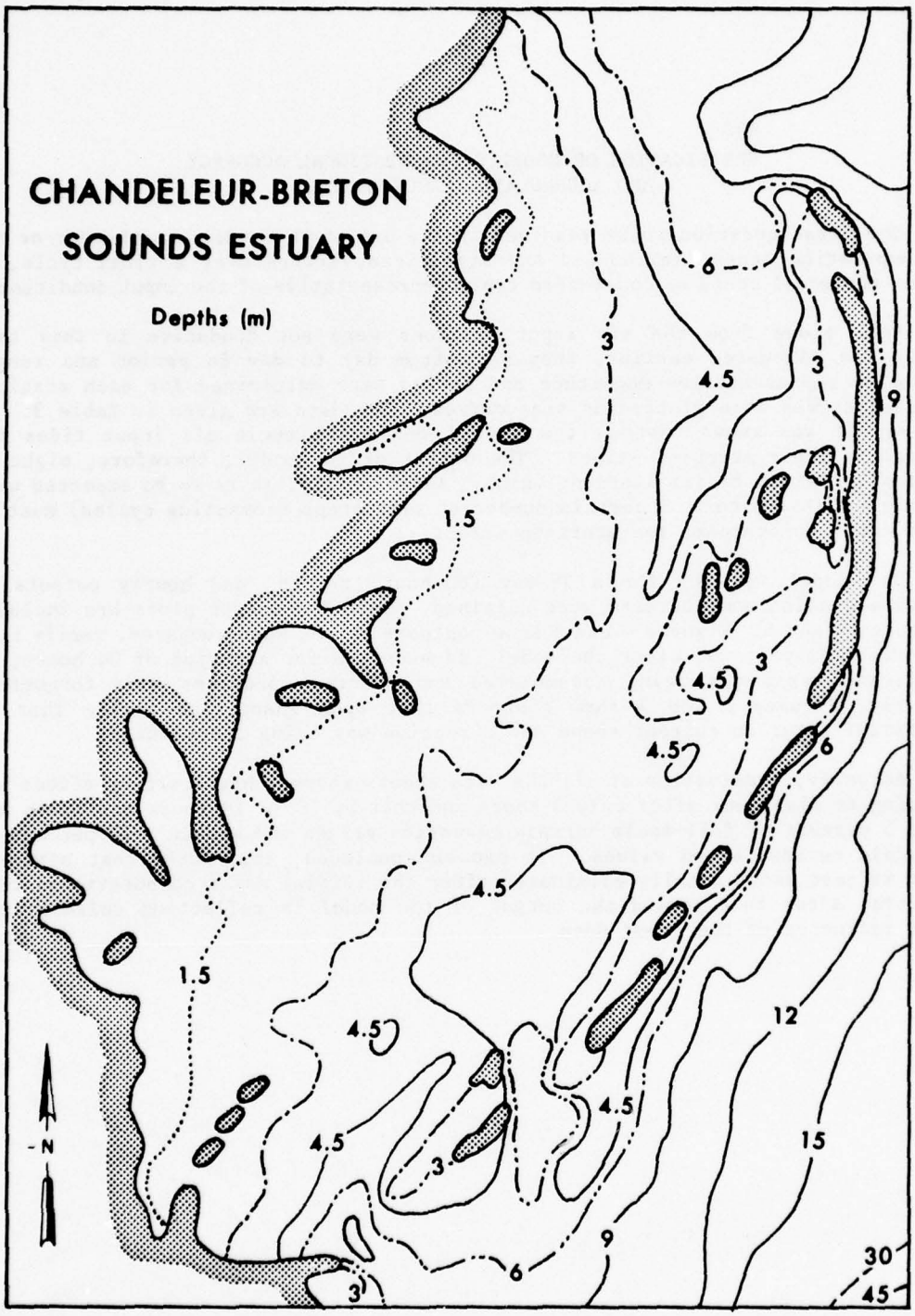

Figure 3. Depth contours in meters as consistent with source charts.

VERIFICATION OF MODEL'S COMPUTATIONAL ACCURACY AND ACCUMULATED ERROR CONTROL

The first question to be resolved in the use of the model was whether or not the computation scheme introduced any significant errors over a tidal cycle, or whether the model could be considered truly representative of the input conditions.

Real tides from the six input stations were not conducive to this test because, as discussed earlier, they vary from day to day in period and range. Instead, a representative magnitude and period were determined for each station, and tidal curves were plotted as sine curves. The data are given in Table 3. In this way it was known that at the end of one tidal cycle all input tides had returned to their starting values. The output of the model, therefore, might be expected to return to its starting value. Additionally, as is to be expected with any model of this nature, a certain number of time steps (computing cycles) must be run in order to overcome the start-up effect.

The model was run for a 2½-day (60-hour) period, and hourly outputs of surface elevation and currents were obtained. Selected output plots are included as Figures 4 and 5. Figures 4 and 5 show contours which, when compared, verify that for surface elevations, after the model had been run for a period of 36 hours, no significant error was being accumulated and start-up problems were forgotten. Similarly, Figures 6 and 7 show contours that upon inspection verify that no significant error in current speed and direction was being accumulated.

Actually, examination of all the data sheets showed that start-up effect was beginning to disappear after only 3 hours and that by 15 to 18 hours the match was within 5 percent of full-scale surface elevation values and within 5-10 percent of full-scale current speed values. It can be concluded, therefore, that start-up effect is just about totally eliminated after the initial day's computational run. Therefore, after this period the output of the model is reflecting reliably the direct influence of the input data.

TABLE 3
INPUT TIDAL HEIGHTS (FT)
SINE CURVE TIDES - TEST DATA

TIME STEP	DAY	HOUR	TIDE STATIONS A	B	C	D	E	F
1	1		.350	.270	.660	.330	.510	.510
2	1	1	.430	.330	.750	.410	.620	.620
3	1		.520	.410	.850	.500	.750	.750
4	1	2	.620	.500	.950	.590	.880	.880
5	1		.730	.590	1.040	.690	1.010	1.010
6	1	3	.840	.690	1.140	.800	1.150	1.150
7	1		.950	.800	1.230	.900	1.290	1.290
8	1	4	1.060	.900	1.310	1.000	1.420	1.420
9	1		1.170	1.010	1.380	1.110	1.550	1.550
10	1	5	1.280	1.110	1.450	1.210	1.680	1.680
11	1		1.390	1.210	1.500	1.300	1.790	1.790
12	1	6	1.470	1.300	1.540	1.390	1.890	1.890
13	1		1.550	1.390	1.570	1.470	1.980	1.980
14	1	7	1.620	1.470	1.590	1.530	2.060	2.060
15	1		1.690	1.530	1.600	1.590	2.120	2.120
16	1	8	1.740	1.580	1.590	1.640	2.160	2.160
17	1		1.770	1.640	1.570	1.670	2.190	2.190
18	1	9	1.790	1.670	1.540	1.690	2.200	2.200
19	1		1.800	1.680	1.500	1.700	2.190	2.190
20	1	10	1.790	1.710	1.450	1.690	2.160	2.160
21	1		1.770	1.690	1.380	1.670	2.120	2.120
22	1	11	1.740	1.670	1.310	1.640	2.060	2.060
23	1		1.690	1.640	1.230	1.590	1.980	1.980
24	1	12	1.620	1.590	1.140	1.530	1.890	1.890
25	1		1.550	1.530	1.040	1.470	1.790	1.790
26	1	13	1.470	1.470	.950	1.390	1.680	1.680
27	1		1.390	1.390	.850	1.300	1.550	1.550
28	1	14	1.280	1.390	.750	1.210	1.420	1.420
29	1		1.170	1.210	.660	1.110	1.290	1.290
30	1	15	1.060	1.110	.560	1.000	1.150	1.150
31	1		.950	1.010	.470	.900	1.010	1.010
32	1	16	.850	.900	.390	.800	.880	.880
33	1		.730	.800	.320	.690	.750	.750
34	1	17	.620	.690	.250	.590	.620	.620
35	1		.520	.590	.200	.500	.510	.510
36	1	18	.430	.500	.160	.410	.410	.410
37	1		.350	.410	.130	.330	.320	.320
38	1	19	.290	.330	.110	.270	.240	.240
39	1		.210	.270	.100	.210	.180	.180
40	1	20	.160	.210	.110	.160	.140	.140
41	1		.130	.160	.130	.130	.110	.110
42	1	21	.110	.130	.160	.110	.100	.100
43	1		.100	.110	.200	.100	.110	.110
44	1	22	.110	.100	.250	.110	.140	.140
45	1		.130	.110	.320	.130	.180	.180
46	1	23	.160	.130	.390	.160	.240	.240
47	1		.210	.160	.470	.210	.320	.320
48	1	24	.260	.210	.560	.270	.410	.410

TABLE 3
INPUT TIDAL HEIGHTS (FT)
SINE CURVE TIDES - TEST DATA

TIME STEP	DAY	HOUR	TIDE STATIONS A	B	C	D	E	F
49	2		.350	.270	.660	.330	.510	.510
50	2	1	.430	.330	.750	.410	.620	.620
51	2		.520	.410	.850	.500	.750	.750
52	2	2	.620	.500	.950	.590	.880	.880
53	2		.730	.590	1.040	.690	1.010	1.010
54	2	3	.840	.690	1.140	.800	1.150	1.150
55	2		.950	.800	1.230	.900	1.290	1.290
56	2	4	1.060	.900	1.310	1.000	1.420	1.420
57	2		1.170	1.000	1.380	1.110	1.550	1.550
58	2	5	1.290	1.110	1.450	1.210	1.680	1.680
59	2		1.380	1.210	1.500	1.300	1.790	1.790
60	2	6	1.470	1.300	1.540	1.390	1.890	1.890
61	2		1.550	1.390	1.570	1.470	1.980	1.980
62	2	7	1.620	1.470	1.590	1.530	2.060	2.060
63	2		1.690	1.530	1.600	1.590	2.120	2.120
64	2	8	1.740	1.580	1.590	1.640	2.160	2.160
65	2		1.770	1.640	1.570	1.670	2.190	2.190
66	2	9	1.790	1.670	1.540	1.690	2.200	2.200
67	2		1.800	1.680	1.500	1.700	2.190	2.190
68	2	10	1.790	1.700	1.450	1.690	2.160	2.160
69	2		1.770	1.690	1.380	1.670	2.120	2.120
70	2	11	1.740	1.670	1.310	1.640	2.060	2.060
71	2		1.690	1.640	1.230	1.590	1.980	1.980
72	2	12	1.620	1.590	1.140	1.530	1.890	1.890
73	2		1.550	1.530	1.040	1.470	1.790	1.790
74	2	13	1.470	1.470	.950	1.390	1.680	1.680
75	2		1.380	1.390	.850	1.300	1.550	1.550
76	2	14	1.280	1.300	.750	1.210	1.420	1.420
77	2		1.170	1.210	.660	1.110	1.290	1.290
78	2	15	1.060	1.110	.560	1.000	1.150	1.150
79	2		.950	1.000	.470	.900	1.010	1.010
80	2	16	.850	.900	.390	.800	.880	.880
81	2		.730	.800	.320	.690	.750	.750
82	2	17	.620	.690	.250	.590	.620	.620
83	2		.520	.590	.200	.500	.510	.510
84	2	18	.430	.500	.160	.410	.410	.410
85	2		.350	.410	.130	.330	.320	.320
86	2	19	.280	.330	.110	.270	.240	.240
87	2		.210	.270	.100	.210	.180	.180
88	2	20	.160	.210	.110	.160	.140	.140
89	2		.130	.160	.130	.130	.110	.110
90	2	21	.110	.130	.160	.110	.100	.100
91	2		.100	.110	.200	.100	.110	.110
92	2	22	.110	.100	.250	.110	.140	.140
93	2		.130	.110	.320	.130	.180	.180
94	2	23	.160	.130	.390	.160	.240	.240
95	2		.210	.160	.470	.210	.320	.320
96	2	24	.280	.210	.560	.270	.410	.410

TABLE 3

INPUT TIDAL HEIGHTS (FT)

SINE CURVE TIDES - TEST DATA

TIME STEP	DAY	HOUR	TIDE STATIONS A	B	C	D	E	F
97	3		.350	.270	.660	.330	.510	.510
98	3	1	.430	.330	.750	.410	.620	.620
99	3		.520	.410	.850	.500	.750	.750
100	3	2	.620	.500	.950	.590	.880	.880
101	3		.730	.590	1.040	.690	1.010	1.010
102	3	3	.840	.690	1.140	.800	1.150	1.150
103	3		.950	.800	1.230	.900	1.290	1.290
104	3	4	1.060	.900	1.310	1.000	1.420	1.420
105	3		1.170	1.000	1.380	1.110	1.550	1.550
106	3	5	1.280	1.110	1.450	1.210	1.680	1.680
107	3		1.380	1.210	1.500	1.300	1.790	1.790
108	3	6	1.470	1.300	1.540	1.390	1.890	1.890
109	3		1.550	1.390	1.570	1.470	1.980	1.980
110	3	7	1.620	1.470	1.590	1.530	2.060	2.060
111	3		1.690	1.530	1.600	1.590	2.120	2.120
112	3	8	1.740	1.590	1.590	1.640	2.160	2.160
113	3		1.770	1.640	1.570	1.670	2.190	2.190
114	3	9	1.790	1.670	1.540	1.690	2.200	2.200
115	3		1.800	1.690	1.500	1.700	2.190	2.190
116	3	10	1.790	1.700	1.450	1.690	2.160	2.160
117	3		1.770	1.690	1.380	1.670	2.120	2.120
118	3	11	1.740	1.670	1.310	1.640	2.060	2.060
119	3		1.690	1.640	1.230	1.590	1.980	1.980
120	3	12	1.620	1.590	1.140	1.530	1.890	1.890

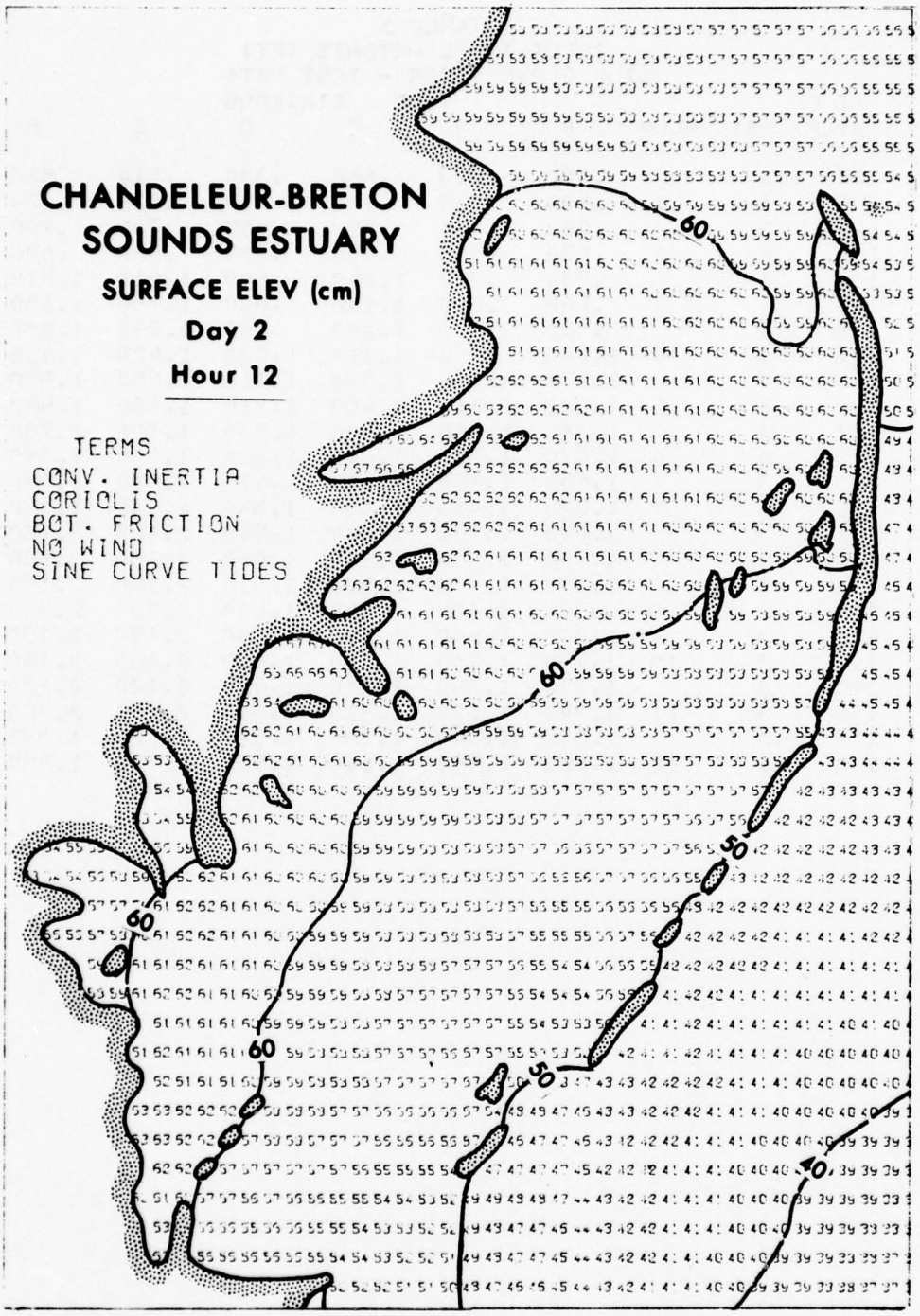

Figure 4. Surface elevations, day 2, hour 12, from sine curve tidal input.

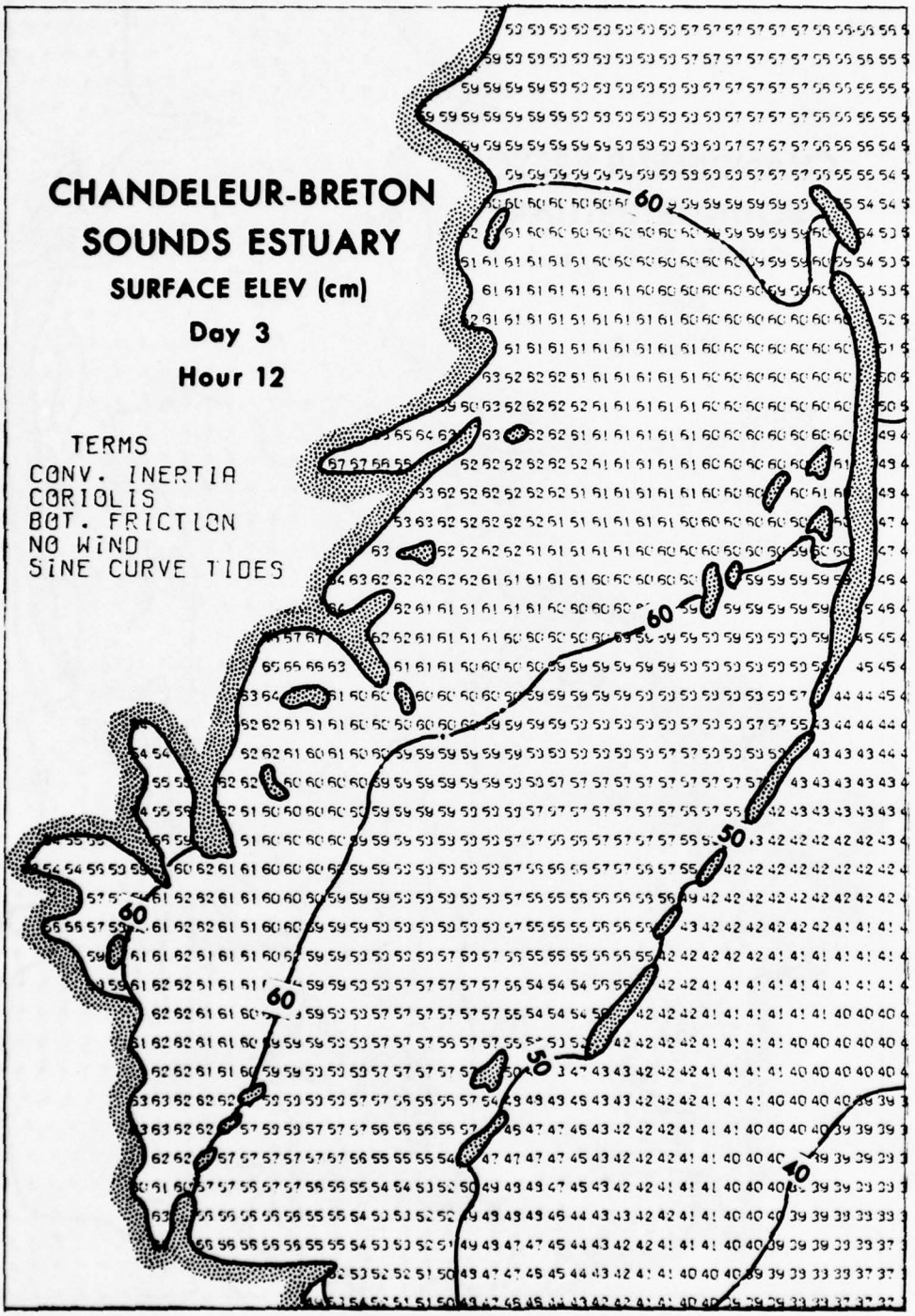

Figure 5. Surface elevations, day 3, hour 12, from sine curve tidal input.

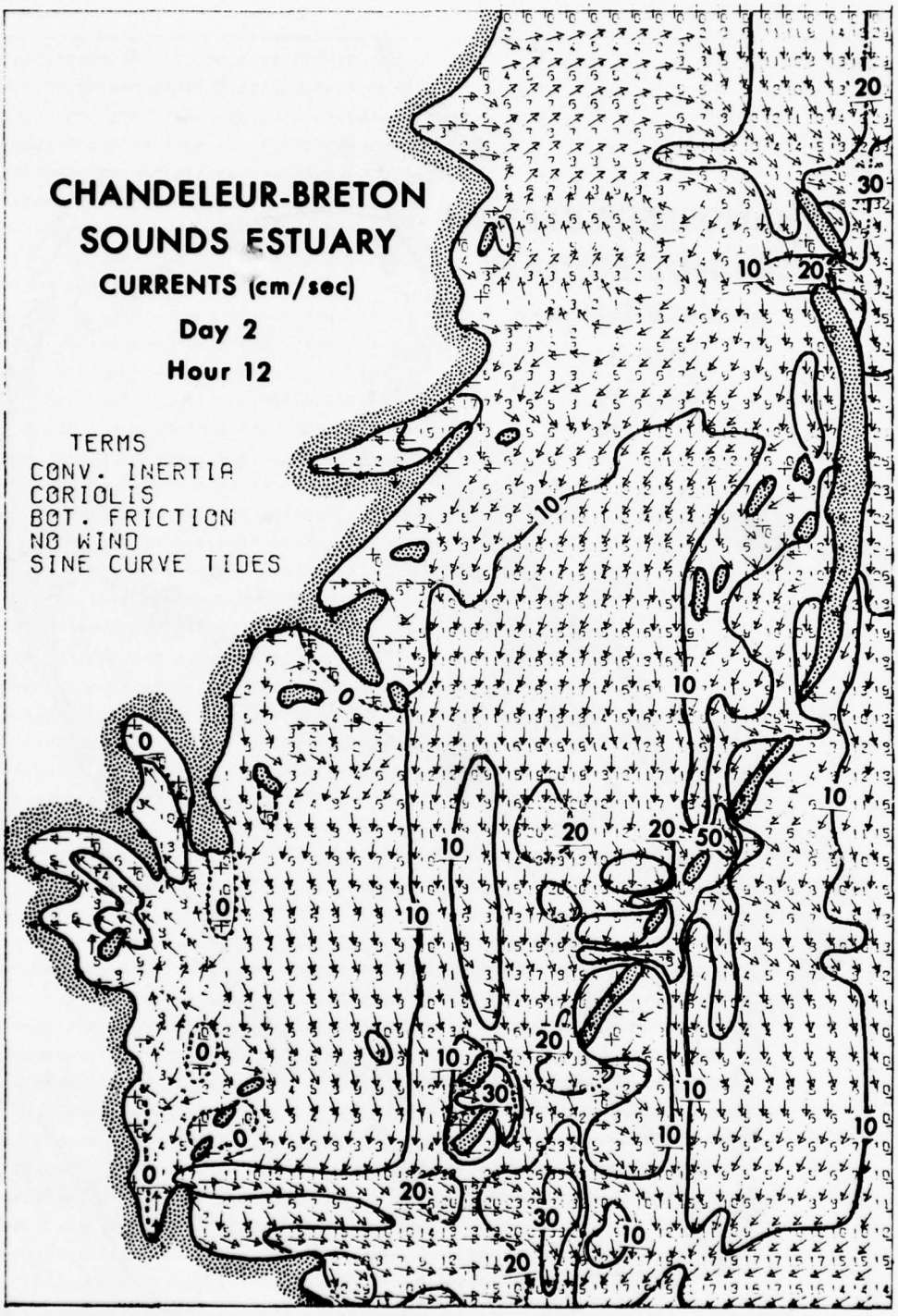

Figure 6. Currents, day 2, hour 12, from sine curve tidal input.

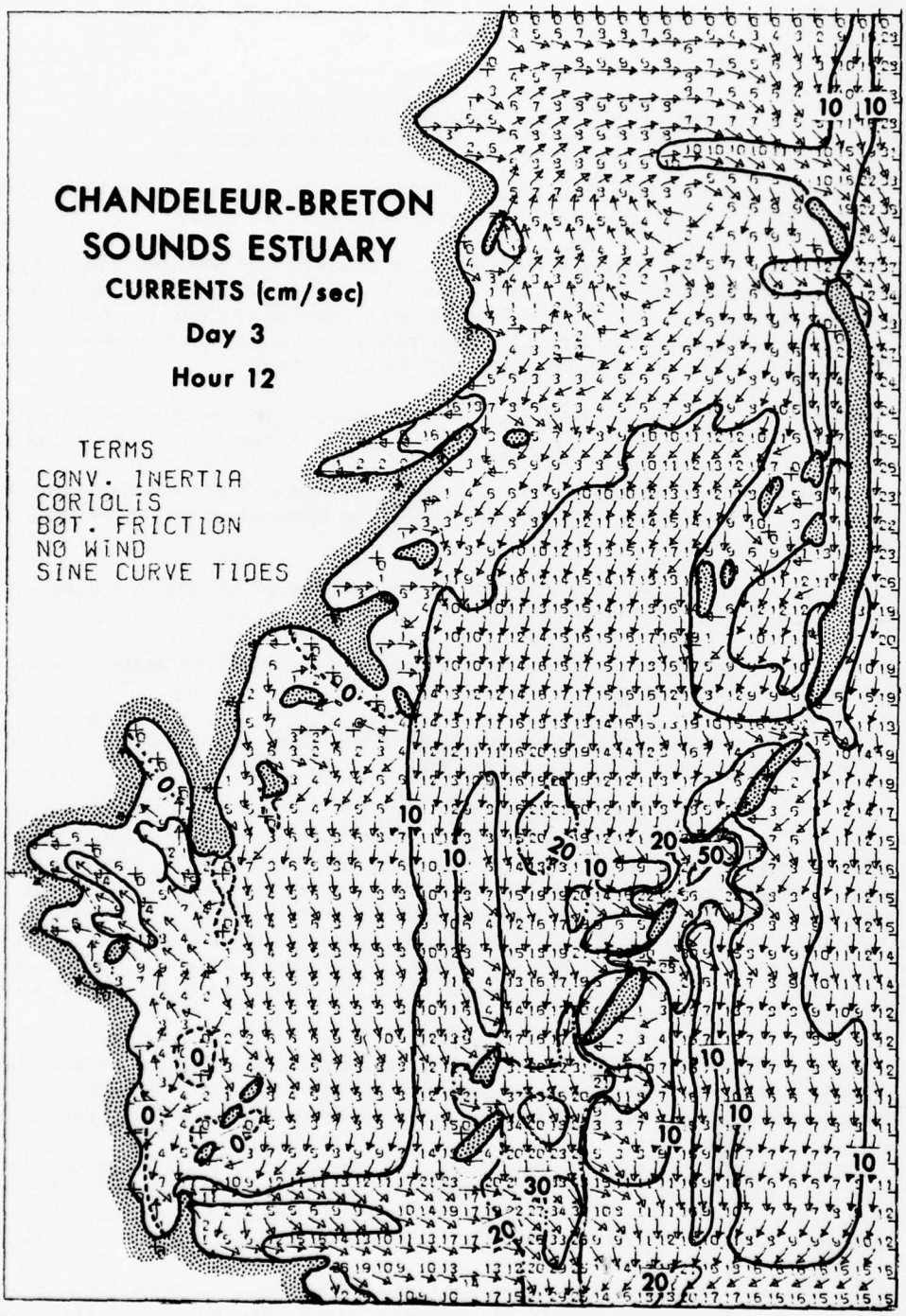

Figure 7. Currents, day 3, hour 12, from sine curve tidal input.

VERIFICATION OF MODEL'S SIMULATION ACCURACY (MODEL OUTPUT VS. OBSERVED FIELD DATA)

Having shown that the model is computationally accurate, the most critical requirement was to test it against real data for true accuracy.

Dates of current observations, station number, and current tidal type are given in Table 1. From this table and Figure 1, where the stations may be located, one can see that during each of the four data-collection periods the combination of stations is different. They are also separated by considerable distance and are each located in areas of specific interest in the estuary.

These facts not only allow 15 straightforward comparisons of model output to observed data, but they also provide information for comment on the following:

1. Each of the four groups of stations contains one or more stations outside and concurrently inside the estuary (assuming the Chandeleur Island-Breton Island arc to be the boundary).

2. The foregoing allows comment on the effect of shallow or deep water or open sea compared to the enclosed estuary.

3. In each group, one or more stations is in a high and another is in a low current velocity location.

4. In each group there is a station near a boundary (open or closed), and there are others several grid distances out from the nearest bound.

5. Observations were made during periods of low tidal range (equatorial tide--22 September 1968), average range (27-28 July and 23-24 August 1968), and finally maximum daily range (tropic tides--30 April-1 May 1968). The tides for 22-24 August 1968 are included as Table 4 because they are the input for several tests. The remainder are not included. To perform these tests, the model was run using tide and wind conditions applicable to the observation dates and times. Note, for example, in Table 4 that the average range is about 0.45 to 0.60 meter and the period is about 25 hours, and for tropic tides the range is 0.75 to 0.9 meter and about 0.15 meter at equatorial range.

Working from the output data listing (which, though tedious, was simple and efficient), component velocities were extracted and tabulated for each hour. The synchronous observed currents were reduced to components by an auxiliary program.

A plotter program was written to accept concurrent field and model data and plot the results, as shown in Figures 8 to 10. In some cases the comparisons were excellent, but others were disturbing. Definitive reasons for the differences are not apparent, but the following suppositions and discussions are warranted.

These plots show that the field data are quite ragged. Local high-frequency disturbances may have been in effect; however, some effect seems attributable to instrumentation malfunction. Actually, raw data were represented by smooth least

TABLE 4

INPUT TIDAL HEIGHTS (FT)

AVERAGE TIDES 0030 22AUG - 1200 24AUG'68

TIME STEP	DAY	HOUR	TIDE STATIONS A	B	C	D	E	F
1	1		.600	.450	.870	.600	.740	.580
2	1	1	.700	.520	.940	.660	.850	.700
3	1		.760	.620	1.000	.750	.970	.840
4	1	2	.860	.700	1.070	.830	1.090	.950
5	1		.950	.780	1.150	.910	1.200	1.060
6	1	3	1.040	.870	1.220	.980	1.300	1.220
7	1		1.140	.960	1.280	1.080	1.400	1.340
8	1	4	1.230	1.050	1.360	1.150	1.520	1.470
9	1		1.320	1.130	1.420	1.230	1.630	1.580
10	1	5	1.400	1.220	1.480	1.320	1.730	1.700
11	1		1.480	1.280	1.520	1.400	1.840	1.800
12	1	6	1.560	1.360	1.560	1.450	1.920	1.880
13	1		1.620	1.420	1.580	1.520	2.000	1.960
14	1	7	1.680	1.480	1.600	1.580	2.070	2.040
15	1		1.730	1.550	1.580	1.630	2.130	2.100
16	1	8	1.760	1.600	1.540	1.660	2.160	2.150
17	1		1.780	1.640	1.480	1.690	2.190	2.190
18	1	9	1.790	1.660	1.420	1.690	2.180	2.180
19	1		1.780	1.680	1.350	1.670	2.130	2.120
20	1	10	1.750	1.680	1.270	1.630	2.080	2.060
21	1		1.720	1.660	1.180	1.580	2.030	2.000
22	1	11	1.680	1.630	1.100	1.520	1.940	1.920
23	1		1.620	1.570	1.020	1.450	1.850	1.840
24	1	12	1.540	1.510	.920	1.370	1.740	1.740
25	1		1.450	1.440	.840	1.300	1.640	1.650
26	1	13	1.360	1.360	.750	1.200	1.520	1.550
27	1		1.270	1.280	.660	1.120	1.400	1.450
28	1	14	1.170	1.200	.580	1.030	1.270	1.350
29	1		1.070	1.110	.500	.940	1.160	1.230
30	1	15	.950	1.010	.420	.850	1.050	1.120
31	1		.850	.910	.350	.760	.920	1.010
32	1	16	.740	.810	.270	.670	.800	.900
33	1		.630	.720	.210	.560	.690	.790
34	1	17	.530	.620	.160	.490	.580	.680
35	1		.450	.520	.110	.400	.470	.580
36	1	18	.360	.440	.100	.320	.360	.480
37	1		.260	.350	.100	.250	.280	.390
38	1	19	.200	.250	.120	.180	.220	.300
39	1		.150	.200	.130	.140	.150	.230
40	1	20	.120	.150	.180	.100	.120	.170
41	1		.100	.130	.230	.100	.100	.100
42	1	21	.100	.100	.280	.100	.100	.100
43	1		.110	.100	.340	.110	.120	.100
44	1	22	.140	.100	.410	.130	.160	.100
45	1		.170	.110	.470	.160	.200	.130
46	1	23	.220	.140	.550	.220	.260	.180
47	1		.280	.180	.600	.280	.350	.240
48	1	24	.360	.240	.660	.350	.440	.330

TABLE 4

INPUT TIDAL HEIGHTS (FT)

AVERAGE TIDES 0030 22AUG - 1200 24AUG'68

TIME STEP	DAY	HOUR	TIDE STATIONS A	B	C	D	E	F
49	2		.450	.300	.750	.430	.530	.430
50	2	1	.520	.370	.810	.500	.650	.520
51	2		.580	.450	.870	.580	.760	.630
52	2	2	.670	.520	.940	.660	.880	.750
53	2		.750	.600	1.020	.750	.990	.880
54	2	3	.820	.680	1.080	.830	1.100	1.010
55	2		.910	.760	1.150	.890	1.200	1.120
56	2	4	1.000	.850	1.200	.970	1.310	1.240
57	2		1.100	.910	1.270	1.040	1.400	1.350
58	2	5	1.180	.980	1.320	1.120	1.500	1.460
59	2		1.260	1.070	1.380	1.200	1.600	1.580
60	2	6	1.340	1.130	1.410	1.260	1.690	1.670
61	2		1.400	1.220	1.450	1.350	1.780	1.750
62	2	7	1.470	1.300	1.470	1.420	1.860	1.840
63	2		1.530	1.360	1.490	1.470	1.930	1.900
64	2	8	1.580	1.430	1.490	1.520	1.990	1.980
65	2		1.630	1.480	1.460	1.560	2.040	2.030
66	2	9	1.670	1.530	1.430	1.600	2.070	2.070
67	2		1.680	1.570	1.400	1.600	2.100	2.100
68	2	10	1.700	1.600	1.350	1.590	2.090	2.090
69	2		1.680	1.600	1.290	1.570	2.070	2.050
70	2	11	1.660	1.600	1.220	1.530	2.030	2.000
71	2		1.620	1.590	1.150	1.480	1.970	1.940
72	2	12	1.580	1.550	1.070	1.410	1.870	1.850
73	2		1.520	1.500	1.000	1.370	1.770	1.770
74	2	13	1.450	1.440	.930	1.300	1.680	1.680
75	2		1.360	1.360	.870	1.240	1.590	1.600
76	2	14	1.290	1.300	.800	1.160	1.490	1.500
77	2		1.200	1.220	.720	1.080	1.370	1.400
78	2	15	1.100	1.150	.660	1.010	1.260	1.310
79	2		1.020	1.060	.600	.930	1.150	1.220
80	2	16	.920	.980	.520	.860	1.060	1.120
81	2		.830	.900	.450	.780	.960	1.030
82	2	17	.750	.850	.400	.700	.860	.920
83	2		.660	.760	.360	.640	.760	.840
84	2	18	.580	.690	.330	.570	.660	.730
85	2		.500	.600	.300	.490	.570	.630
86	2	19	.450	.550	.300	.440	.480	.550
87	2		.380	.470	.300	.400	.420	.480
88	2	20	.330	.400	.310	.350	.380	.380
89	2		.310	.350	.330	.320	.320	.320
90	2	21	.300	.320	.350	.300	.300	.300
91	2		.300	.300	.390	.300	.300	.300
92	2	22	.300	.300	.430	.300	.300	.300
93	2		.300	.300	.480	.320	.350	.320
94	2	23	.320	.310	.530	.360	.380	.340
95	2		.350	.320	.580	.390	.420	.370
96	2	24	.400	.360	.650	.440	.500	.430

TABLE 4

INPUT TIDAL HEIGHTS (FT)

AVERAGE TIDES 0030 22AUG - 1200 24AUG'68

TIME STEP	DAY	HOUR	TIDE STATIONS A	B	C	D	E	F
97	3		.450	.400	.700	.490	.570	.490
98	3	1	.500	.450	.760	.530	.660	.550
99	3		.680	.500	.830	.580	.730	.650
100	3	2	.650	.560	.890	.650	.850	.750
101	3		.700	.610	.950	.720	.930	.850
102	3	3	.770	.670	1.000	.800	1.020	.950
103	3		.860	.740	1.050	.860	1.110	1.040
104	3	4	.950	.800	1.100	.940	1.200	1.130
105	3		1.020	.870	1.160	1.000	1.300	1.220
106	3	5	1.100	.940	1.210	1.070	1.380	1.300
107	3		1.170	1.000	1.250	1.120	1.460	1.400
108	3	6	1.250	1.070	1.300	1.200	1.550	1.500
109	3		1.320	1.320	1.130	1.250	1.630	1.570
110	3	7	1.390	1.210	1.360	1.320	1.700	1.660
111	3		1.440	1.270	1.390	1.350	1.760	1.740
112	3	8	1.480	1.330	1.400	1.400	1.800	1.800
113	3		1.520	1.400	1.400	1.420	1.860	1.860
114	3	9	1.560	1.420	1.400	1.450	1.920	1.920
115	3		1.580	1.450	1.380	1.470	1.950	1.950
116	3	10	1.600	1.480	1.350	1.490	2.000	2.000
117	3		1.600	1.490	1.300	1.500	2.000	2.000
118	3	11	1.600	1.500	1.250	1.500	2.000	2.000
119	3		1.590	1.500	1.200	1.480	1.950	1.950
120	3	12	1.560	1.500	1.130	1.450	1.850	1.850

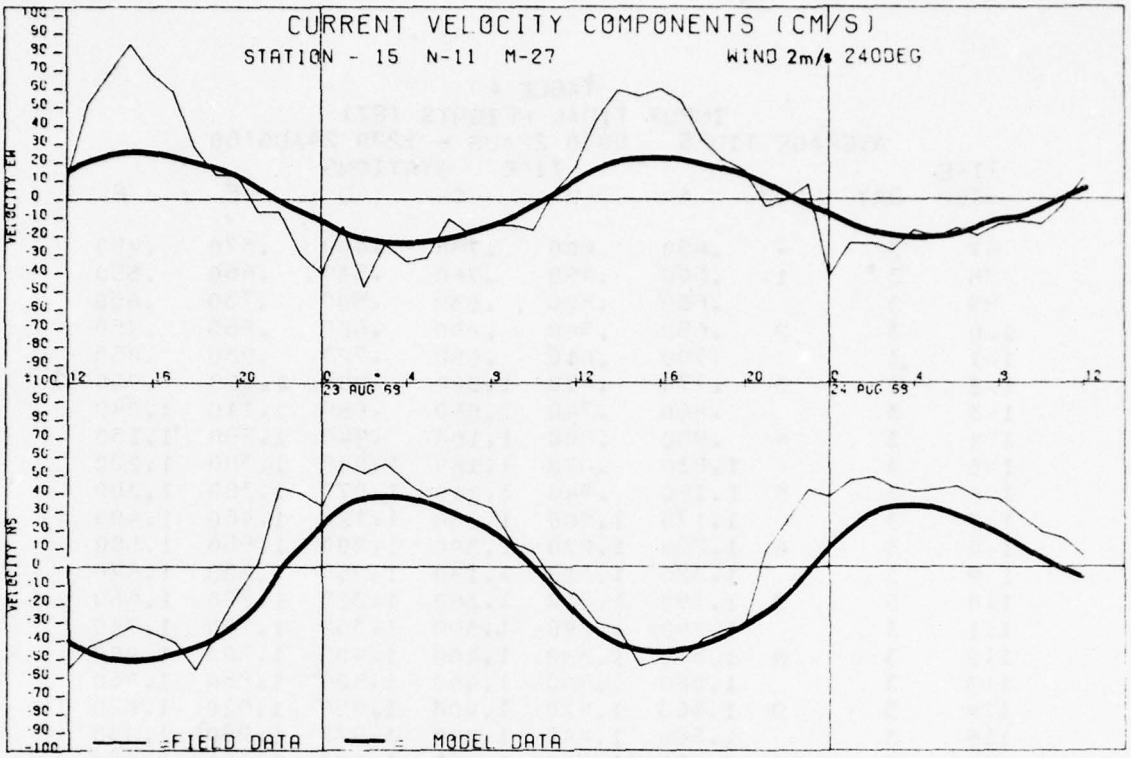

Figure 8. Comparison, real to model currents, station 15.

squares fit, Fourier Series curves; but, though more presentable, the true nature of the data was not apparent. The good comparisons with model data tended to look too good, and the raggedness, which might have partially explained some of the poor fits, was also lost. The uncorrected data were thus chosen for illustration. In any event, individual current component values, especially for comparative purposes, might reasonably be assumed accurate within 5 to 10 cm/sec (0.1 to 0.2 knot) at best.

There was little difficulty in discerning curve frequency when the amplitudes were large, and in some cases, particularly at stations 10 and 15 (the latter is illustrated in Fig. 8), the model and field data fit rather well. It is noted, of course, that these stations are located in the main channel and entrances just north and south of Breton Island, where currents are more pronouced in both amplitude and direction.

It was somewhat more difficult to discern a period for the low-amplitude data, but in most cases (stations 3, 5, 6, 12, 13, 18, and 19) the model data appeared to be a good simulation of both period and amplitude. Figure 9 (station 3) is typical. It was particularly interesting to note that both the model and the field data showed the rather uniform amplitude and long period that would be expected during an equatorial tide cycle (stations 2, 3, 5, and 13).

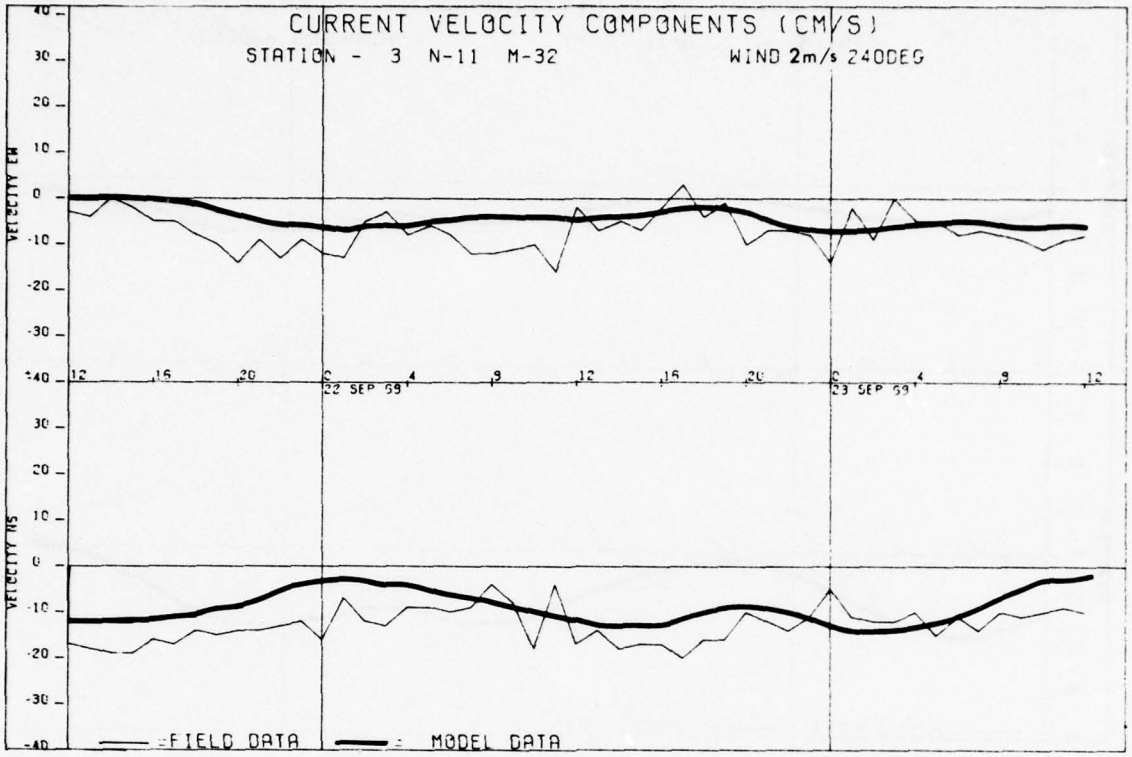

Figure 9. Comparison, real to model currents, station 3.

Comparisons for stations 2 (Fig. 10), 8, and 9 do not fit well in one component direction and possibly each for the same reason: all three are near the edge of the model area. The east-west data for stations 8 and 9 look particularly ragged, a situation that may be the effect of a local open-sea disturbance. Neither this nor what might be a small phase shift could be expected to be accurately simulated by the interpolation of smooth predicted input tides.

The real discrepancy, however, appears to lie with the side wall effects of the model. The poor fit is with the east-west component of station 2 (Fig. 10) and with the north-south component of stations 8 and 9. In all three cases the problem direction is normal to the adjacent open boundary. Stations 8 and 9 are on row 2, which is only one row in from the boundary.

It seems logical, therefore, that, in the same way that a time step lag was required to eliminate start-up effects, the model requires a few grid points' buffer from an open bound before its input effect is properly merged. The comparisons of field and model data for stations 4, 10, and 20, which were taken during a tropic tide period, also suggest a boundary effect to be the cause of observed discrepancies. The field data reflect the exaggerated range difference, but only station 10 is a good comparison. Station 20 is only one computational point from a boundary and does not match in its east-west component. Likewise, station 20 is diagonally one point away from an upper and lower boundary, and its north-south component velocity comparison is not good.

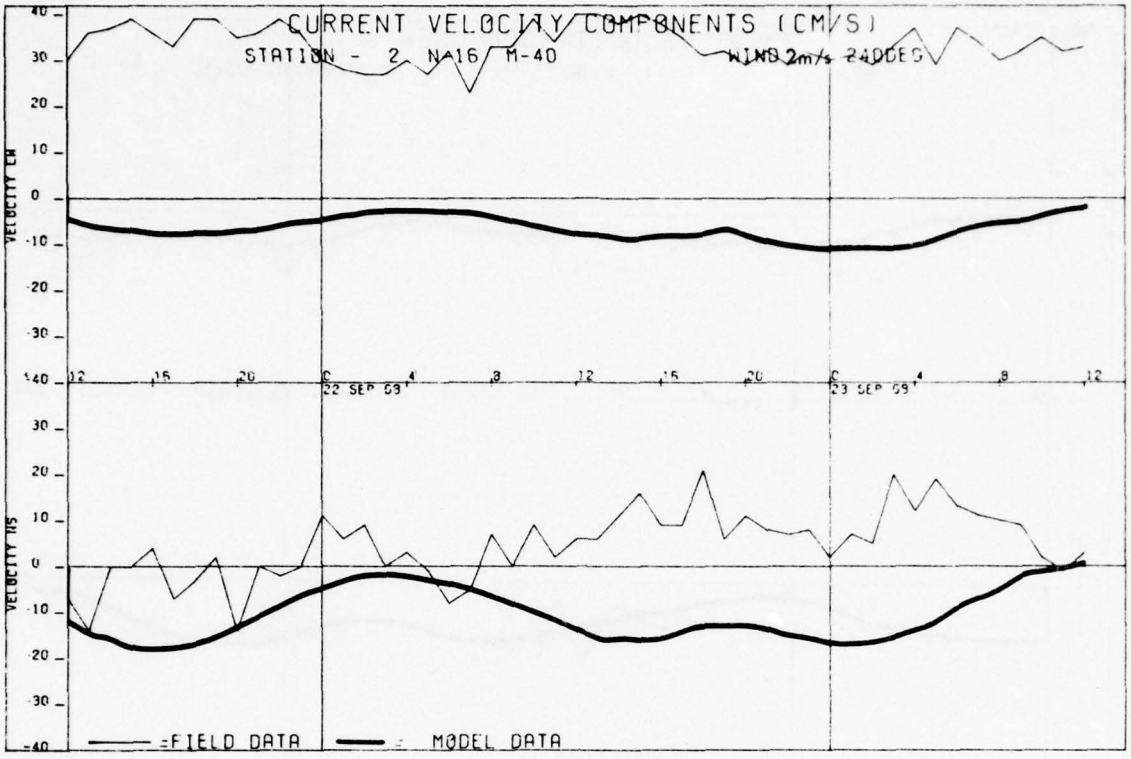

Figure 10. Comparison, real to model currents, station 2.

Station 4 is an enigma. It is possible that the input depths in the area are not too accurate. The field data were recorded at a depth of 3 meters. At the coordinates for station 4 there is a model depth of 6 meters and an atypical (for this estuary) rather abrupt rise on all sides. Increased model depth does have the effect of reducing current amplitude (which is the comparison discrepancy).

In summary, it may be concluded, considering the good comparisons, the ragged field data, and the explanations for those points where comparisons were not good, that the computational model simulation accuracy is quite reasonable.

A caveat is necessary, however. As demonstrated, the model is simulating a real area. There are numerous irregular-shaped boundaries. It is the author's opinion that the model is giving a realistic gross simulation of the area, but details around edges, sharp points, etc., may be suspect. This situation, too, should not be unreasonable to investigators who have worked with this type problem in that considerable interpretation is warranted and should be expected in certain areas. Simulation in essence will establish rational trends, such as over wide, unrestricted areas or even narrow, long embayments. Single points, however, may remain suspect.

The easiest way, of course, to resolve the doubt, if detail is needed at a given point, would be to model that small area at a much larger scale than used in the gross model. Input to the large-scale model can come from the gross model at the points where confidence in their accuracy allows its use.

DETERMINATION OF THE EFFECT OF TERMS

Testing the effect of various terms in the equations of motion was made possible by systematic application of the optional term controls, which are, as described earlier, a feature of the computational model.

The model was run, except for the wind tests, using tidal data for the period 22-24 August 1968 (shown in Table 4), during which average tidal range conditions existed. It may be assumed that, had equatorial or tropic tidal conditions existed, the following results would be somewhat exaggerated.

Basically the method used, except for the wind tests, was to run the model with as few terms in effect as possible and then to run it three more times, each time adding one of the three subject terms. From the output listing at a matrix of every fifth grid point the hourly values of surface elevation and velocity for two tidal cycles were then recorded for each run. The tabulated differences provided the data for the following observations.

Coriolis. The effect of inclusion of these terms was to increase the surface elevation about 2-8 percent of the full local range. Ranges were 35 cm in the southeastern corner and up to 60 cm near the northwestern corner of the model. The actual magnitude of the terms' contributions was 1-3 cm (5 cm maximum).

Upon inclusion of the Coriolis terms the surface elevation rose most, about 34 cm on south-to-north flow inside the estuary and only 1-2 cm on the north-to-south flow outside. Generally these are the directions of the more pronounced steady and slightly faster flows.

Generally current speed was decreased 1-10 cm/sec (about 17 cm/sec maximum). The greatest effect (5-15 cm/sec) was outside the estuary on the more pronounced north-to-south flow. Inside the estuary the decrease was only 1-3 cm/sec.

As might be expected when this term was included, generally the currents were turned to the right (azimuth increase) from 1 to 60 degrees in the rising and falling tides, when currents were stronger. At slack periods at high and low tides there were occasional shifts as much as 90 degrees.

In summary, therefore, Coriolis terms can have a 2-10 percent net effect on surface elevations and current speeds with an expected directional turning effect of 10-20 degrees or more, provided, of course, that the study area is large enough in area to show an effect.

Convective inertia. These terms are often considered negligible and thus omitted from computing schemes. As the following will indicate, they are not exactly negligible, but their effect is rather small (at least in this model), not too consistent, and just about at the accuracy confidence level for the model. Upon inclusion this term had negligible (1 cm maximum) effect on surface elevation. To stretch a point, one might detect a slightly greater effect inside the estuary than outside. Upon inclusion of these terms, current speeds generally

increased 1-5 cm/sec when currents were maximum, at rising and falling. This was not entirely consistent, however, since this was the case primarily on the southeastern end of the model and current speeds decreased 1-3 cm/sec on the northeastern and northern sides of the model. Upon including these terms, current direction or azimuth increased 1-24 degrees (currents turned to the right) on rising tides and paradoxically decreased 1-2 degrees on ebbing tides on the outside of the estuary. Inside the estuary, however, the azimuth effect was even more inconsistent, varying between ± 5 degrees on both rising and falling tides at various points. The maximum azimuth increase inside the estuary was 10 degrees.

In the Leendertsee-type model the boundary conditions for these non-linear field accelerations are only poorly understood; despite these tests, it is difficult to gauge the importance of these terms.

Bottom friction. Bottom friction is the major term in the computational system of equations used to model an estuary and, along with the continuity, local acceleration, body force (gravity), and if applicable wind and Coriolis terms, it should not be omitted in shallow estuary studies.

Surface elevation as a result of including this term was generally raised 5-25 cm, which is about 25 to 50 percent of the tidal range. Because the friction term is primarily a function of current speed, the term was most effective when currents were maximum, during ebb and flood tides. At the slack of high and low tides surface elevations on occasion decreased 5-15 cm, or about 5 to 20 percent of full-scale values.

Generally, current speed was decreased by 10 to 50 cm/sec during maximum ebb and flooding current periods and on occasion up to 65 cm/sec at low tide when friction was included.

The effect on current direction or azimuth was not consistent, but it did cause changes at some points up to ±150 degrees at high tide. Generally the shift was clockwise (azimuth increase) by 10 to 50 degrees. The effect was generally less at maximum ebb and flood.

Wind: estuary response to sudden start and stop. This phase of the study was undertaken to provide information on the estuary's response to a suddenly started and equally suddenly stopped wind, as might be the case in a frontal passage.

In this test it was again necessary to use the input sine curve tidal data listed in Table 3 so that cyclic repetition could be verified. The same data output that was used previously to verify the model's computational accuracy was therefore used again as the "no wind" condition.

A second run was made, with one change. Input cards added a 12.9-m/sec (25-knot) or 8.6-m/sec (18.6-knot) wind blowing to the southwest (240°) down the long axis of the estuary. Control cards were set to start this wind after a 24-hour period to eliminate start-up effect, and finally the wind was stopped after 12 hours and the model was run another day to provide information on settling time.

The first question was whether the wind had reached a steady state and, if so, when.

The procedure used was to record the hourly surface elevation, current speed, and azimuth at a matrix of every fifth grid point throughout the model. The differences at each point for successive hours were listed and inspected. When the

differences no longer changed, wind effect had reached steady state. Steady state occurred at day 2, hour 16, which was 16 hours after the wind had started.

The wind had been programmed to stop completely at day 2, hour 24, which means it began to ramp out in 20 percent increments beginning four time steps or 2 hours earlier. Plots of the steady-state wind effect (differences from the "no wind" condition) 3 hours before the wind stopped are shown in Figures 11 and 12 for surface elevation and currents, respectively. Figures 13 and 14 show the day 2, hour 24, or first full wind stop, differences. Figures 15 and 16 show the surface elevation and current difference effects 3 hours after the wind had stopped.

Figures 11 and 12 indicate that the model showed the effect of a steady-state 12.9-m/sec (25-knot) wind blowing down the estuary (240°). The surface was somewhat depressed in the lee of the Chandeleur chain and rose uniformly to more than 20 cm at the southwestern end of the estuary. Currents were shifted to the right (in line with the wind) about 20 to 30 degrees, and some points showed completely reversed flow. Current speeds increased more than 10 cm/sec on the northern edge of the model, gradually decreased to -5 cm/sec about one quarter of the way to the south, and finally increased again to more than 20 cm/sec as the wind increased its fetch to the southwest. Figures 11-16 were used to illustrate this effect because so much of it depends on the configuration of the estuary.

In the surface elevations (Fig. 11), for example, the slope might run up to 30 cm at the southwestern end. This long-axis wind-induced slope of about 3×10^{-6} agrees very well with the 4×10^{-6} figure observed for wind set-up by Kjerfve (1973) in Caminada Bay, just west of the Chandeleur-Breton Sounds estuary.

Figures 13 and 14 show results for the first hour after the wind had stopped. One can see the immediate leveling response of the estuary as compared to the set-up attitude shown by the steady-state wind in Figures 11 and 12. Figures 16 and 17 show that, 3 hours after the wind had stopped, its effect was negligible.

In summary, a sudden start and stop to a wind, such as might be experienced by the passage of a weather front, had a dramatic effect on the estuary. It took about 12-16 hours for the estuary's response to reach steady state in building up to the wind, but it took only about 3-6 hours for it to return to normal. Actually, it was 12 hours before there was no detectable trace of wind effect.

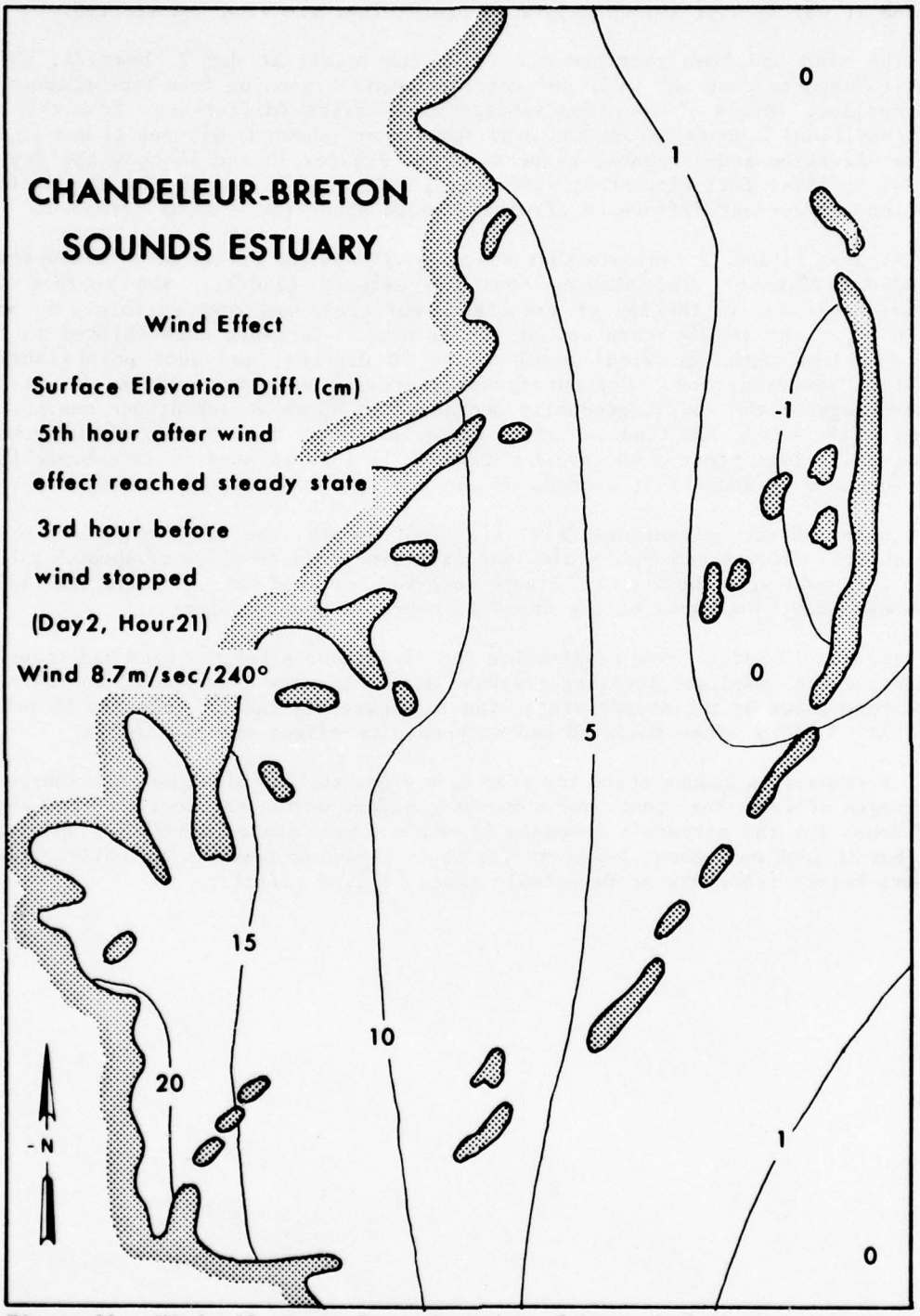

Figure 11. Wind effect, surface elevation, 3 hours before wind stop.

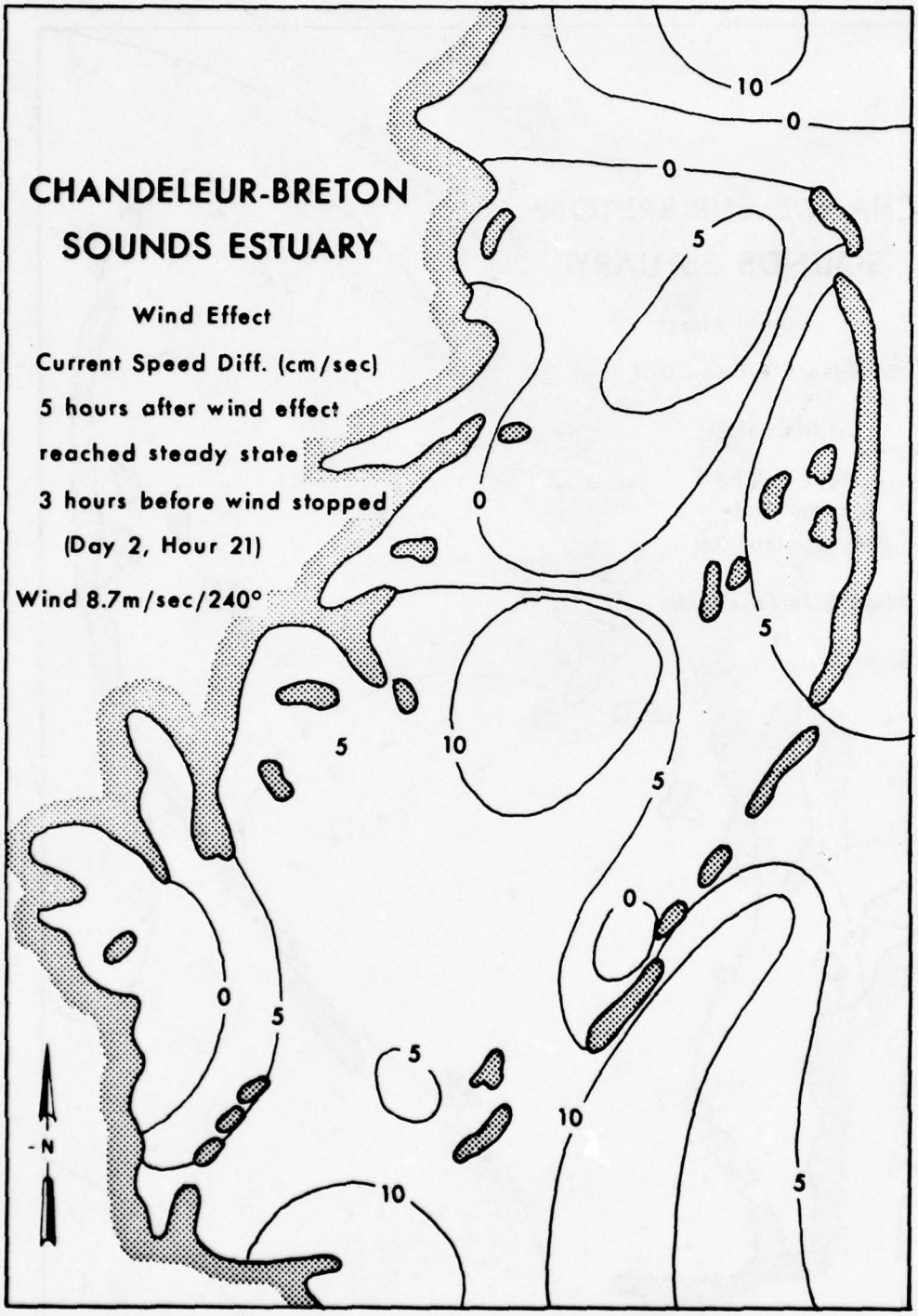

Figure 12. Wind effects, currents, 3 hours before wind stop.

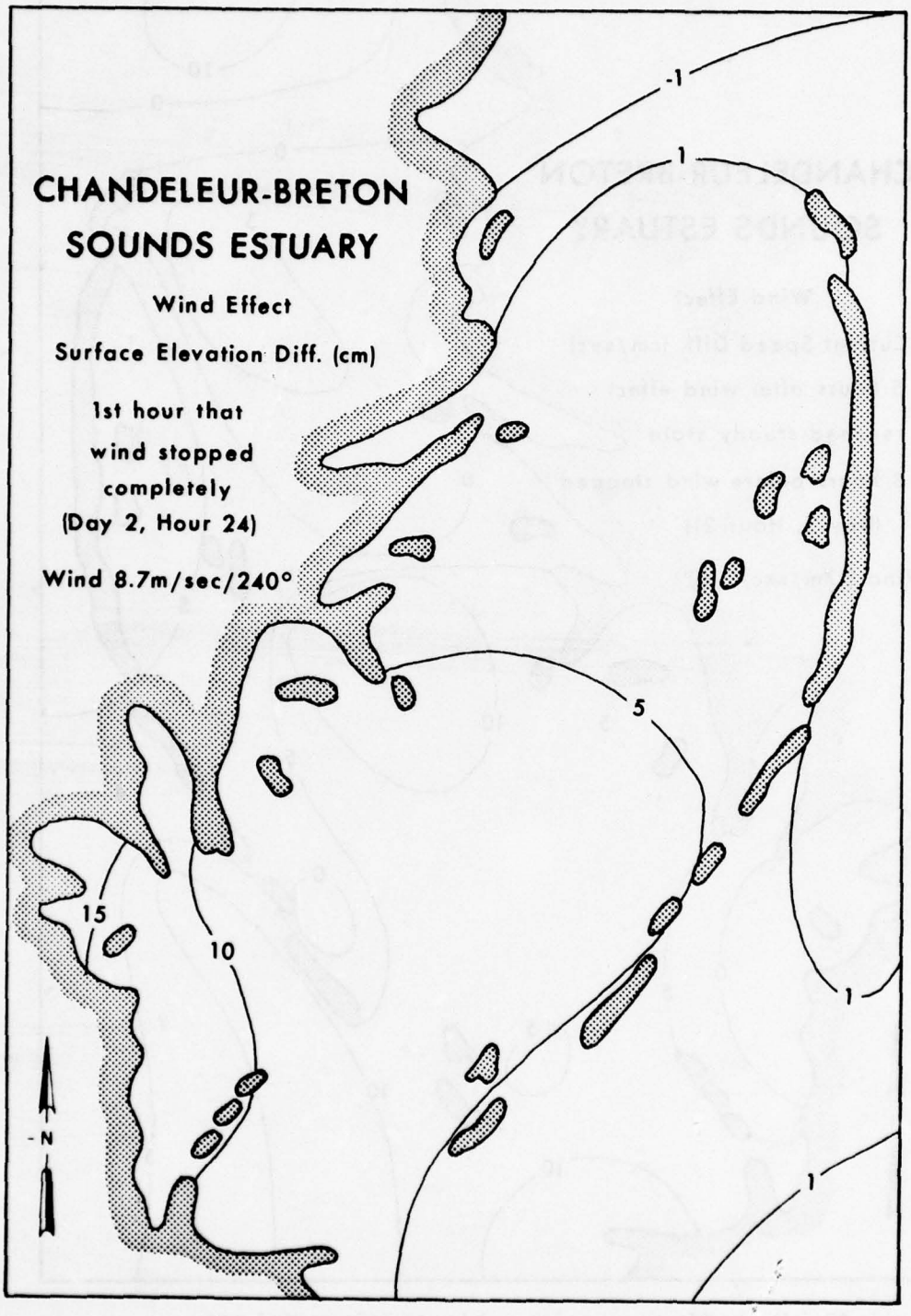

Figure 13. Wind effect, surface elevation, 1st hour of complete wind stop.

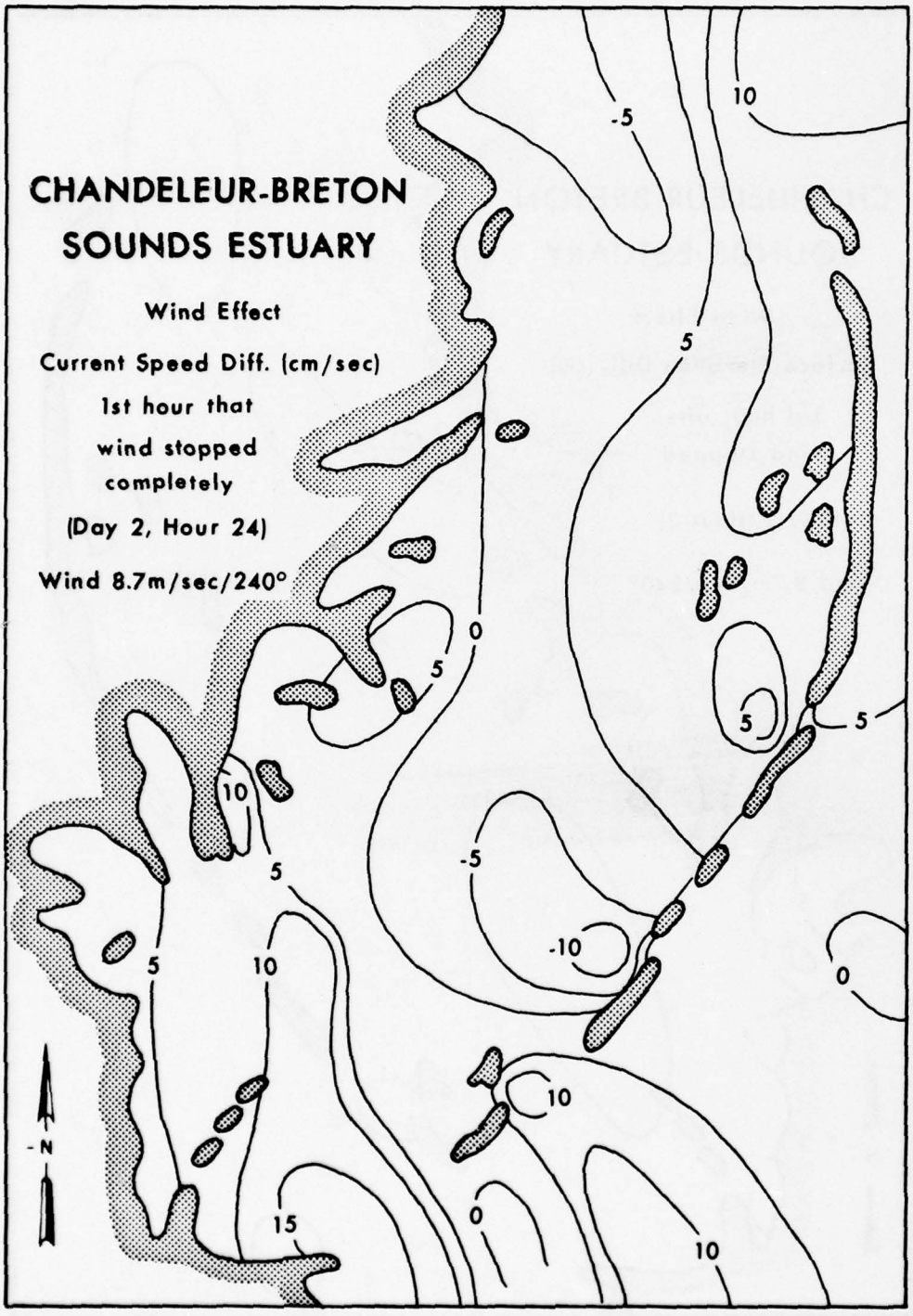

Figure 14. Wind effect, currents, 1st hour of complete wind stop.

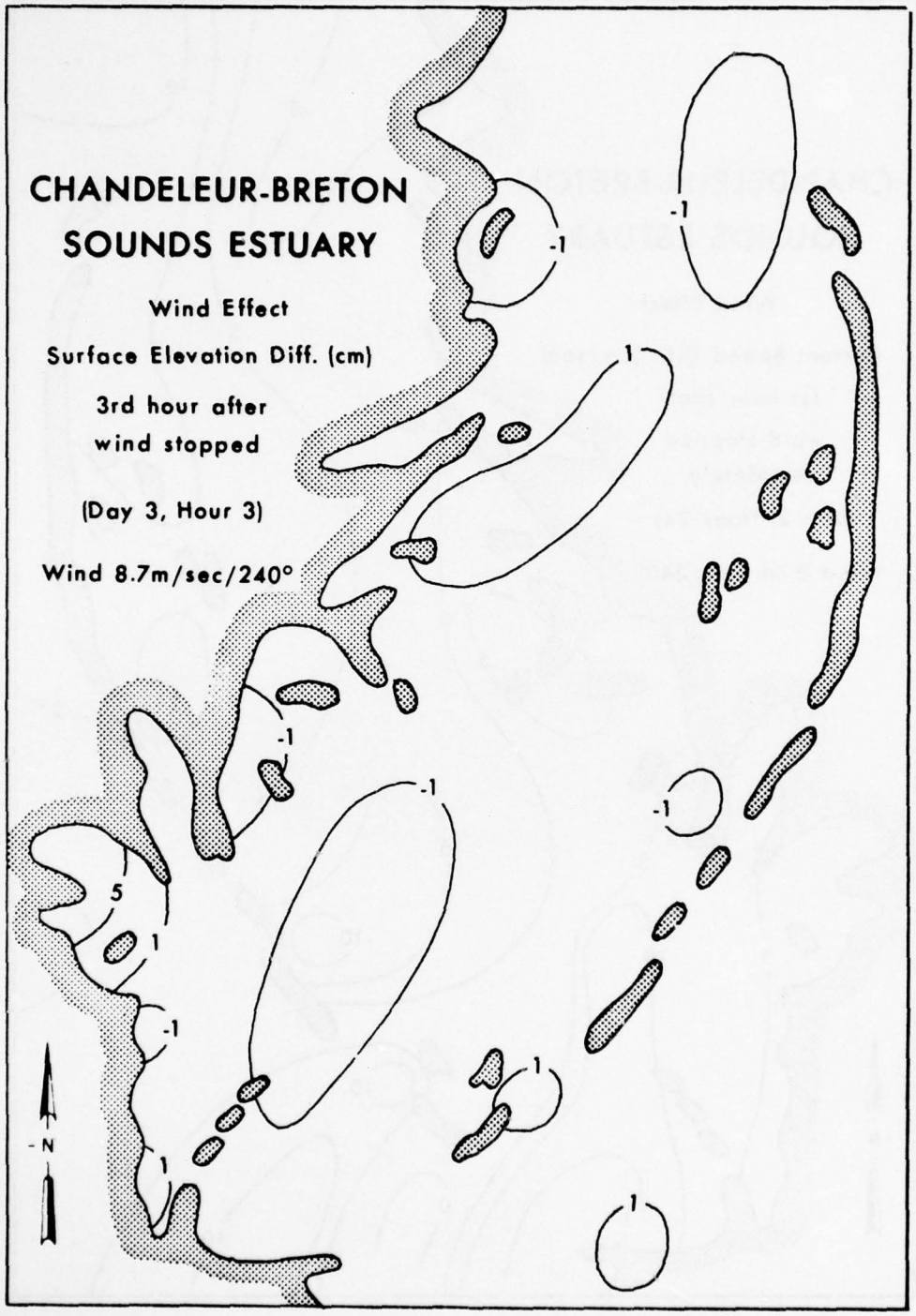

Figure 15. Wind effect, surface elevation, 3 hours after wind stop.

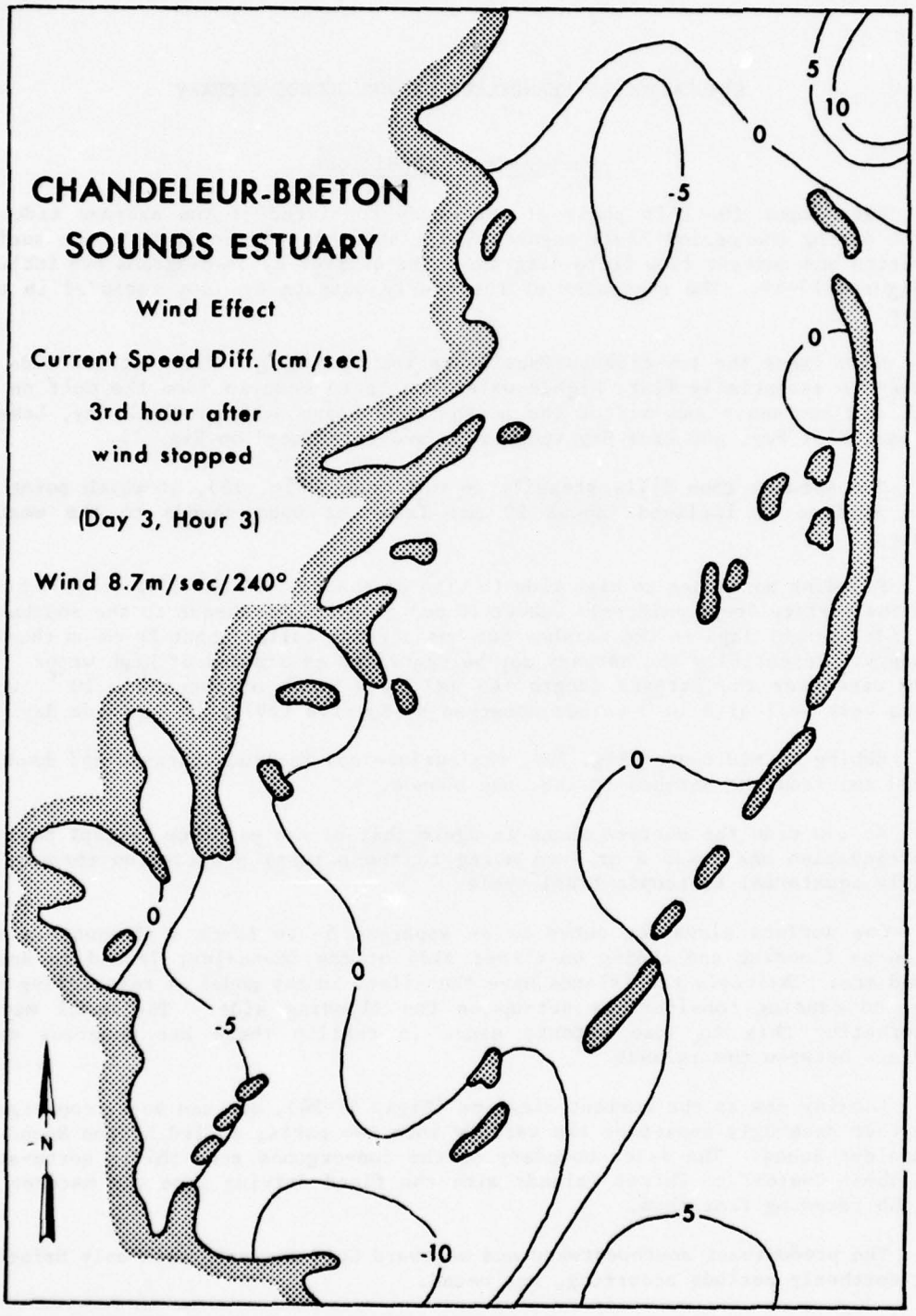

Figure 16. Wind effect, currents, 3 hours after wind stop.

SIMULATION OF CHANDELEUR-BRETON SOUNDS ESTUARY

Average Tidal Conditions

Data input for this phase of the study consisted of the average tides in effect during the period 22-24 August 1968 (Table 4). The output is the surface elevation and current flow field diagrams. The quarter-cycle diagrams are included as Figures 17-24. The remainder of the hourly outputs are not included in this report.

Note first the low-tide surface elevation form (Fig. 17). At low tide the estuary is essentially flat; higher water starts to come in from the Gulf on the north and southeast and out of the marshes and bays, such as Black Bay, Lake La Fortuna, Eloi Bay, and Drum Bay (positions are referenced on Fig. 1).

The estuary then fills steadily to mid range (Fig. 18), at which point the whole surface is inclined (about 20 cm) from the open bounds to the western marshes.

Flooding continues to high tide (a rise of about 55-60 cm) (Fig. 19). At high tide the surface drops uniformly (about 10 cm) from the northeast to the southwest. The tidal height lags in the marshes but has already fallen about 20 cm on the Gulf boundary. Essentially the estuary may be described as a mound of high water. The 10-cm rise over the estuary length (45 km) is a slope of about 2×10^{-6}, which agrees very well with 10^{-6} values observed by Kjerfve (1973) in Caminada Bay.

Ebbing to mid range (Fig. 20), the surface now inclines outward and downward (20-30 cm) from the marshes to the open bounds.

At low tide the surface shape is again that of the past low, except that the mean elevation has risen 6 or 7 cm owing to the natural progression through the monthly equatorial to tropic tidal cycle.

One surface elevation noted is an apparent 5- to 10-cm difference in elevation on flooding and ebbing on either side of the Chandeleur Island to Breton Island arc. Obviously the islands have the effect in the model of restricting free flow and causing considerable set-up on the flooding side. The model may be accentuating this to some extent, since in reality there are numerous small channels between the islands.

Looking now at the current diagrams (Figs. 21-24), one can see a convergence zone that seemingly separates the estuary into two parts, called Breton Sound and Chandeleur Sound. The exact boundary of the convergence zone shifts north-south from about Comfort to Chicot Islands with the flood driving into the marshes and the ebb receding from them.

The predominant southwestward and westward Gulf current, with only brief and weak northerly periods occurring, was noted.

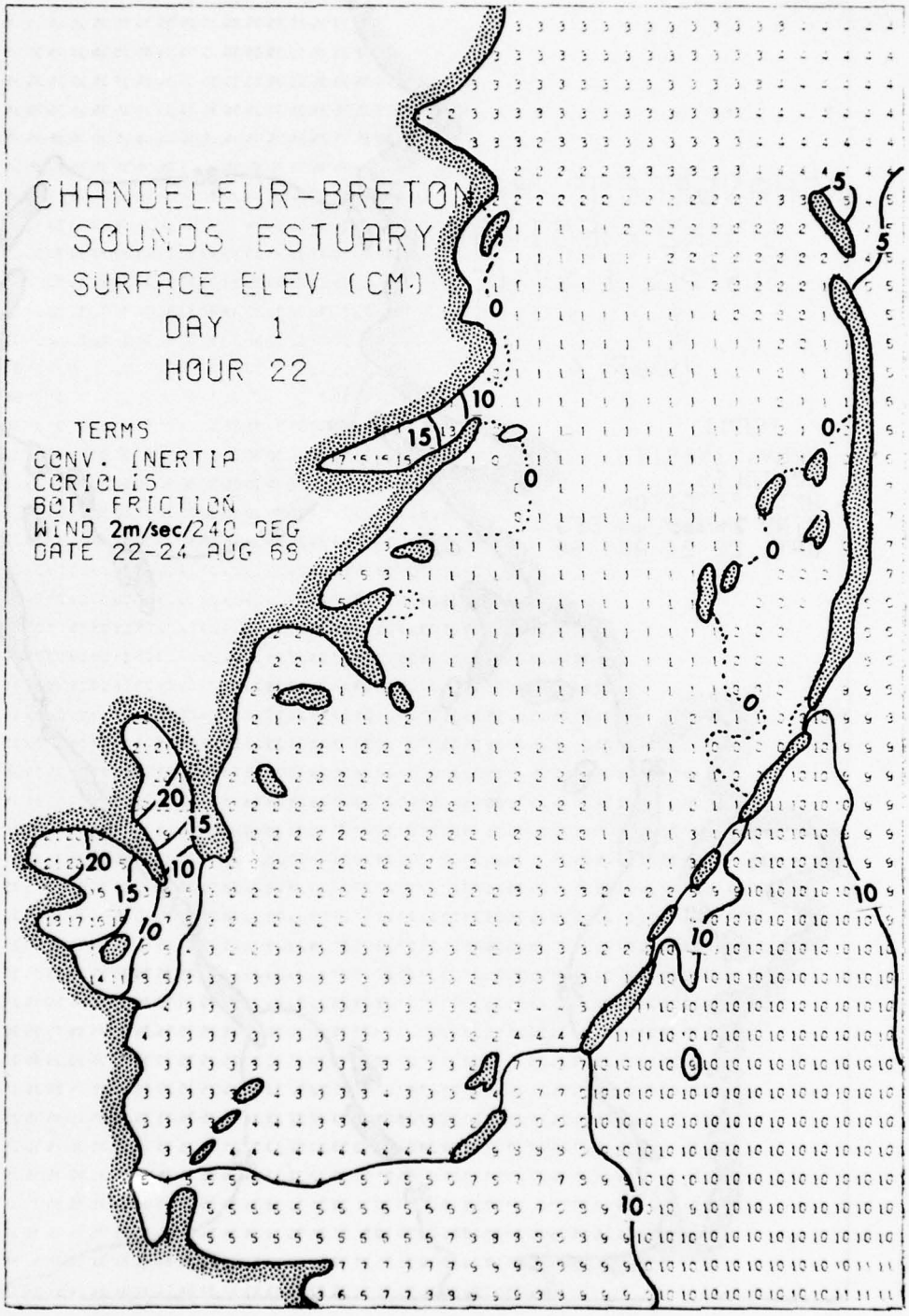

Figure 17. Average tides, surface elevation, low tide.

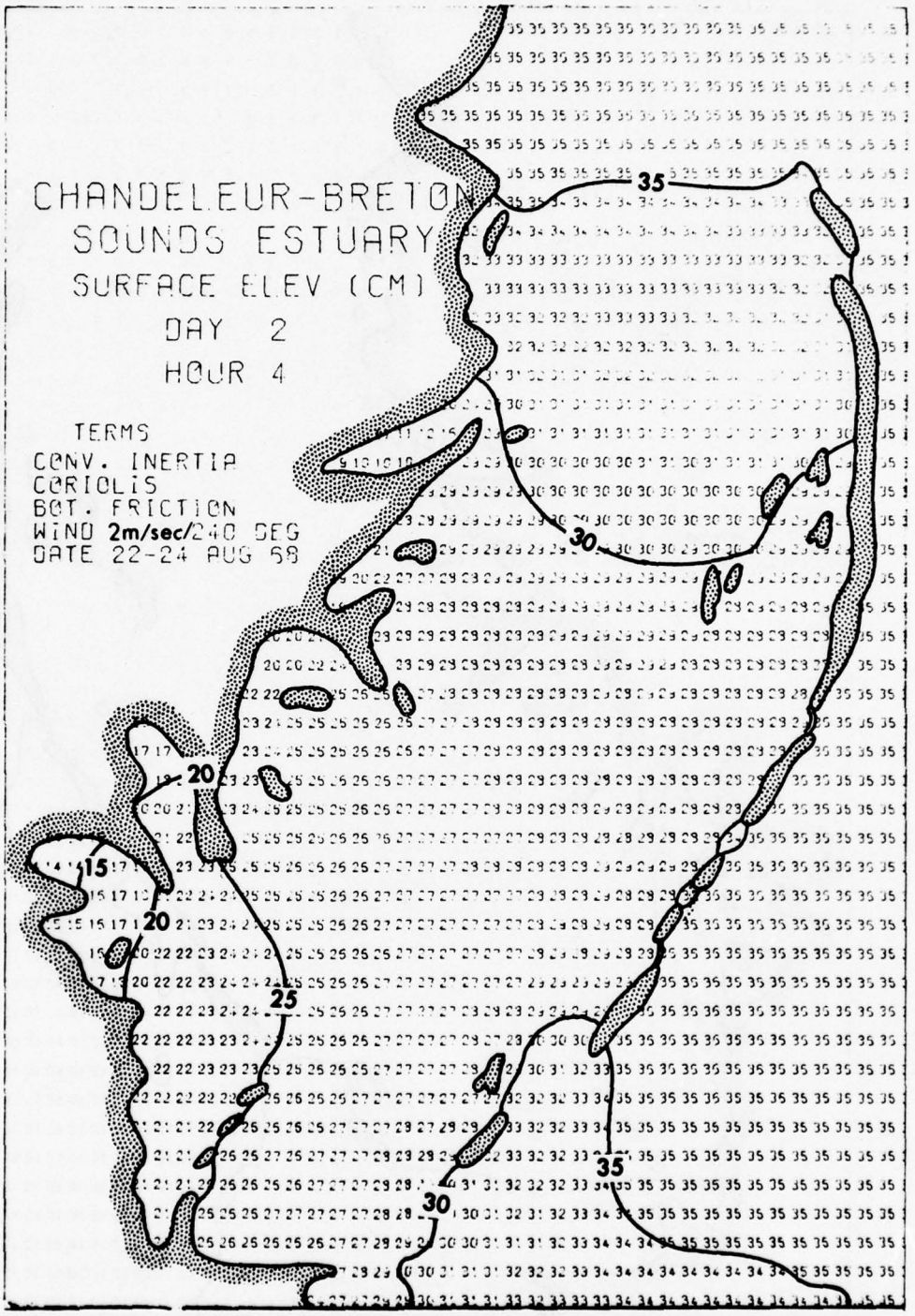

Figure 18. Average tides, surface elevation, maximum rising.

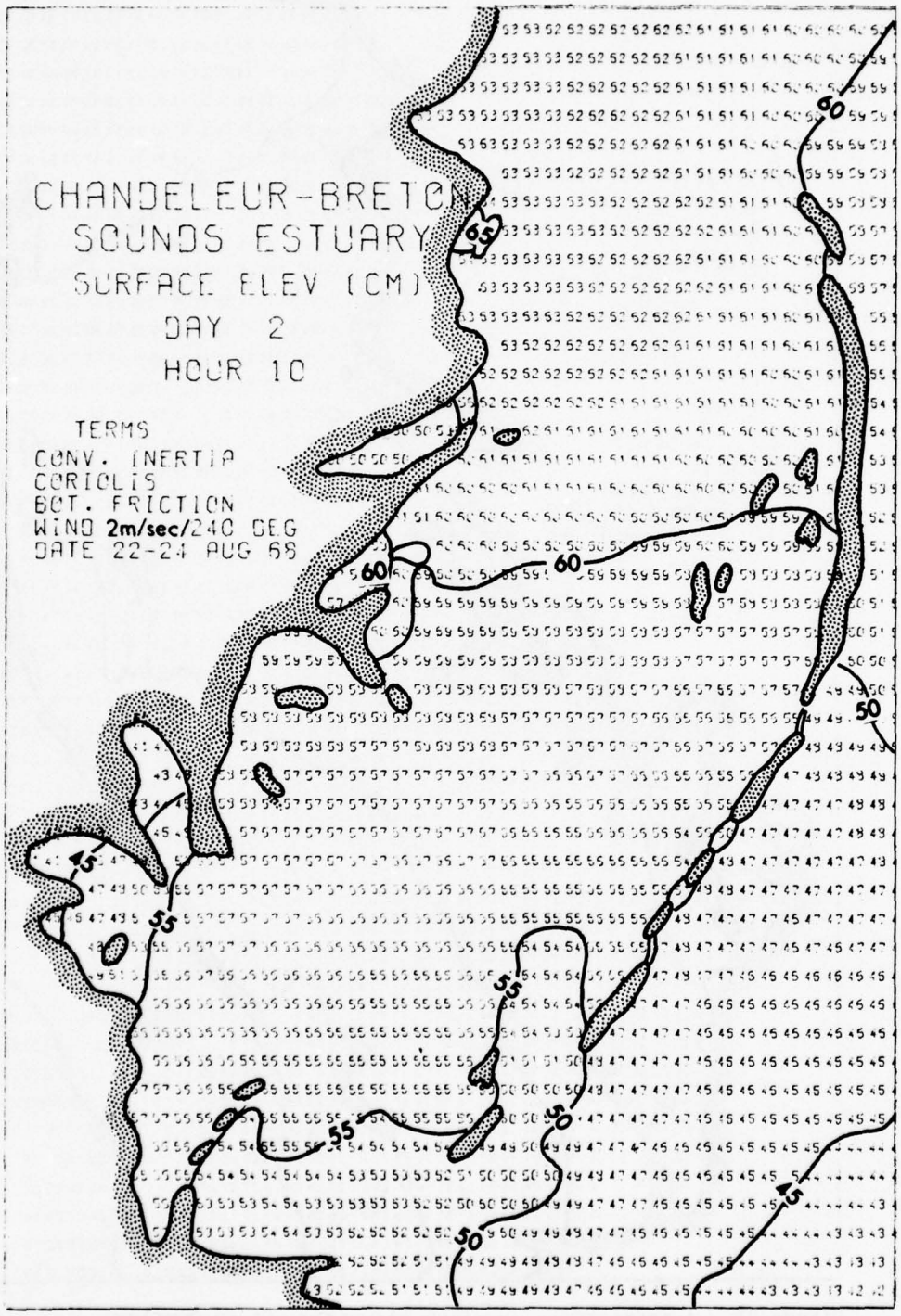

Figure 19. Average tides, surface elevation, high tide.

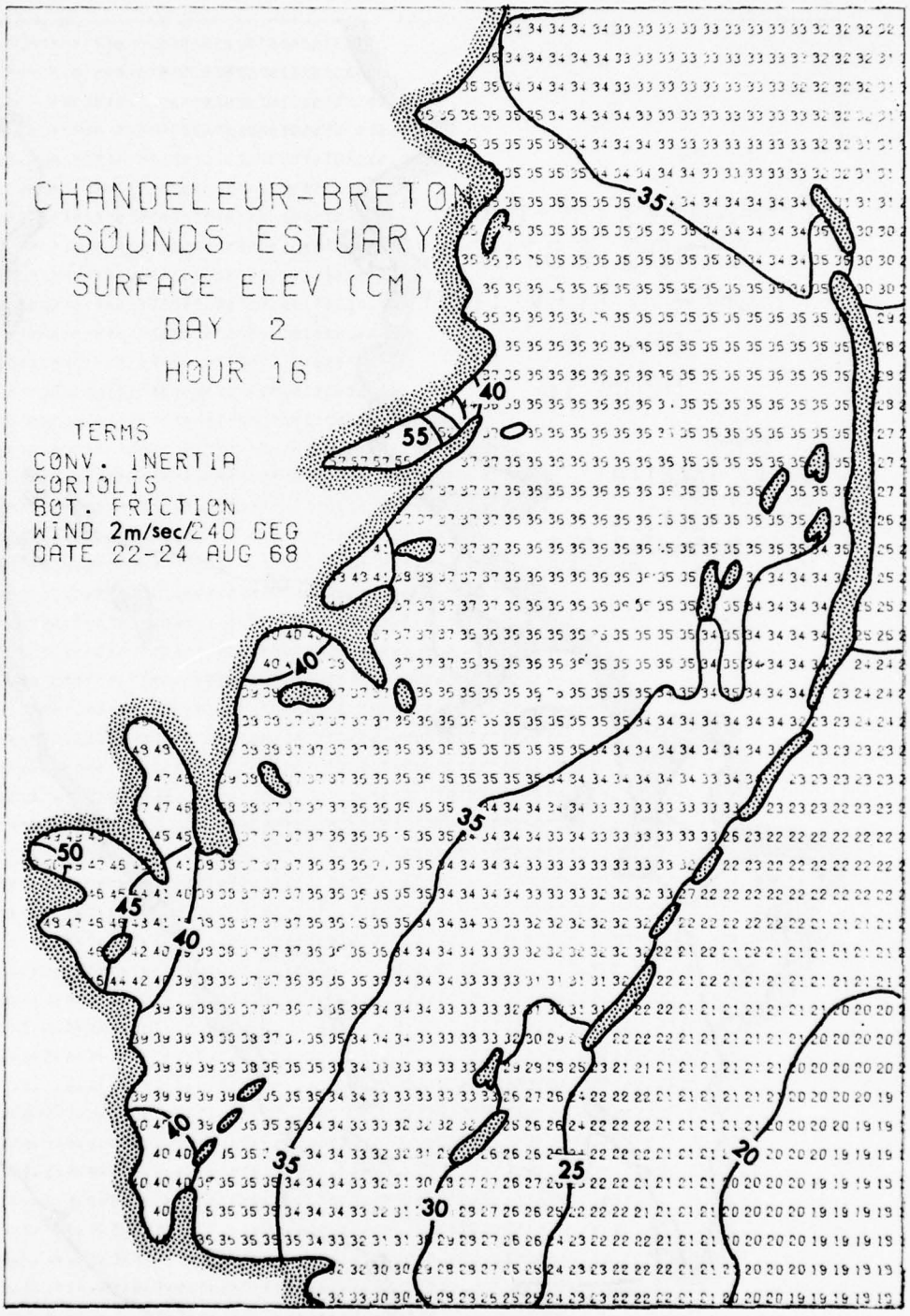

Figure 20. Average tides, surface elevation, maximum ebbing.

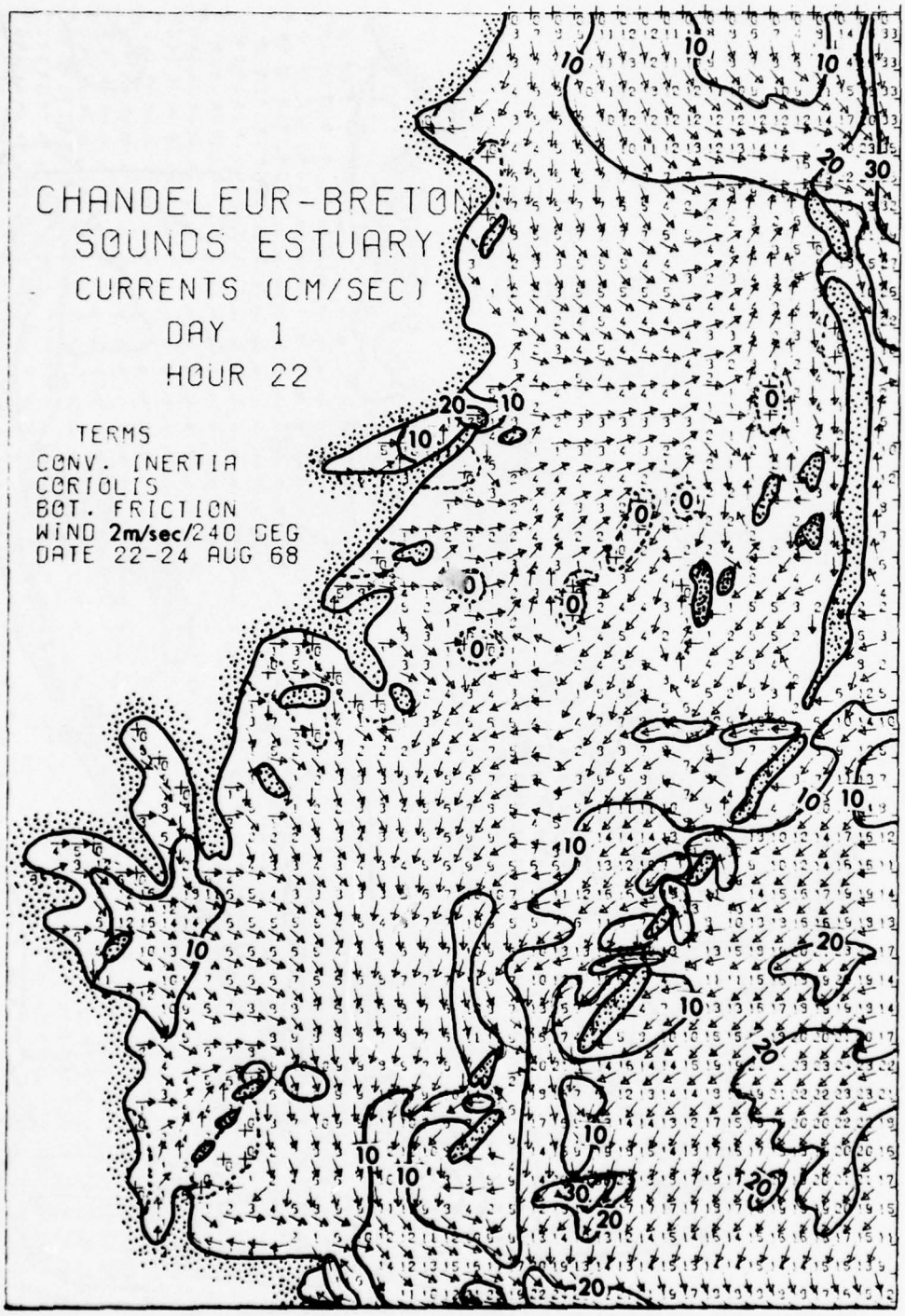

Figure 21. Average tides, currents, low tide.

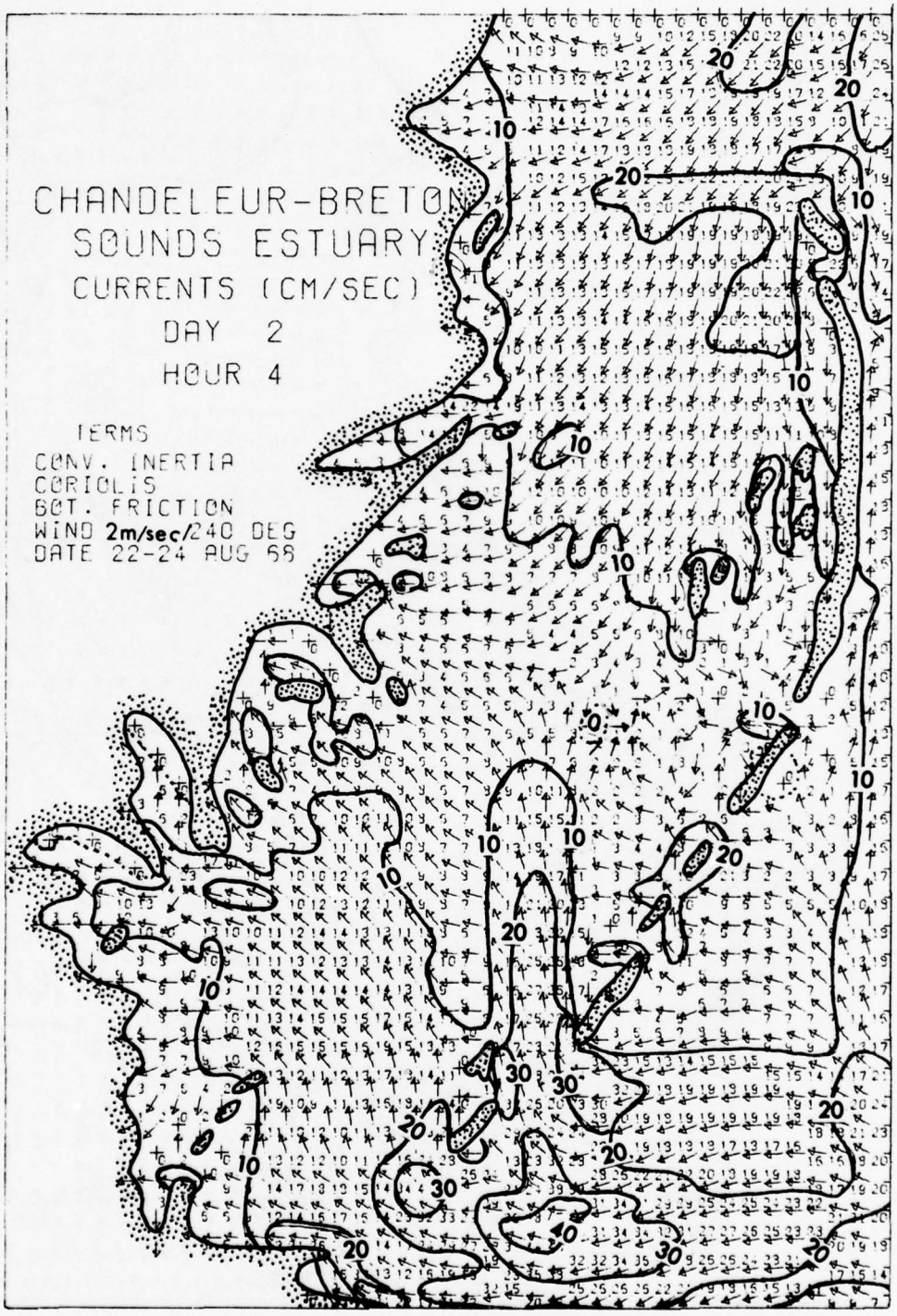

Figure 22. Average tides, currents, maximum rising.

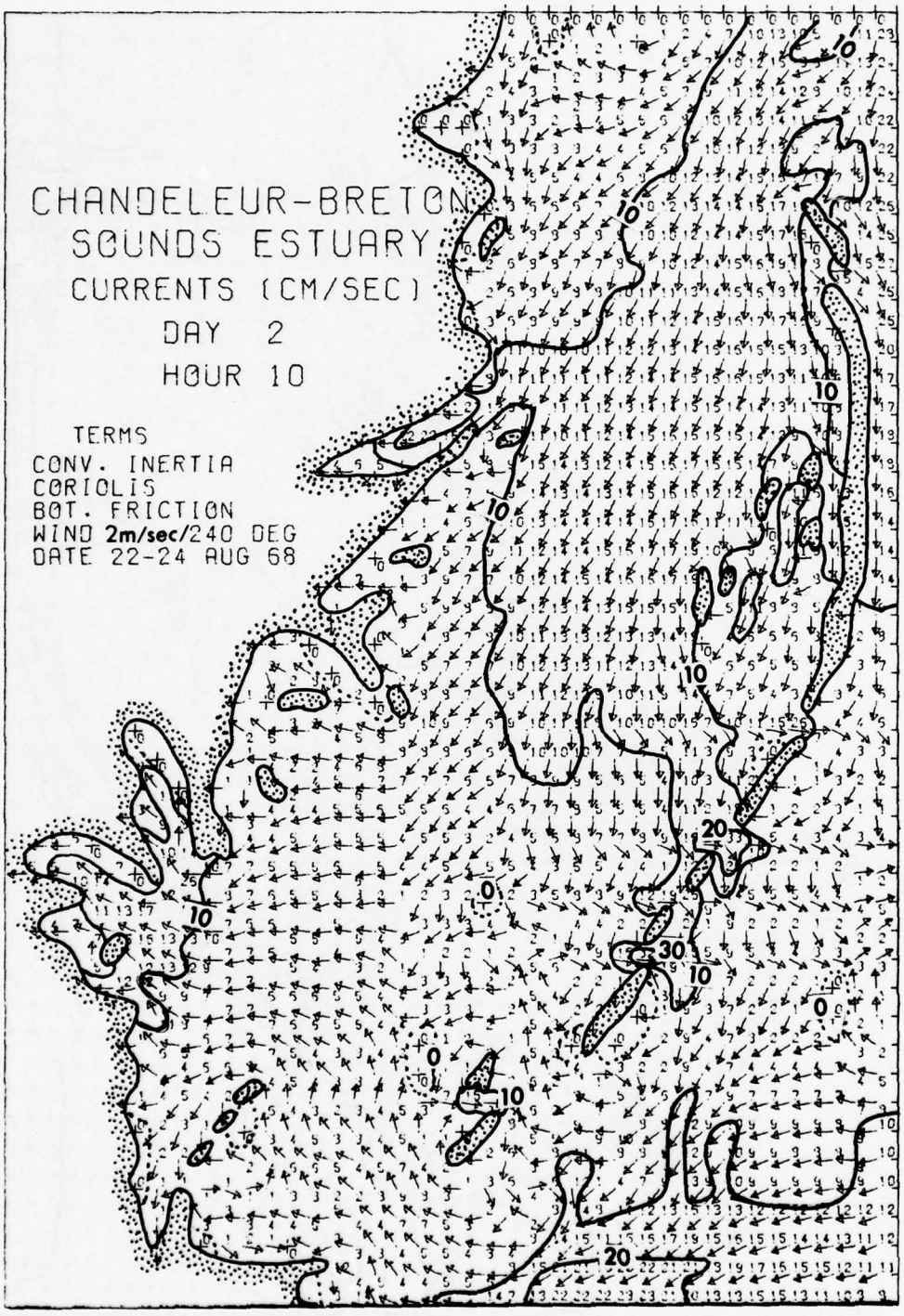

Figure 23. Average tides, currents, high tide.

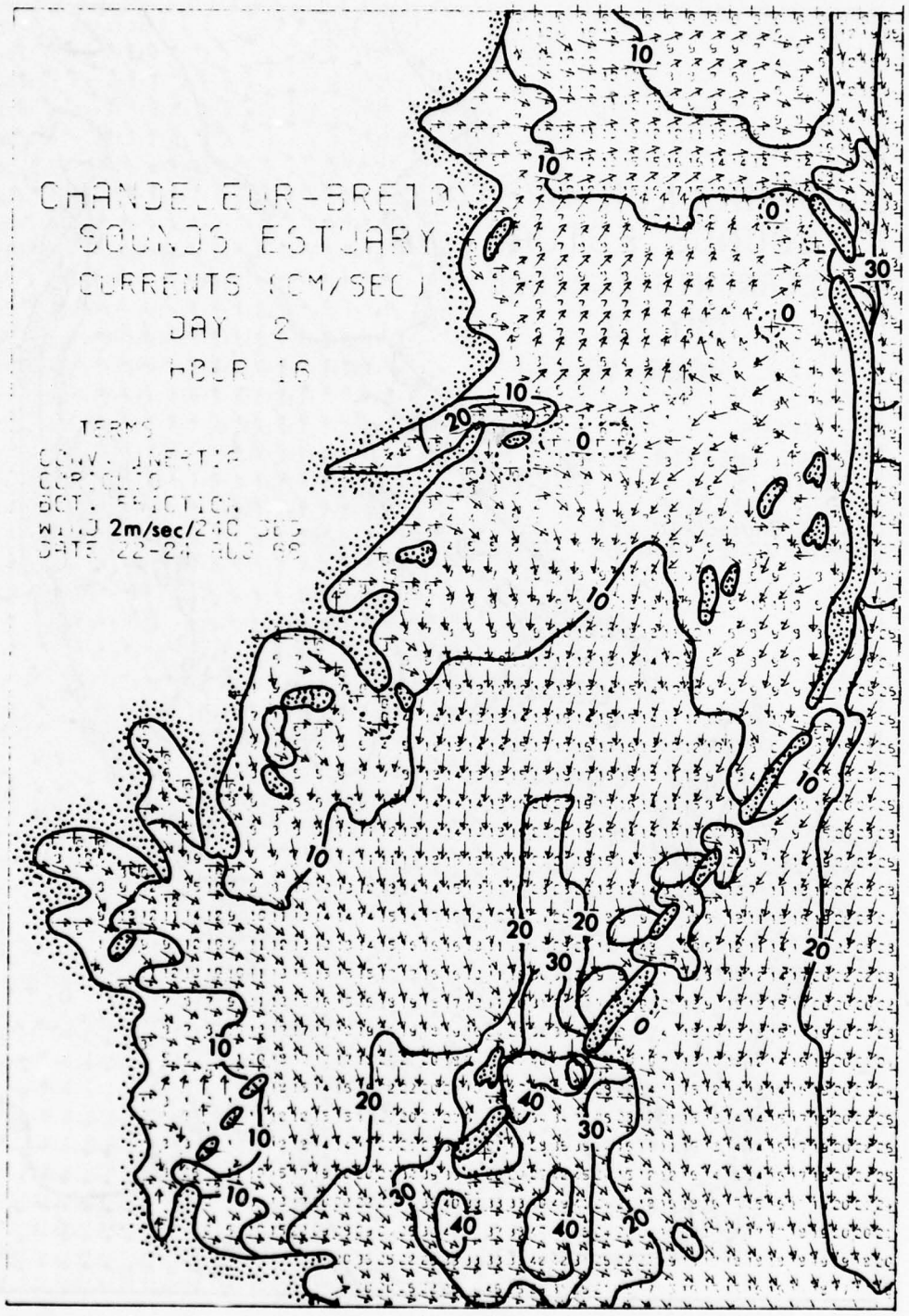

Figure 24. Average tides, currents, maximum ebbing.

The strongest currents come in around Breton Island, ergo the scour channels shown earlier in Figure 3.

At low tide within the estuary the currents are weak and confused, as one would expect. Several weak gyres and countercurrents exist, but do not last long.

The incoming tide and current start first from around Breton Island, but by mid range the currents from the north have become well established and are beginning a relentless intrusion southward through the estuary. Note from Tables 2 and 4 that the tides at Lonesome Bayou, at the Breton Island entrance, lead the rest, but that the ranges are greater on the northern end.

By the time the otherwise normal high-tide slack should have been in effect, the currents from the north totally dominated. Throughout most of the estuary, except north of a line from Mitchell Island to the North Islands, the ebbing currents then ran out to the southeast past Breton Island.

Attempting to correlate these surface elevation and current field patterns with an identifiable wave form is somewhat speculative, since the model simulates real conditions, not ideal cases, and several superimposed and inseparable wave systems are probably in effect. A description is given in a later section of a rather successful simulation by use of two opposing Kelvin waves.

Wind Effect--On, Off, and Along Shore

In giving a physical description of the Chandeleur-Breton Sounds estuary as shown by a model of its water surface elevation and current flow field, it is necessary to show the effect of reasonably typical strong winds. To do this, a wind of 7.0 m/sec (13.5 knots) was modeled as blowing on the estuary from four critical orthogonal directions (040°, 130°, 220°, and 310°). These are the approximate onshore, offshore, and alongshore directions. To accentuate the effect, tidal input was from a tropic tidal period. The tides are from the period 12-13 June 1968.

As in previous tests, the procedure was to run the model in a "no wind" condition and then run it again with the same input data but including the critical wind. The output plots of surface elevations and current flow fields were then compared. The figures shown to illustrate the maximum effect are those of the high tropic tide of the diurnal cycle on which the model was run. Figures 25-26 are the "no wind" case, and Figures 27-34 are the wind effect cases. The remainder of the output diagrams that were referred to in making the following observations are not included.

The wind directions (040°,130°, 220°, and 310°) are headings, not sources, as in most climatological tables, and are the approximate axial directions of the estuary. It is therefore possible to observe maximum onshore, offshore, and alongshore effects.

040° wind. The 040° wind is a northeasterly alongshore wind. The effect generally was to depress the surface elevation of the estuary (Fig. 27) by about 10 cm, primarily by forcing the water out the northern end past Chandeleur Island. The downwind water surface slope is not greatly affected, however. Since the northern boundary was fluid, there was no set-up, but one may observe, by comparing Figures 25 and 26 with Figures 27 and 28, that there is a scooping effect on the southwestern (lee) end of the estuary. Note the 20-cm set-down in the bay adjacent to Black Bay, in the southwestern corner of the Sound.

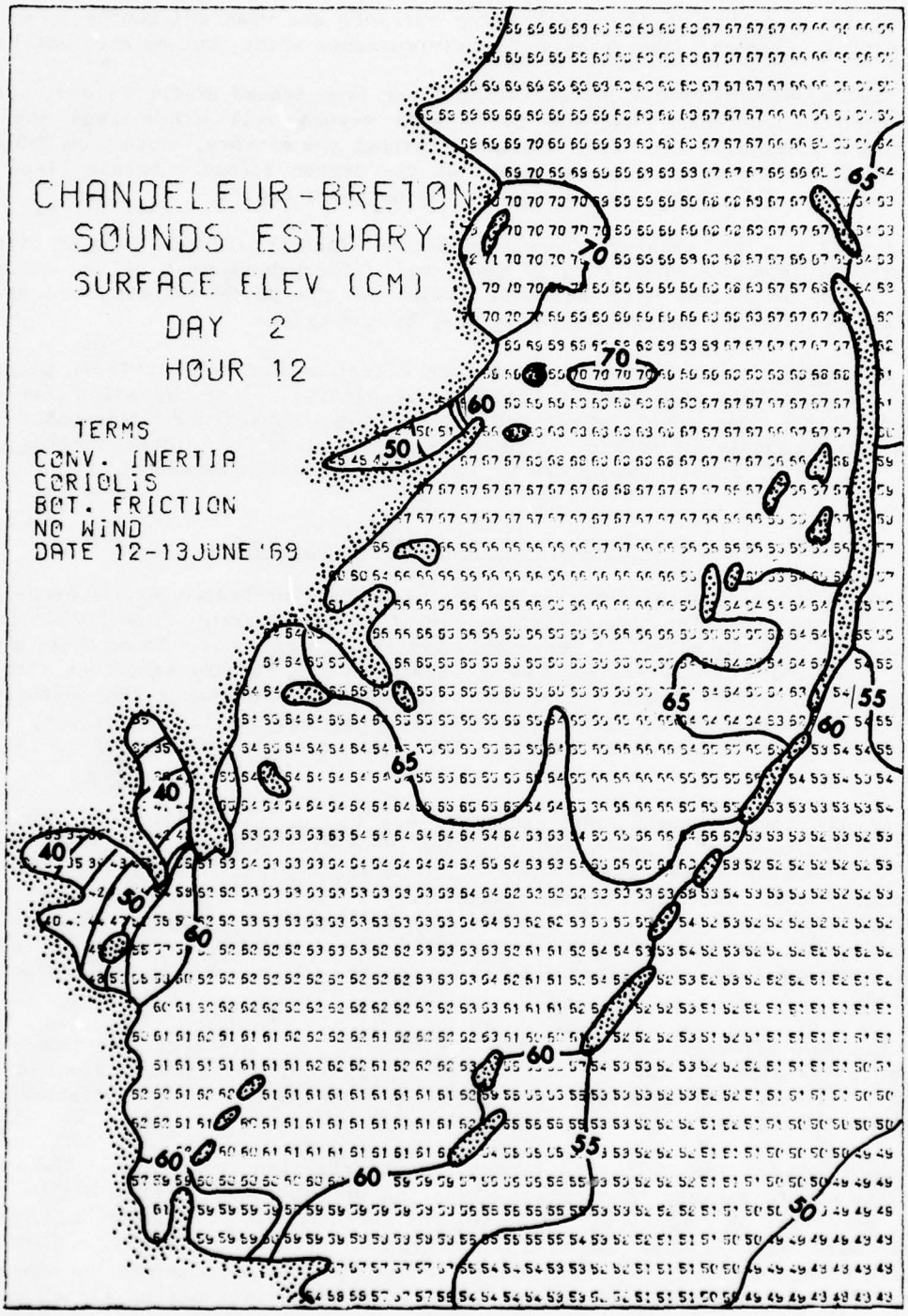

Figure 25. Wind effect test, surface elevation, no wind.

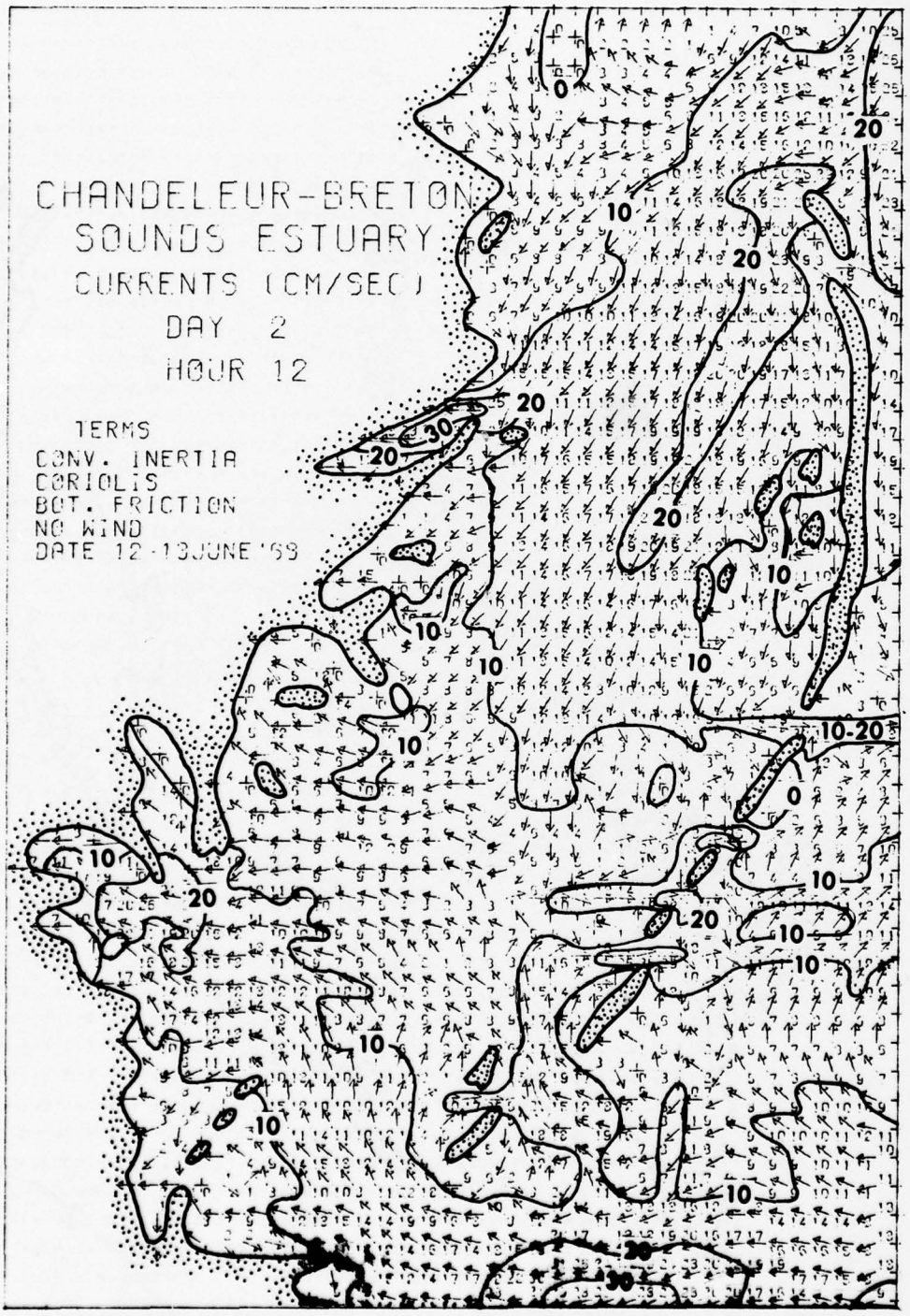

Figure 26. Wind effect test, currents, no wind.

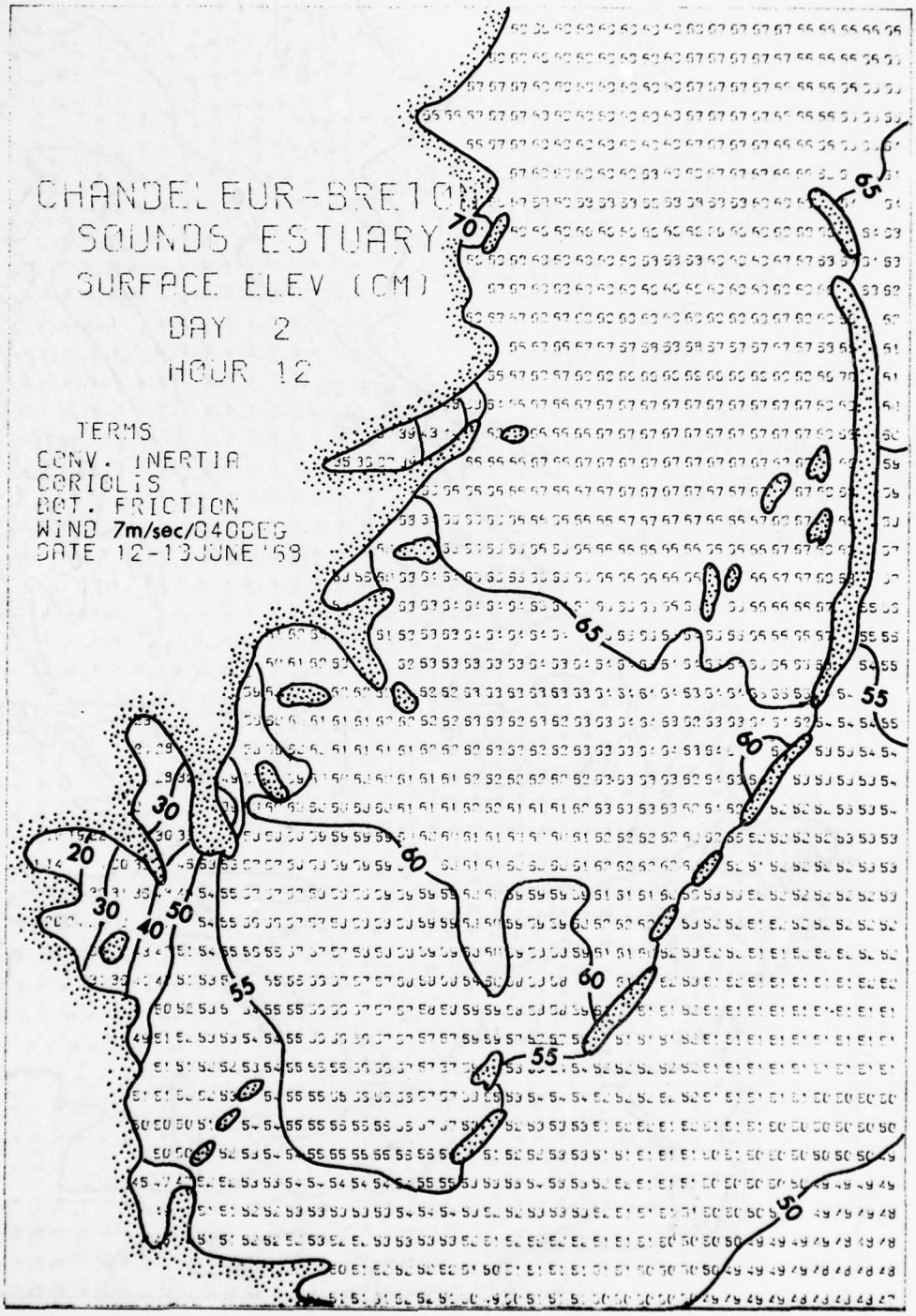

Figure 27. Wind effect test, surface elevation, wind 7 m/sec/040°.

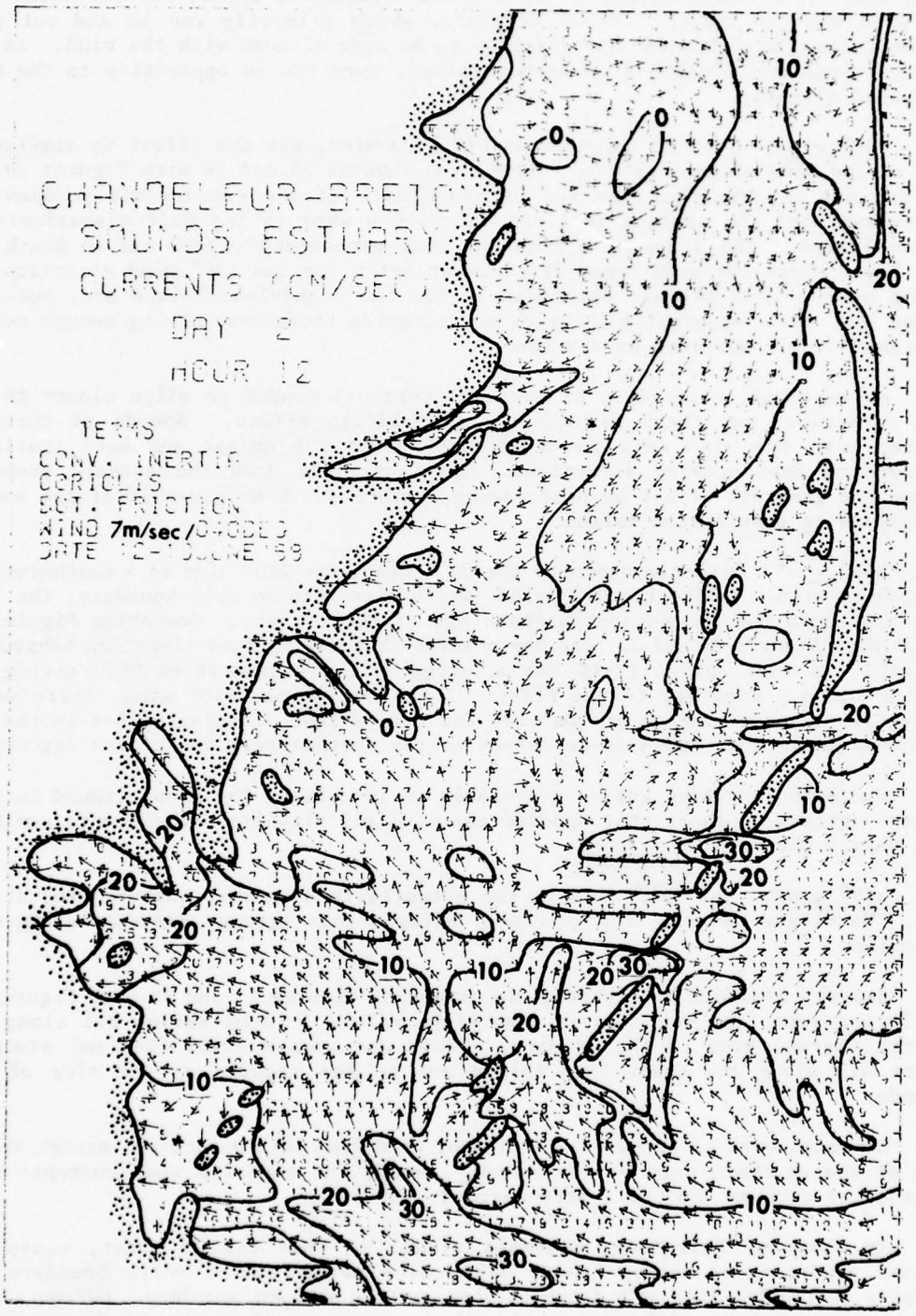

Figure 28. Wind effect, currents, wind 7 m/sec/040°.

As might be expected, most of the currents that were in opposition to the wind, i.e., in a southwesterly direction, were reduced in speed, whereas those with the wind were increased. Cross currents, which primarily run in and out past Breton Island, were turned only slightly to be more aligned with the wind. In the passage south and southwest of Breton Island, currents in opposition to the wind increased slightly.

130° wind. The 130° wind is an offshore wind, but the effect is similar to that of the 040° alongshore wind. Comparing Figures 25 and 26 with Figures 29 and 30, one may observe that the lee or marsh side of the estuary was scooped out (depressed) and the surface inclined steadily upward to the Gulf elevation near Breton Island. The scooping action was most pronounced (10-20 cm) in Black and Eloi Bays, where the wind began its longest fetch for the 130° wind direction. A slight set-up (2-3 cm) was developed inside the Chandeleur Island arc, but only around low tide. Apparently incoming and outgoing tides were strong enough not to be significantly overcome by the wind.

As expected, especially at low tide currents tended to align closer to the wind direction, but there was surprisingly little effect. Speeds of currents aligned with the wind were increased only about 2-5 cm/sec and were similarly retarded on the incoming direction. Cross currents down the estuary probably showed the greatest effect by penetrating farther south as a result of the southward flushing past Breton Island.

220° wind. Directly opposite the 040° wind, the 220° wind is a southwesterly alongshore wind. Unlike the 040° wind, which blew into an open boundary, the 220° wind blew into the leveed southwestern end of the estuary. Comparing Figures 25 and 26 with Figures 31 and 32, one may observe that the surface elevation behaved as expected: a true set-up (5-10 cm) occurred in the southwest on both rising and falling tides. Contrary to the effect of the reciprocal 040° wind, there was a generally raised elevation at low tide and some slight scooping effect in the lee of the North Islands and a 10-cm set-up at the southwestern end of the estuary.

Currents responded quite predictably in increasing the wind-aligned current speeds, decreasing those that opposed the wind and aligning all currents somewhat more toward the wind.

310° wind. The 310° wind is the potentially dangerous onshore wind direction. Hurricane Camille, for instance, entered this estuary somewhat along this direction.

Exactly as would be expected, in comparing Figures 25 and 26 with Figures 33 and 34 one sees that there was a generally uniform 5-15-cm set-up all along the western (marsh) side of the estuary. There was even a small (2-3 cm) scooping effect all along the Chandeleur Island arc on the estuary or lee side of the islands.

Currents were affected very little by wind from this direction, except at low tide at the northern part of the estuary, where the normally weak currents were reversed as much as 180° to a northwesterly direction.

In summary, therefore, moderate winds, in this case 7 m/sec, cause the obvious wind-aligned set-up (about 5-20 cm) blowing into a solid boundary, or scooping on the lee side of a fetch if blowing into an open boundary. Currents tend to align themselves with the wind and increase or decrease their speed in accordance with their relative direction to that of the wind.

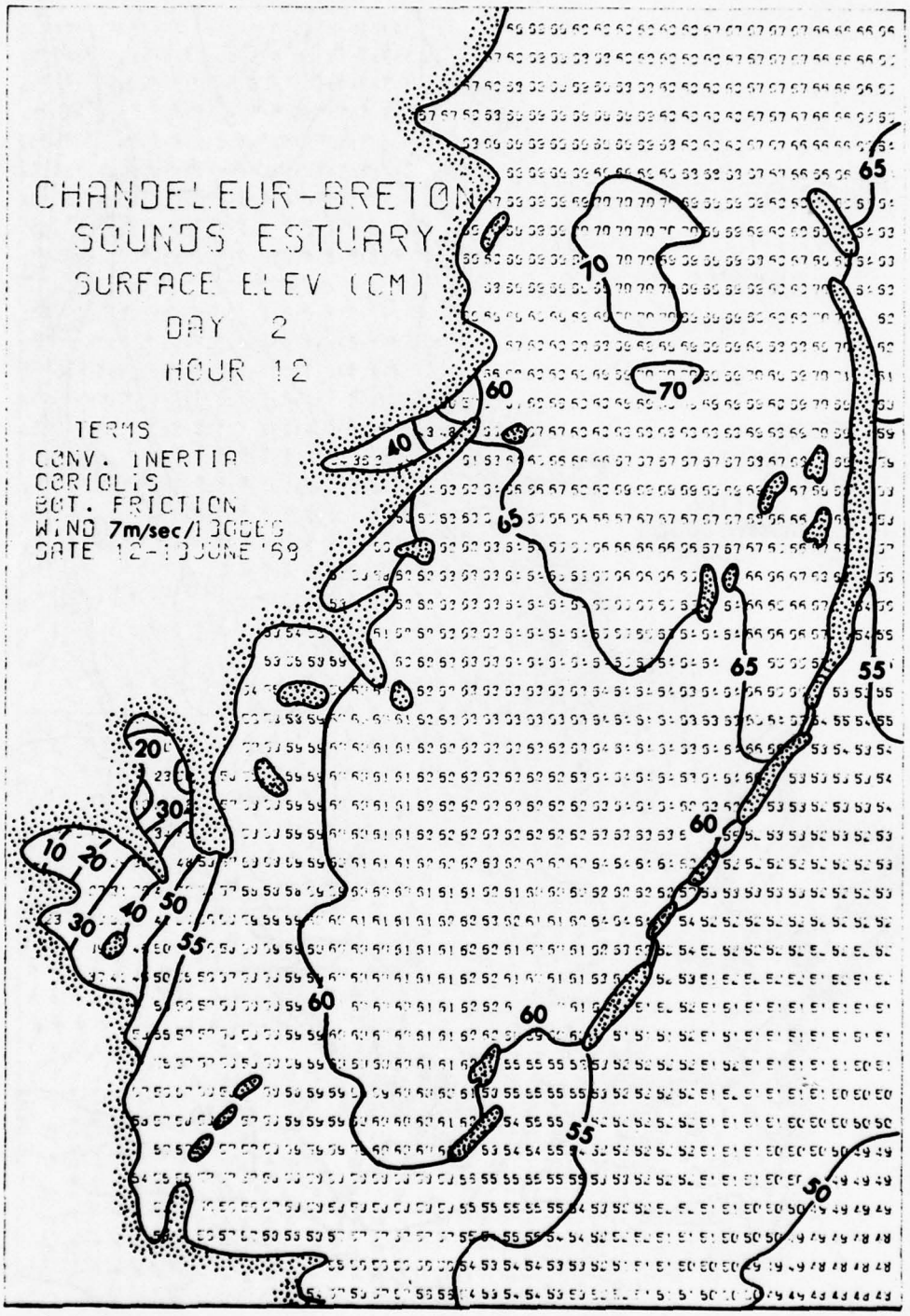

Figure 29. Wind effect test, surface elevation, wind 7 m/sec/130°.

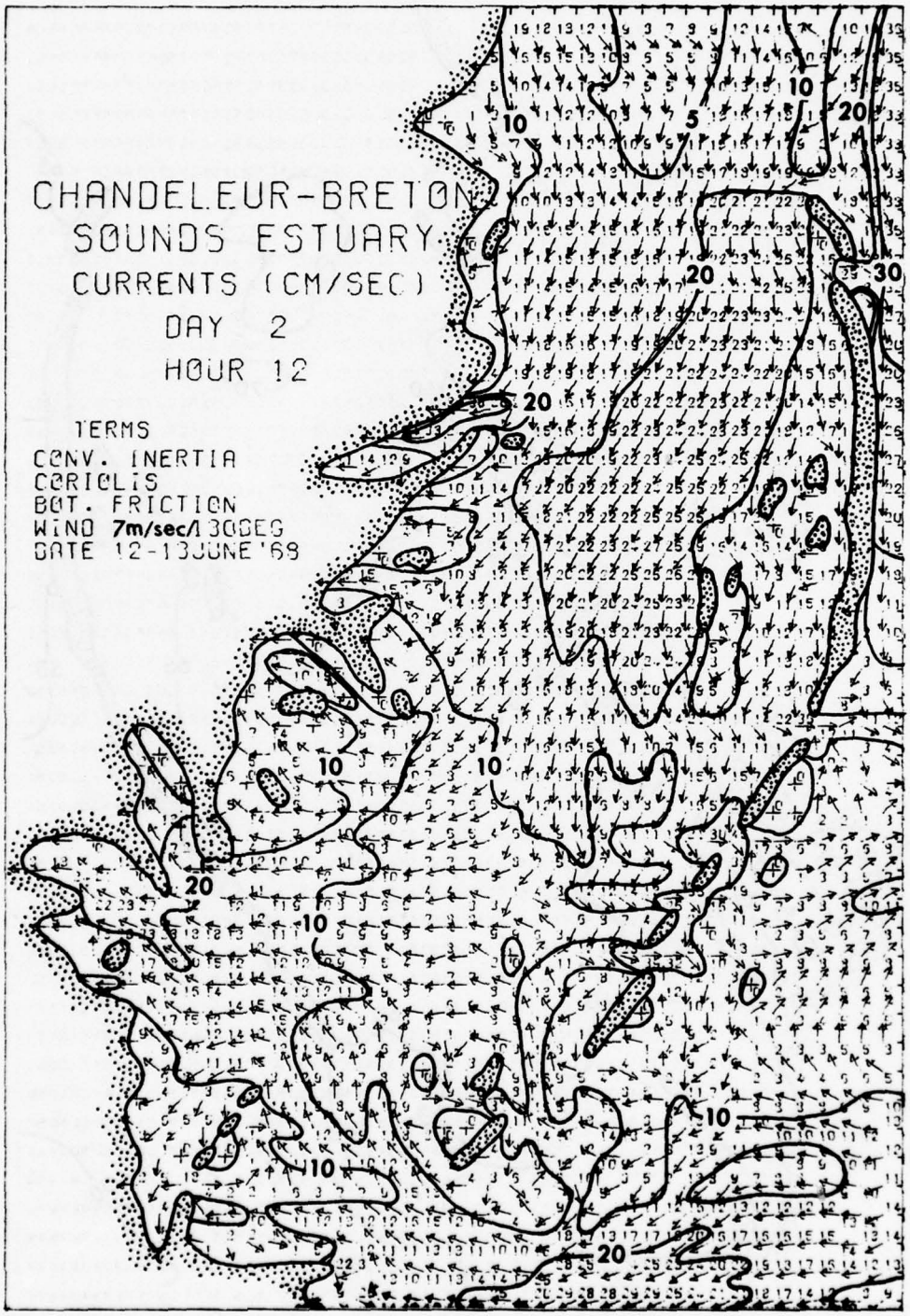

Figure 30. Wind effect, currents, wind 7 m/sec /130°.

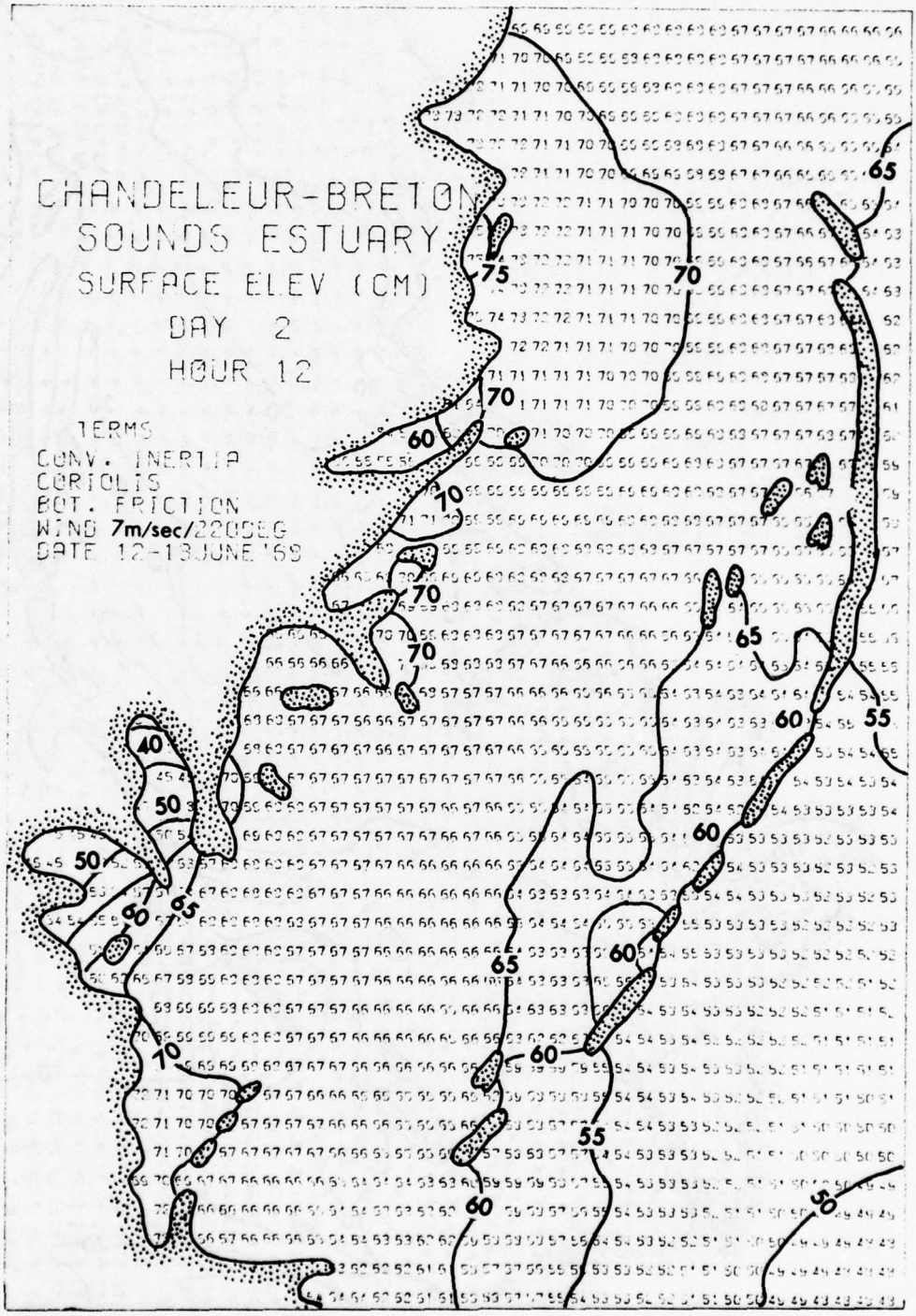

Figure 31. Wind effect, surface elevation, wind 7 m/sec/220°.

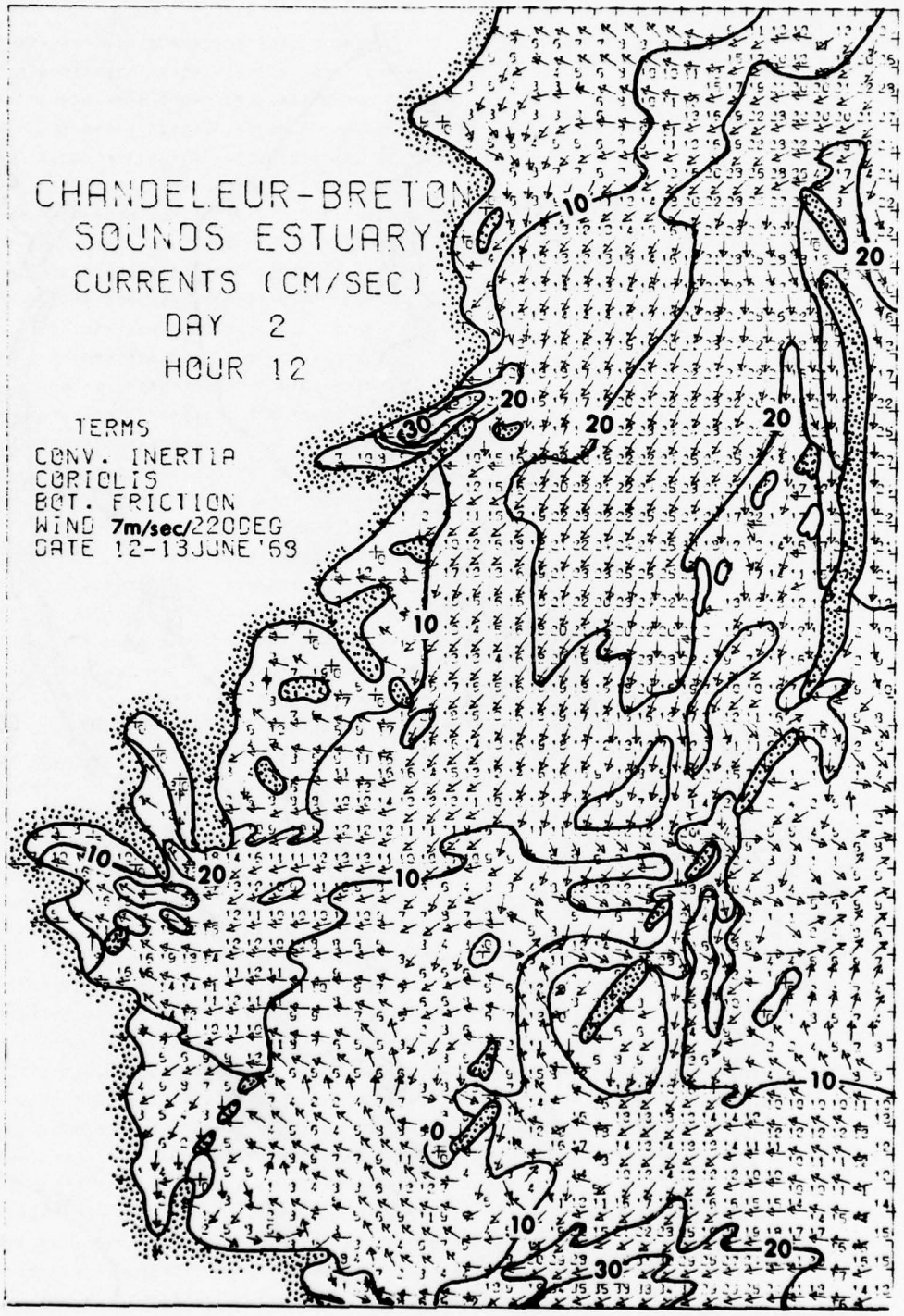

Figure 32. Wind effect, currents, wind 7 m/sec/220°.

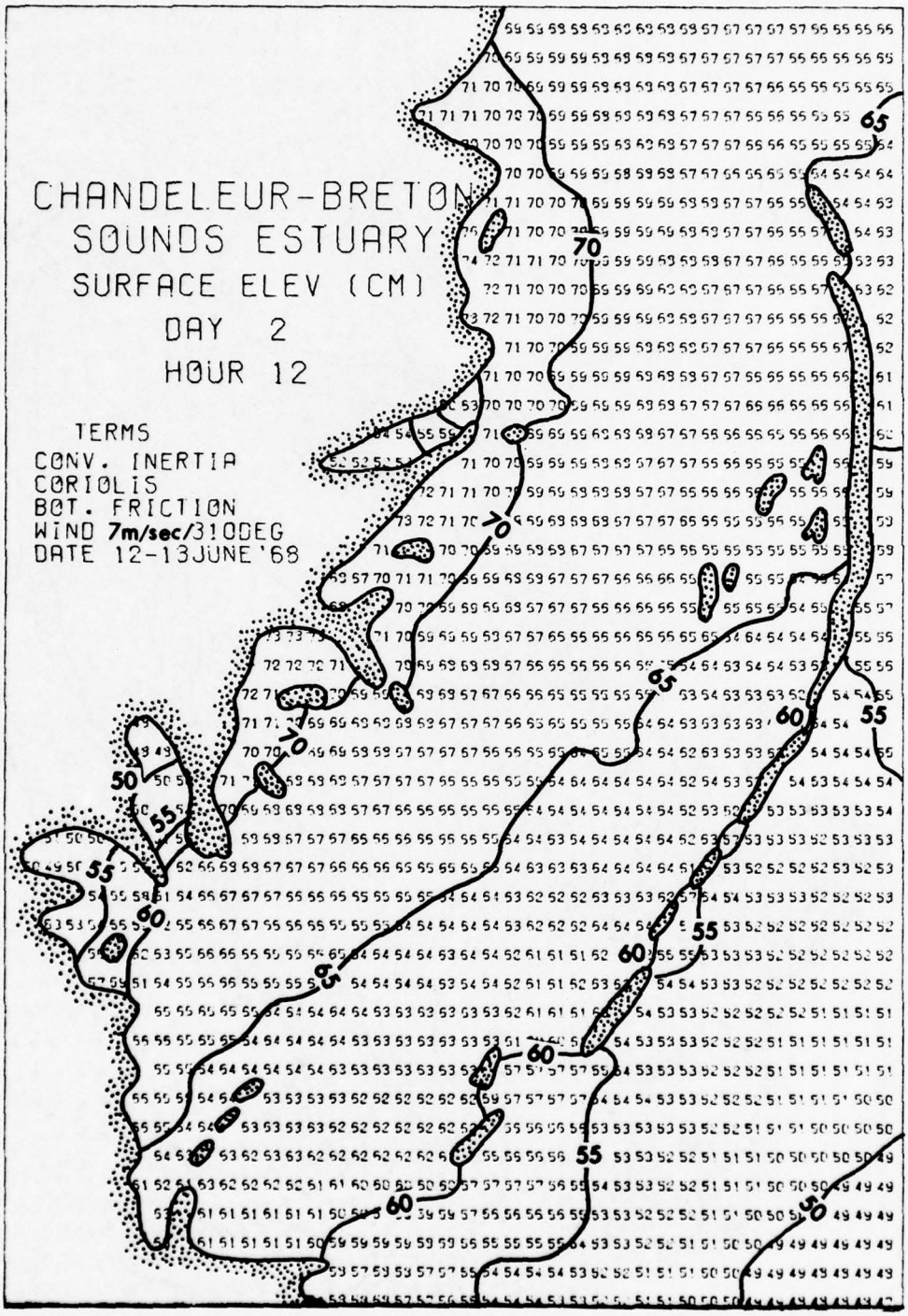

Figure 33. Wind effect test, surface elevation, wind 7 m/sec/310°.

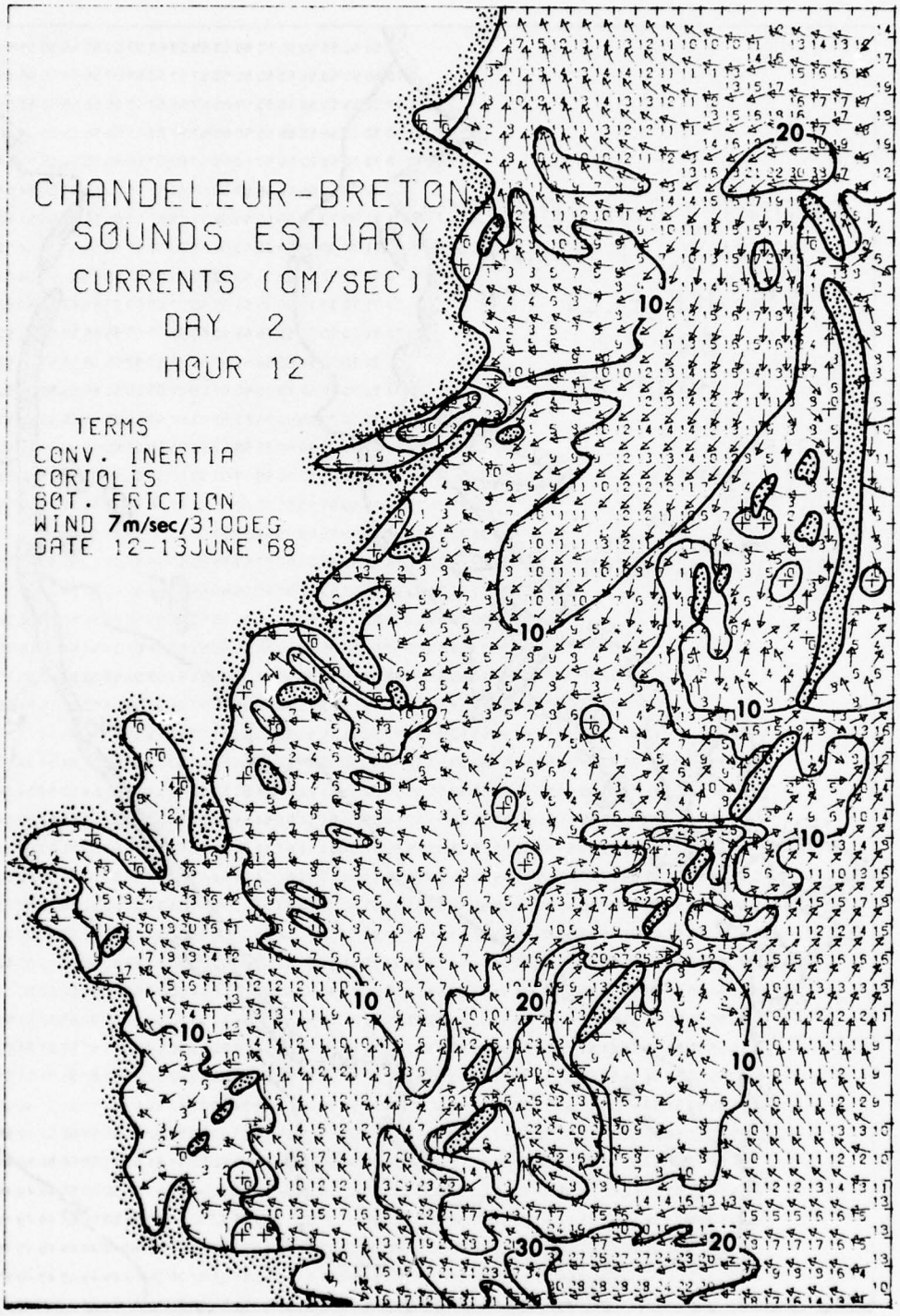

Figure 34. Wind effect, currents, wind 7 m/sec/310°.

Separate tests have also shown that winds around 3-4 m/sec have a barely discernible effect of possibly 1 or 2 cm in surface elevation differences and a similar 1-2-cm/sec current speed alteration. At wind speeds of about 2 m/sec or less, any effect is negligible.

Co-Range and Co-Tidal Lines

Both co-range and co-tidal lines are of considerable interest to the investigator of any large estuary. Engineers and planners of many types of coastal structures depend to a considerable degree on knowing where the greatest and least ranges will occur. A pier's location, for example, would be ideal if there were no alongside surges and rise and fall to the tides. Large-scale loading and offloading operations are economically time dependent, and moving ships' moorings to accommodate ships affected by pier motions is time consuming and expensive. Engineers, planners, and environmentalists interested in protecting or preserving a given coastal area, or given a choice of areas in which to establish a natural refuge, would be considerably assisted by knowledge of these areas of maximum and minimum range.

To obtain these data for a period of one tidal cycle, maximum and minimum surface elevation and corresponding times were determined from the computer output data listings for a grid of every fifth point throughout the model area. The range difference at each point was plotted on a model grid. High and low tide lag times from a base time were treated similarly. The results were contoured and are therefore the co-range and co-tidal lines. Figures 35-37 are the co-range, co-high-tide, and co-low-tide lines for the estuary, as shown by the model, when driven by the average tides shown in Table 4.

The point or area of maximum range noted on Figure 35 is in the vicinity of Deep Pass, from Brush to Martin Islands (see Fig. 1).

Tropic and equatorial tidal periods were also examined but do not change the pattern appreciably except as would be expected, i.e., during tropic tides the range differences are somewhat exaggerated and during equatorial tides are somewhat decreased from those shown in Figures 35-37.

It seems evident from the higher ranges shown around Deep Pass and net volume flow data, which will be discussed in the next section, that the increased tidal action in this area is a major contributor to the erosion of the St. Bernard Delta.

Finally, one may observe from Figure 37 that the Mississippi River Gulf Outlet Canal is located in about as reasonable a position as could be expected with respect to moderate tidal range.

Net Volume Flow

Finally, in completing a hydrodynamic physical description of the Chandeleur-Breton Sounds estuary, one must consider net volume flow.

The volume flow data presented in Table 5 were obtained and summarized from the model computer output data listings using the east-west cross section (N-24, Fig. 35). Volume flow figures from the data listings for every point along the cross section for a tidal cycle were tabulated and summed. The results shown in Table 5 suggest the following:

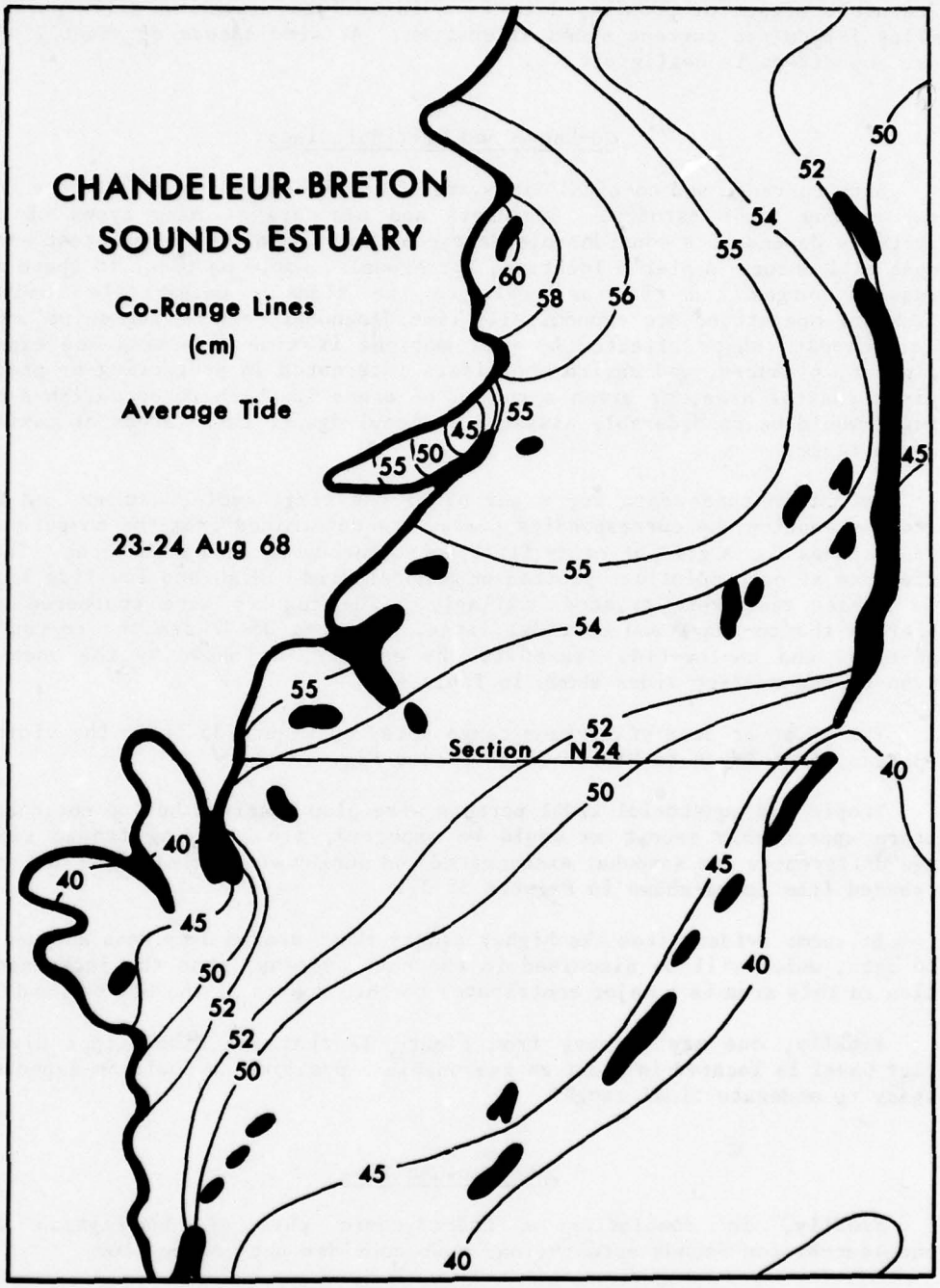

Figure 35. Co-range lines for average tides. Tropic tides show similar field, but maximum is 92 cm, minimum is 65 cm. Equatorial tide ranges vary from zero throughout to a similar field with 28 cm maximum and 10 cm minimum.

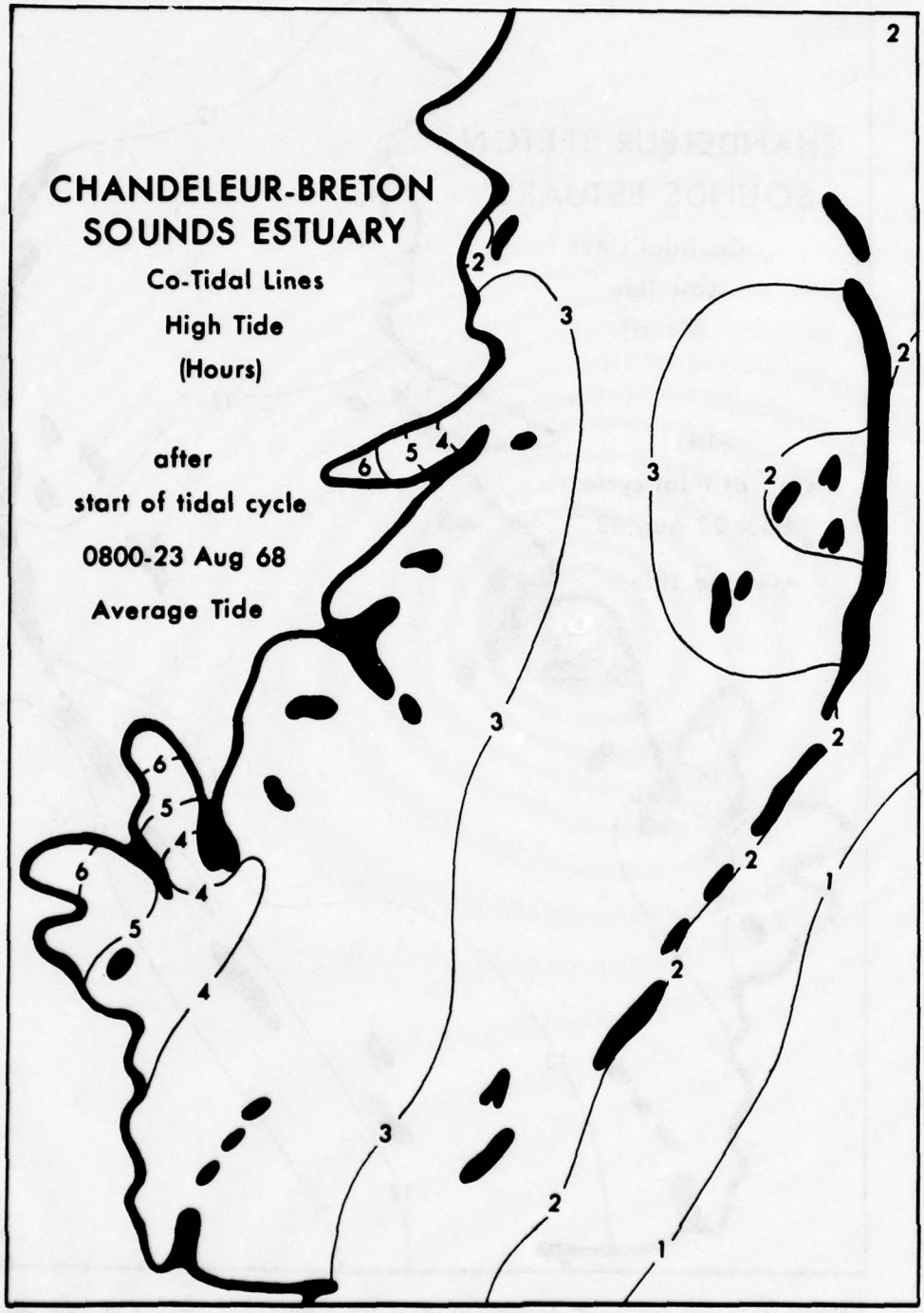

Figure 36. Co-high-tide lines for average tides. Tropic and equatorial tides show similar fields.

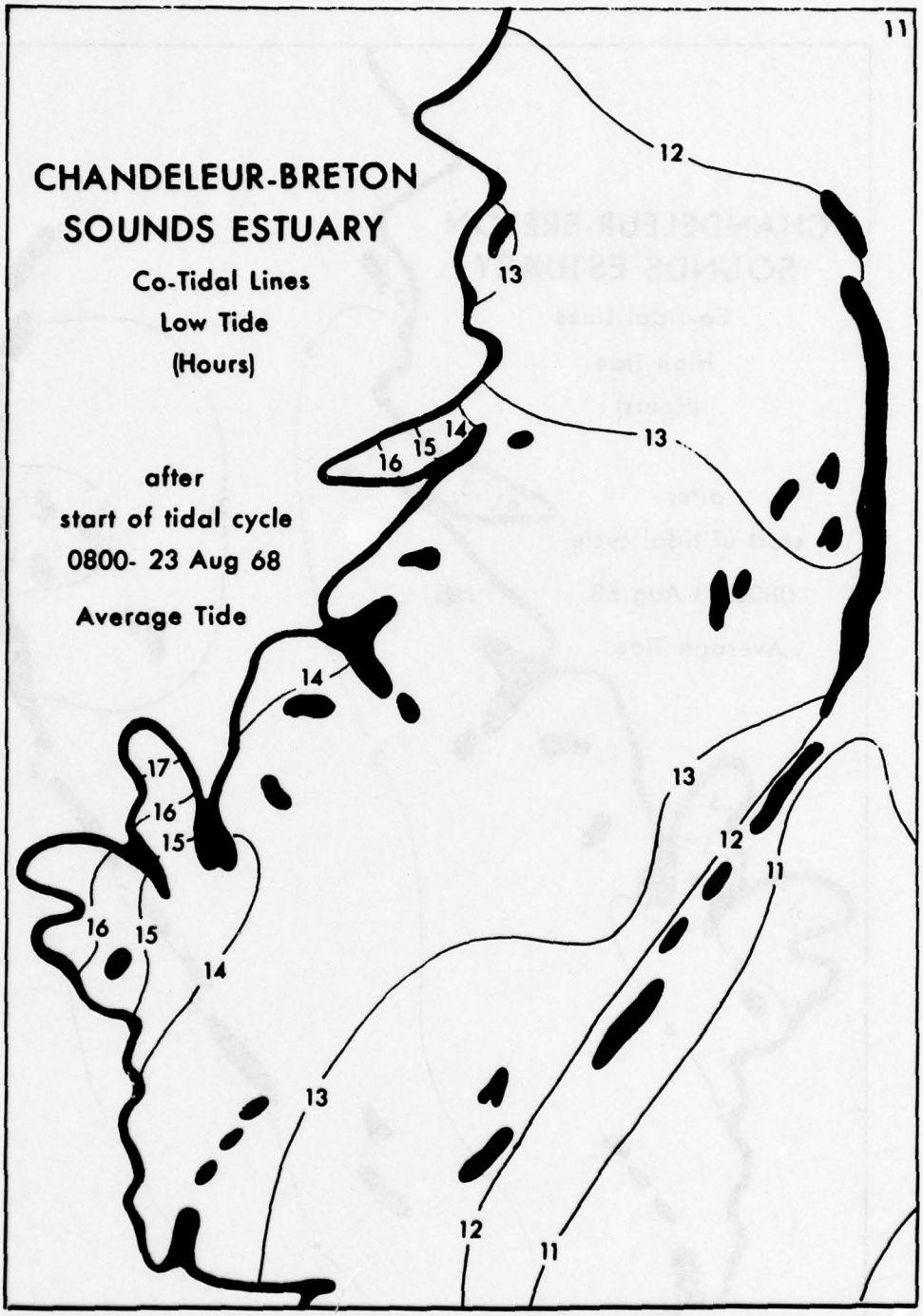

Figure 37. Co-low-tide lines for average tides. Tropic and equatorial tides show similar fields.

Table 5

North-South Volume Flow across Cross Section N-24

Dates	Tide		Wind		Net Flow	
1968	Description	Range (m)	Speed (m/sec)	Heading (°)	Direction	$m^3/sec \times 10^{-2}$
12-13 June	Tropic	0.9	7	220	South	3100
12-13 June	Tropic	0.9	7	130	South	2650
22-23 Sept	Equatorial	0.2	2.1	240	South	2540
28-29 July	Average	0.45	0		South	1940
23-24 Aug	Average	0.54	0		South	1800
12-13 June	Tropic	0.9	0		South	1350
29-30 Apr	Average	0.48	3.2	330	South	1200
12-13 June	Tropic	0.90	7	310	North	250
12-13 June	Tropic	0.90	7	040	North	560

Tropic Tides: Range 0.9 meter

Dates	Tide		Estuary Orientation		Net Flow	
	m/sec	Heading (°)	Long Axis	Cross Axis	Direction	$m^3/sec \times 10^{-2}$
12-13 June	7	220	040-220		South	3100
12-13 June	7	130		130-310	South	2650
12-13 June	0				South	1350
12-13 June	7	310		130-310	North	250
12-13 June	7	040	040-220		North	560

1. There is a net flow across this midline in a north-to-south direction. If wave action is, for example, eroding the northern part of the delta, the littoral transport of material is southward and probably out past Breton Island. From energy studies discussed in a later section it is known that the energy flux to the south is quite pronounced. Basically, energy and volume flow in from all entrances but flow out primarily to the south.

2. Net volume flow is maximum when the tidal range is greatest and a strong wind is blowing down the long axis of the estuary.

3. Net volume flow to the south becomes progressively less as a combination of wind speed and direction and tidal range become more adverse.

4. Net volume flow will, or can, be shifted to the north with a strong onshore wind, or at maximum by a strong wind blowing northward up the long axis of the estuary. One concludes, therefore, that a 7-m/sec wind blowing up the estuary will balance or overcome normal tidal drift to the south.

FURTHER DISCUSSION AND PHYSICAL IMPLICATIONS

Theoretical Wave Form

Attempting to correlate the surface elevation and current flow patterns, discussed earlier, with an identifiable wave form was somewhat speculative, since the model-simulated conditions are distorted from the ideal cases by natural topographic and bathymetric features.

To this end, however, profiles were plotted for the locations shown on Figure 38. The north-south (N-S) profile is shown in Figure 39. The orthogonal profiles are shown in Figure 40. Below each surface elevation profile are the profiles of the current speed components in the plane of the profile.

Inspecting Figures 39 and 40, one sees the indications of standing wave forms. In Figure 39 it appears from the strong north-south current flow, which damps out in a convergence zone somewhat north of the mid-latitude of the estuary, that the total wave form is made up of two waves, i.e., one from the northern entrance and one from the southern. The cross-channel wave forms and currents indicated in Figure 40 suggest a cross-channel seiching effect.

From the co-range lines discussed earlier one recalls the higher ranges on the west or right side of a strong current entering from the north.

These factors suggested two opposing north-south Kelvin waves. A Kelvin wave describes the wave form and geostrophic current which, in general, result from the balance of pressure gradient or slope force and Coriolis force. Basically, in a Kelvin wave the current runs normal to a wave front that slopes up to the right of the current (in the northern hemisphere). Following the development of Platzman (unpublished notes, 1965), the Kelvin wave height (ζ) and speed (U) are:

$$\zeta_{(x,y,t)} = \zeta_{o(y)} \cos k\,(x - ct)$$

$$U_{(x,y,t)} = U_{o(y)} \cos k\,(x - ct) \qquad (22)$$

where $C = \sqrt{gh}$ = wave propagation speed
h = channel depth
x = down-channel coordinate
y = cross-channel coordinate
b = channel width
t = time
$k = 2\pi/L$ = wave number
T = wave period
$L = CT$ = wave length

The origin of the coordinates is at the center of the channel, where x = 0 with +y to the right when looking in the direction of propagation. Then, letting

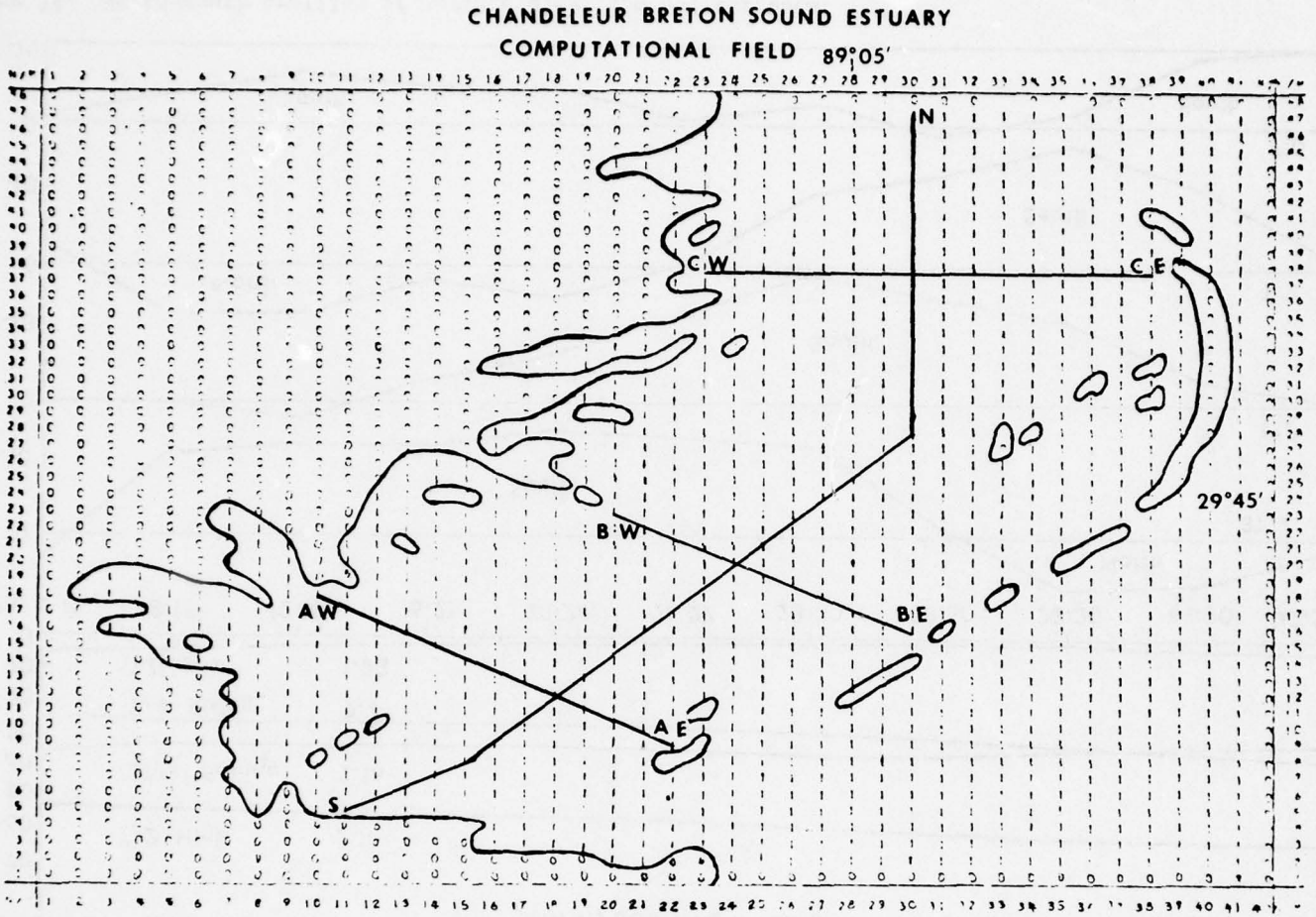

Figure 38. Cross section profile index.

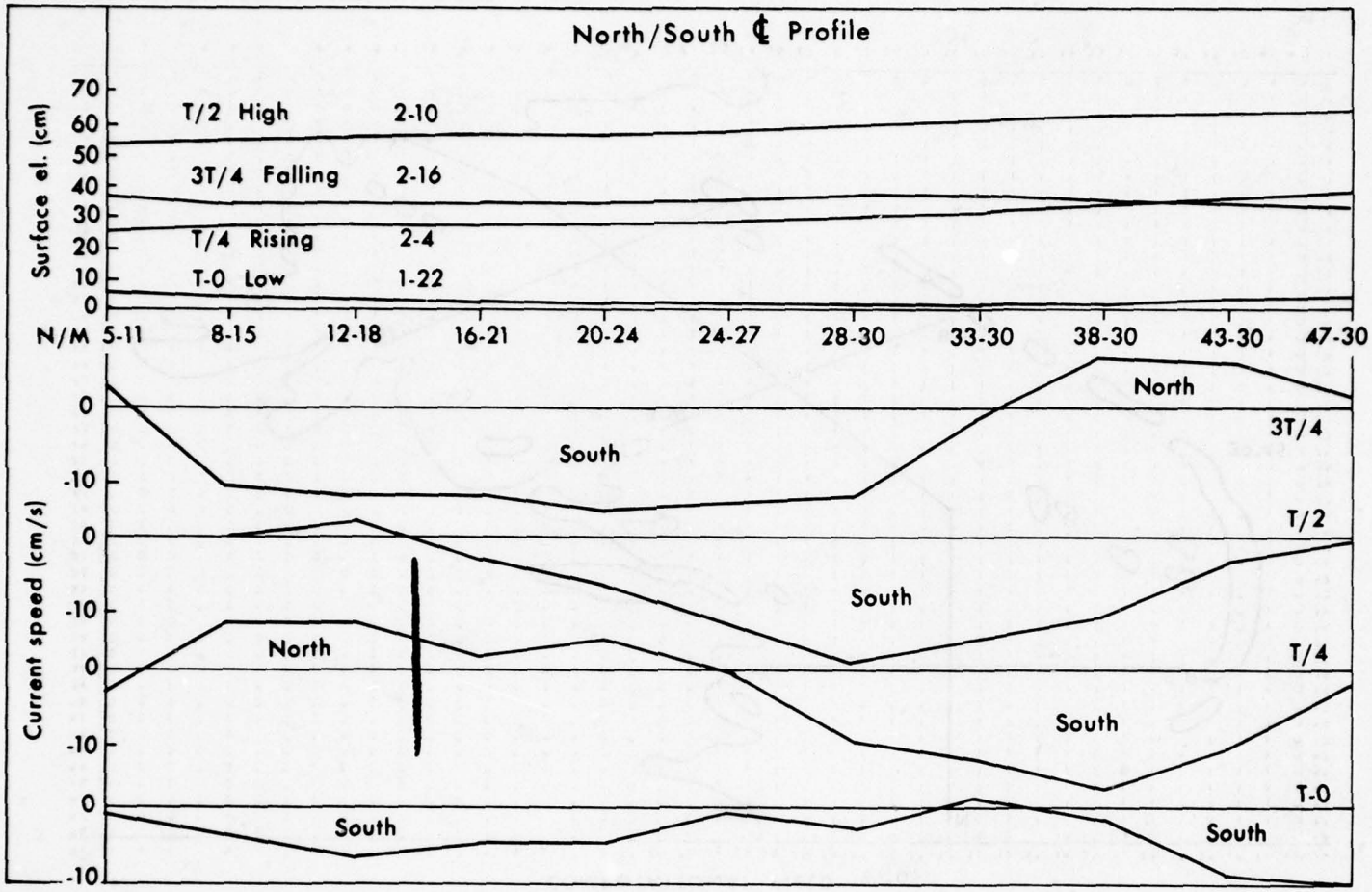

Figure 39. North-south profiles of surface elevation and currents.

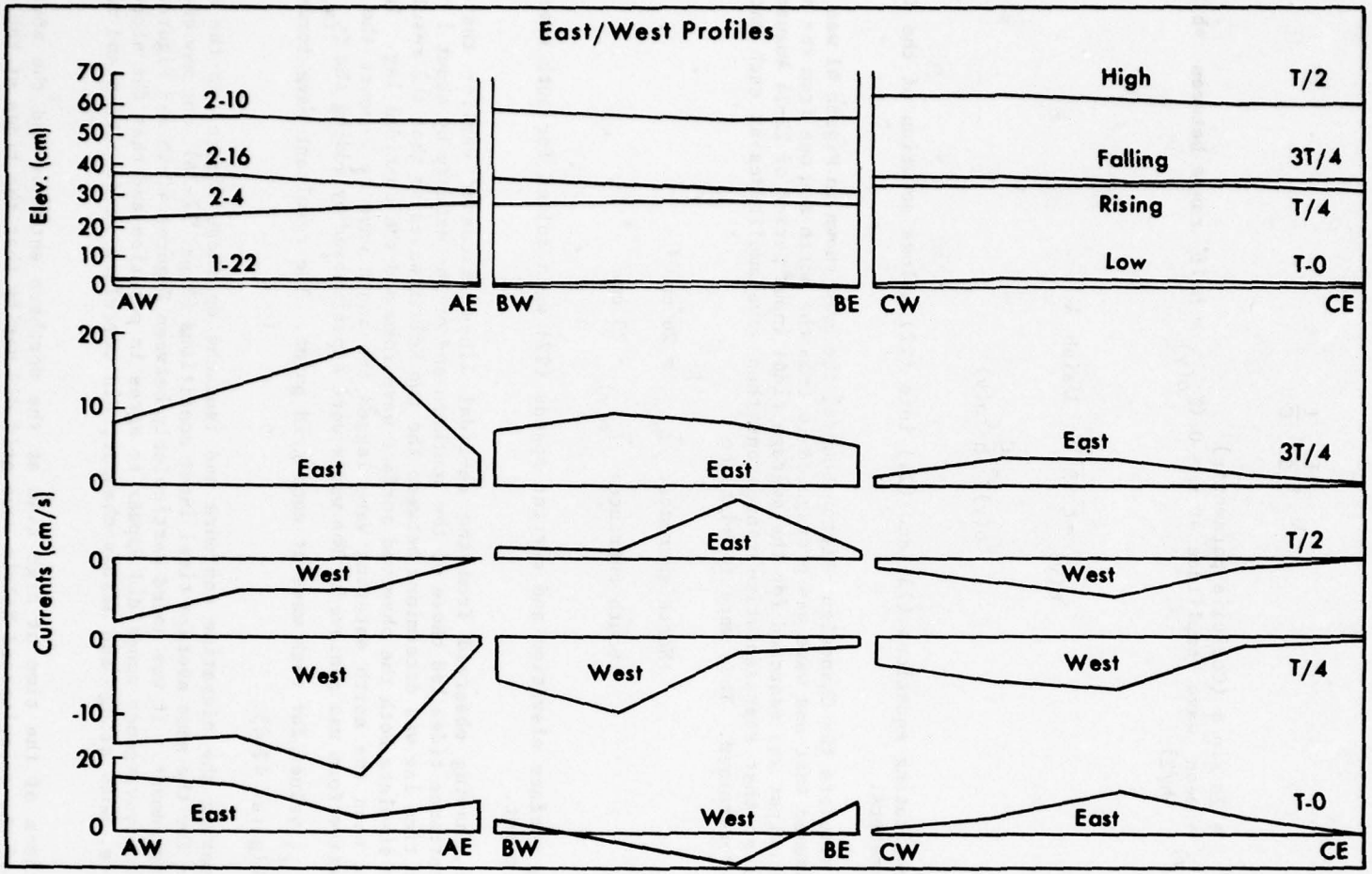

Figure 40. East-west profiles of surface elevation and currents.

$$y' = y/(b/2)$$

and

$$\lambda = \frac{b}{2} \cdot \frac{f}{C}$$

where f = $2\omega \sin \phi$ (Coriolis parameter)
$\bar{\zeta}_{o(y)}$ = mean wave amplitude at $x = 0$ ($\zeta_{o(y)}$ = half range between +b/2 and -b/2)

then

$$\zeta_{o(y)} = \bar{\zeta}\ \ell^{-\lambda y'}\ \lambda/\sinh\ \lambda \tag{23}$$

$$U_{o(y)} = \frac{C}{h}\,\zeta_{o(y)} \tag{24}$$

Substituting equations (23) and (24) into (22) allows solution of the Kelvin wave parameters.

To simulate the Chandeleur-Breton Sounds, the grid shown in Figure 41 was used. It was assumed that one wave was propagated in from the north and one from the south. The model output was searched for the average tidal input period of 22-24 August 1968 (Table 4) so that representative ranges and then wave amplitudes at each entrance could be determined. They were found to be

North entrance: $\bar{\zeta}_{o(y)} = 26$ cm

South entrance: $\bar{\zeta}_{o(y)} = 23$ cm

The hourly surface elevation and current speeds (22) were solved for both waves at each grid point.

Then, having observed from the co-tidal lines discussed earlier that the northern entrance tides led those of the southern end of the estuary by about 1 hour, the proper time lag was determined between the two Kelvin waves so that the resultant wave would simulate both the observed surface wave form and the co-tidal lag. It was found that when the north entering wave lagged the south wave by 2 hours the most representative form was achieved. The waves were superimposed by adding the $\zeta_{(x,y,t)}$ and $U_{(x,y,t)}$ values for each wave at each grid point. The resultant wave forms are shown by Figures 42-45.

Comparing the elevation contours and isotachs on these figures to the model simulation for the same average tidal input conditions (Figs. 17-24). one may observe the good agreement. It was noted particularly between Figures 42-45 and Figures 17-20 that the convergence zones did appear to agree in position and that the slopes of the surface, both along- and across-channel, did correlate in direction and magnitude.

A check of the time of high tide at the northern entrance and the southern entrance of the superimposed Kelvin wave grid did verify that the tides at the north

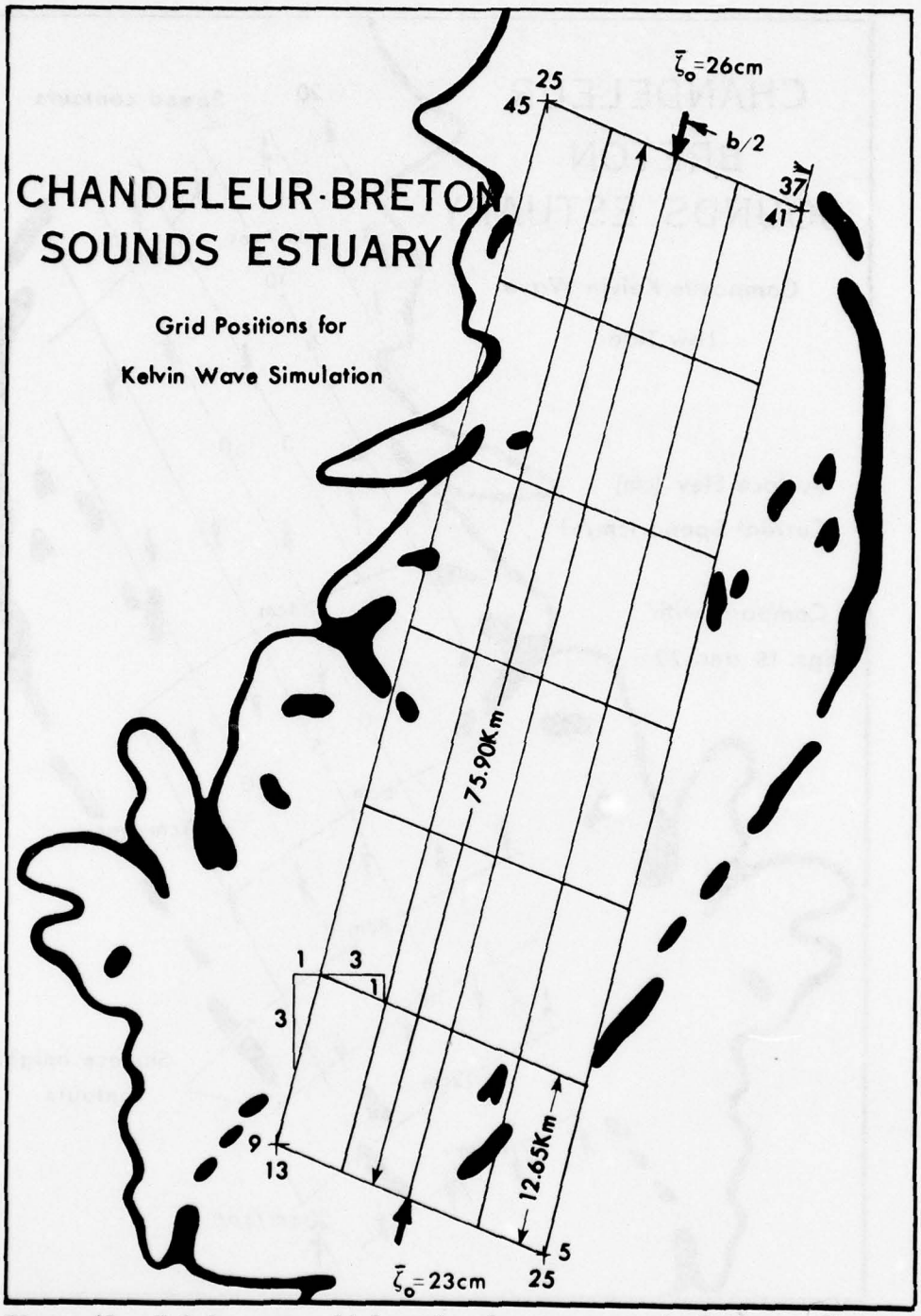

Figure 41. Kelvin wave grid location for two wave simulations. Waves from north $\bar{\zeta}_o$ = 26 cm, waves from south $\bar{\zeta}_o$ = 23 cm, b/2 = 12.65 km, C = 600 cm/sec, T = 24.84 hr.

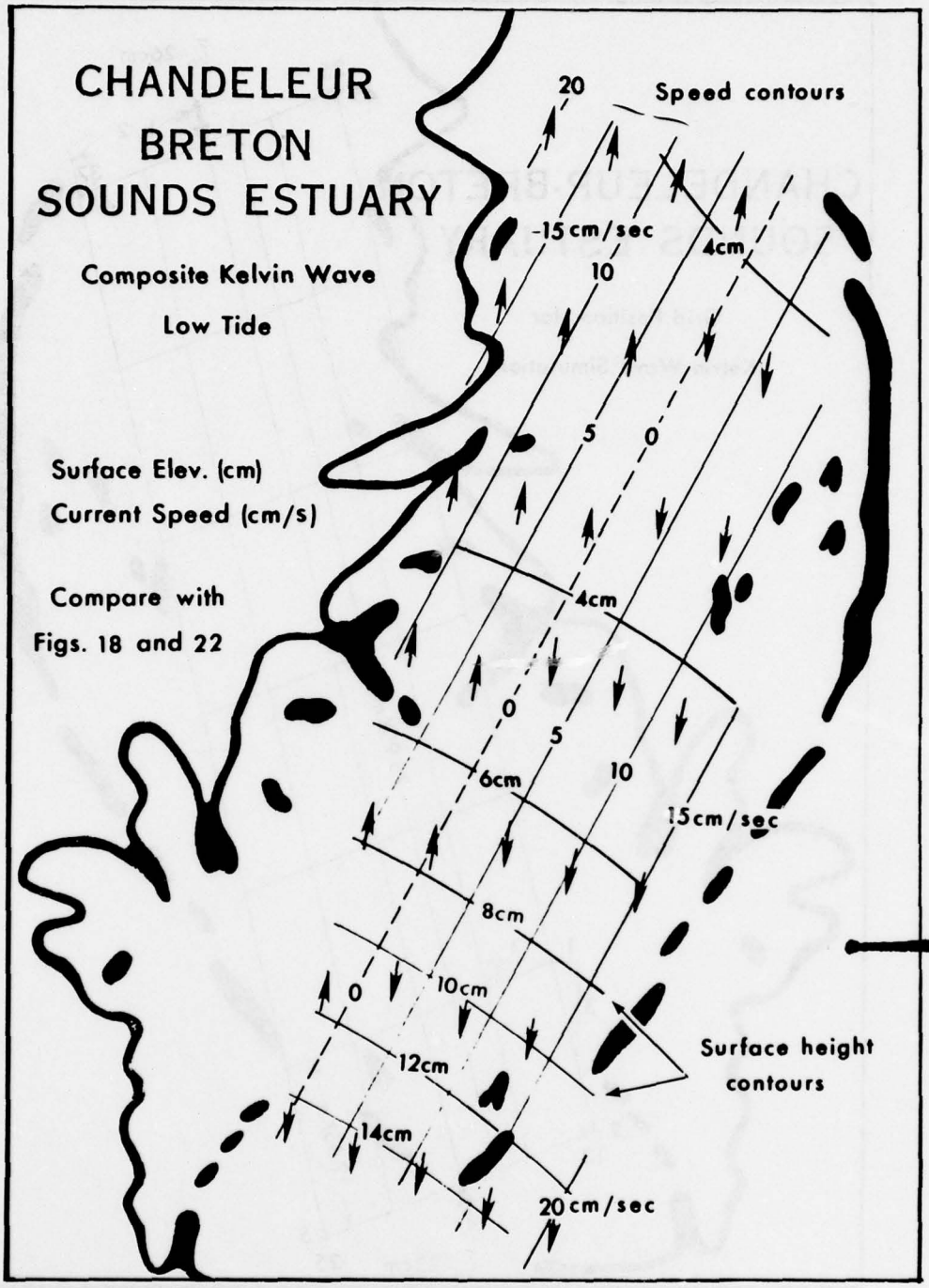

Figure 42. Composite Kelvin wave for low tide, resultant of adding north and south wave values at each grid point. Wave from north lags by 2 hours.

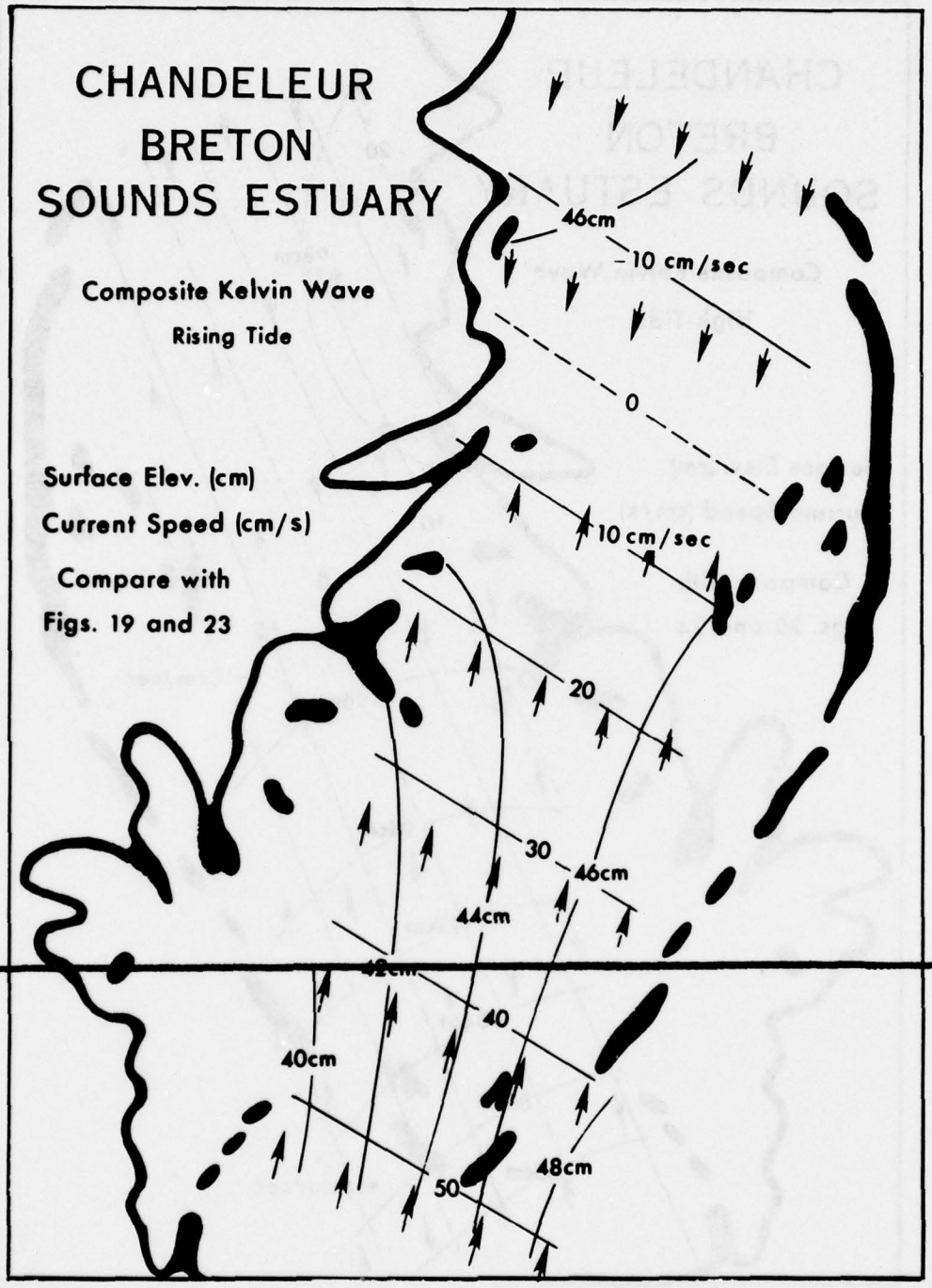

Figure 43. Composite Kelvin wave for maximum rising tide, resultant of adding north and south wave values at each grid point. Wave from north lags by 2 hours.

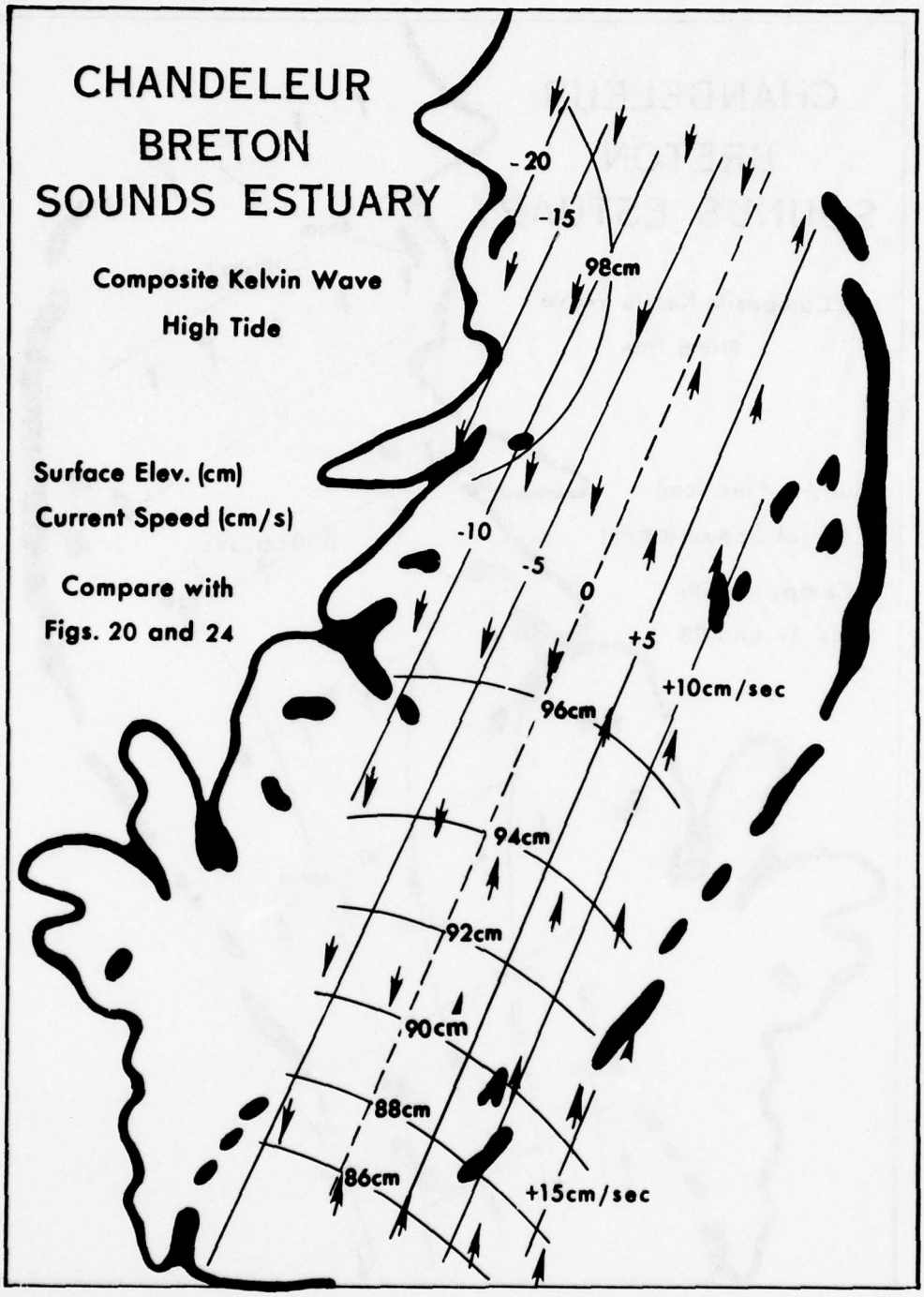

Figure 44. Composite Kelvin wave for high tide, resultant of adding north and south wave values at each grid point. Wave from north lags by 2 hours.

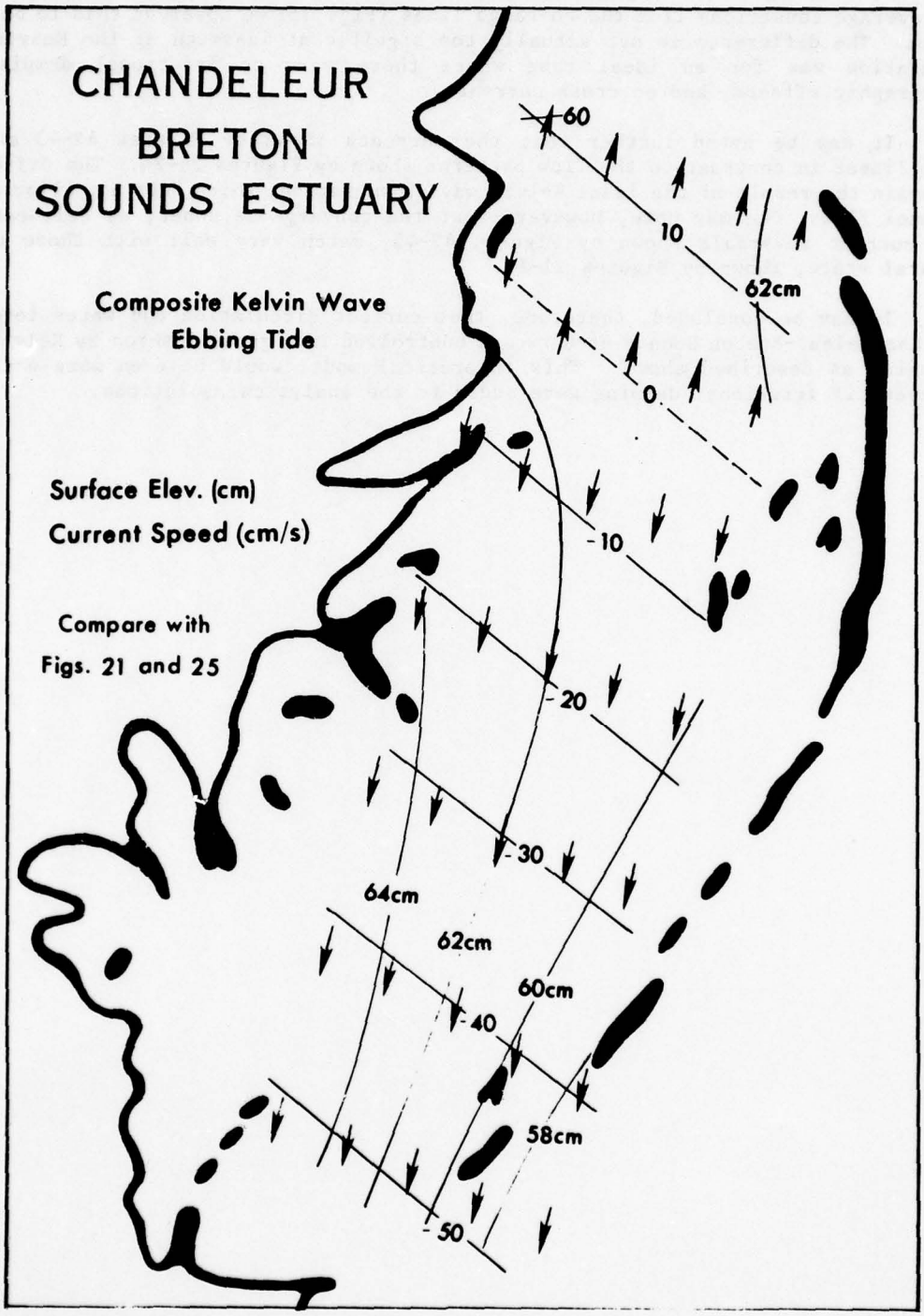

Figure 45. Composite Kelvin wave for maximum ebbing tide.

led those at the south by 1 hour, as required in the real estuary. One may note, however, that the tidal range for the Kelvin wave formulation is over 90 cm, whereas for average conditions from the co-range lines (Fig. 35) we observed this to be about 60 cm. The difference is not actually too significant inasmuch as the Kelvin wave simulation was for an ideal case where there were no frictional damping, no topographic effects, and no cross currents.

It may be noted further that the currents shown by Figures 42-45 are all rectilinear in contrast to the flow patterns shown by Figures 21-24. The difference is again the result of the ideal Kelvin wave formulation, which does not allow cross-channel flow. One may note, however, that the convergence zones, as delineated by the current reversals shown by Figures 42-45, match very well with those of the natural state, shown by Figures 21-24.

It may be concluded, therefore, that current circulation and water levels in the Chandeleur-Breton Sounds estuary are controlled in a gross fashion by Kelvin wave dynamics as described above. This theoretical model would be even more accurate, however, if frictional damping were added to the analytical solutions.

ENERGY BALANCE

Energy balance, and particularly the energy dissipation by frictional motions in shallow seas and embayments, has been a topic of discussion and study for more than 50 years. Street (1917) may have begun the interest with his discussion of frictional dissipation by tides. Taylor (1919), however, with his energy balance of the Irish Sea, may have created the greatest interest by showing a simple way to account for input energies and frictional dissipation, plus a practical application of the effect of the moon on the energy balance of a body of water. Jeffreys (1920) and Heiskanen (1921) soon tabulated figures that accounted for much of the worldwide shallow-water-area energy dissipation.

More recent studies have been limited to smaller areas and have been characterized by more detail and less gross approximation. The latter was the characteristic of the early work.

In chronological order, McLellan (1958) did work on the energy considerations and particularly the moon's effect on the Bay of Fundy. Miller (1966) discussed the tidal flux versus frictional method of determining energy dissipation. Blanton (1969) used the methods developed by Ippen and Harleman (see Ippen, 1966) to determine energy dissipation in Coos Bay, Oregon. Stock and Filloux (1975) provided information on the energy balance in widely separated areas, the Gulf of California and the Adriatic Sea. Garrett (1975) discussed tidal response in gulfs as a function of the energy input and dissipation. Levine and Kenyon (1975) studied the energy balance in Narragansett Bay.

The investigation of the energy balance in the Chandeleur-Breton Sounds estuary adds detail and precision to the foregoing body of knowledge. The area is 10 times larger than Narragansett Bay, 10 times smaller than the Irish Sea, and generally 5 to 7 times smaller than all the other areas of study. It is certainly the shallowest of all the study areas and has the lowest energy. It is the one area in the group subject to a diurnal tide. It has by far the lowest current speeds, and, finally, there was considerable detail available so that approximations are not so dominant as they might be in other studies.

The data for the energy balance came from the model output for the estuary, with the model run on the average tidal input given in Table 4.

It was possible to compute and determine the energy flux directly and from an energy balance between the input energy sources and the frictional dissipation.

The energy balance is shown by the formula:

$$\partial E/\partial t = E_I - E_D + W_M \qquad (25)$$

where $\partial E/\partial t$ = the rate of change of energy in the system
E_I = tidal input energy flux across the boundaries of the system
E_D = frictional dissipation of energy inside the system
W_M = the work done on (by) the moon on (by) the system

Total energy E is given by

$$E = KE + PE$$

where KE = kinetic energy
PE = potential energy

$$E = \frac{1}{2} \rho \int_A (h+\zeta)\, S^2\, dA + \frac{1}{2} \rho g \int_A \zeta^2 dA \qquad (26)$$

where h = depth below MSL
ζ = surface elevation above MSL
S = current speed
dA = unit area

The rate of change of energy in the Sound $\partial E/\partial t$ was determined directly from the use of equation (26); all input came from the model for each grid point on an hourly increment for a full diurnal cycle.

Total, kinetic, and potential energy for the estuary, which has a surface area of 3.2×10^{13} cm^2, was plotted and is shown by Figure 46. Total energy E and energy flux $\partial E/\partial t$ are given in Table 6.

Inspecting Figure 46 and Table 6, one may observe the relatively low total energy (average $\simeq 8 \times 10^{18}$ ergs) and maximum energy of only 17×10^{18} ergs as compared to the much larger values for most of the areas considered in the previously mentioned studies.

One sees, of course, from equation (26) that total energy is a function of total area, average depth, current speed, and surface elevation. The Chandeleur-Breton Sounds averages are:

Depth $\approx$ 500 cm (16 ft)
Speed $\approx$ 10 cm/sec
Amplitude = 10 cm

In most previous studies depths were greater; e.g., Taylor (1919) used h = 6800 cm. Most wave amplitudes were on the order of 150-200 cm and current speeds were between 100 and 150 cm/sec. One may observe from Figure 46 that total energy for this estuary is primarily a function of potential energy or the influence of tide level.

A comparative energy balance was obtained by following Taylor (1919) and McLellan (1958), where, using the time-averaged version of equation (25)

$$\langle \partial E/\partial t \rangle = \langle E_I \rangle - \langle E_D \rangle + \langle W_M \rangle \qquad (27)$$

Previous investigators have usually assumed $\langle \partial E/\partial t \rangle = 0$ and have investigated only the steady-state energy balance. This study, however, also determines the hour-by-hour time-dependent balance and the importance of $\langle \partial E/\partial t \rangle$ in the time-averaged balance.

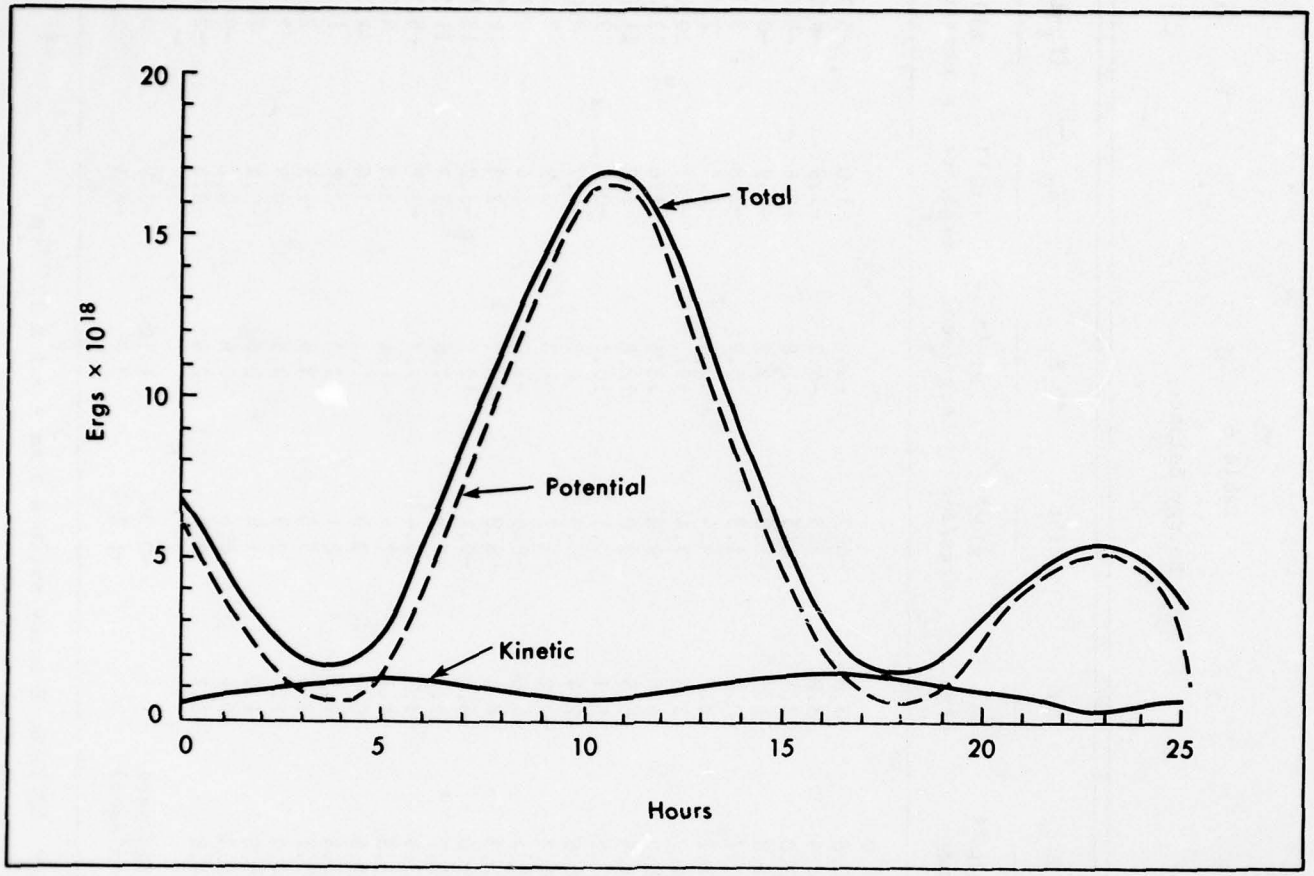

Figure 46. Total energy in Chandeleur-Breton Sounds showing contribution from potential and kinetic energies.

AD-A053 358 LOUISIANA STATE UNIV BATON ROUGE COASTAL STUDIES INST F/G 8/8
A NUMERICAL STUDY OF CURRENTS, WATER SURFACE ELEVATIONS, AND EN--ETC(U)
FEB 78 W E HART N00014-75-C-0192
UNCLASSIFIED TR-250 NL

2 OF 2
AD
A053358

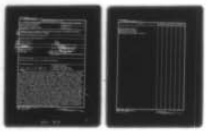

END
DATE
FILMED
6-78
DDC

Table 6

Energy Balance

Hour	E	ΔE	$\Delta E/\Delta t$	E_I	$-E_D$	(E_I-E_D)
	$x10^{18}$ ergs	$x10^{18}$ ergs	$x10^{14}$ ergs/sec	$x10^{14}$ ergs/sec	$x10^{14}$ ergs/sec	$x10^{14}$ ergs/sec
-1	7.9					
0	6.8	-3.0	-4.2	-4.2	-1.0	-5.2
1	4.9	-3.8	-5.3	-4.2	-1.8	-6.0
2	3.0	-3.1	-4.3	-1.8	-2.6	-4.4
3	1.8	-1.3	-1.8	2.2	-2.9	-0.7
4	1.7	0.9	1.3	5.9	-2.8	3.1
5	2.7	3.2	4.4	9.5	-2.5	7.0
6	4.9	5.3	7.4	12.1	-2.1	10.0
7	8.0	6.6	9.2	13.6	-1.6	12.0
8	11.5	6.5	9.0	12.8	-1.2	11.6
9	14.5	5.1	7.1	10.1	-0.8	9.3
10	16.6	2.4	3.3	4.7	-0.7	4.0
11	16.9	-1.2	-1.7	-1.3	-0.9	-2.2
12	15.4	-4.6	-6.4	-7.0	-1.4	-8.4
13	12.3	-6.4	-8.9	-10.2	-2.3	-12.5
14	9.0	-6.6	-9.2	-10.2	-3.2	-13.4
15	5.7	-5.7	-7.9	-7.8	-3.7	-11.5
16	3.3	-3.9	-5.4	-4.7	-3.8	-8.5
17	1.8	-1.7	-2.4	-1.4	-3.5	-4.9
18	1.6	0.0	0.0	1.3	-3.0	-1.7
19	1.8	1.5	2.1	3.3	-2.3	1.0
20	3.1	2.5	3.5	3.9	-1.5	2.4
21	4.3	2.1	2.9	3.4	-0.9	2.5
22	5.2	1.0	1.4	1.5	-0.4	1.1
23	5.3	-0.4	-0.6	-0.6	-0.2	-0.8
24	4.8	-1.7	-2.4	-2.4	-0.4	-2.8
Avg. (10^{14}ergs/sec)			-0.36	1.14	-1.9	-0.76
Avg. (ergs/cm^2/sec)			-1.2	3.7	-6.1	-2.4

where $\Delta E/\Delta t = \Delta E/7200$, Estuary surface area = $3.1 \times 10^{13} cm^2$

Input tidal energy flux as shown by Taylor (1919) is

$$E_I = \rho g \int_0^L h\,\zeta(S \sin\alpha)\, d\ell + \frac{1}{2} \int_0^L (\sin\alpha)\,(2g\zeta^2 + hS^2 + \zeta S^2)\, d\ell \qquad (28)$$

where

$S \sin\alpha$	=	the current speed normal to the plane of the estuary entrance
α	=	the direction of the current relative to this plane
L	=	total length of the entrance
$d\ell$	=	differential distance

Other terms are as defined under equation (26).

Frictional dissipation of energy flux is:

$$E_D = \kappa \int_A \rho\, S^3\, dA \qquad (29)$$

where all terms have been defined previously. The dimensionless constant $\kappa \approx 2 \times 10^{-3}$ is the familiar approximation for the frictional constant.

We can further assume that, owing to the small amplitude of the tidal wave, the shallow depths, and the relatively small area of the Chandeleur-Breton Sounds estuary, the moon effect W_M is negligible. Therefore, the energy balance is between the input energy flux E_I and the frictional dissipation of energy E_D.

To compute these terms, as when computing the total energy E, the variables h, ζ , S, and α were taken from the computer output listing of the model at hourly intervals for a full tidal cycle. Actually, since all the parameters had been extracted, E_D was computed at the same time as E, KE, and PE.

Energy flux through each entrance was computed separately, but also using the model data at each entrance grid point. The input energy flux from the major northern and southern entrances and the sum of the other five small entrances are plotted in Figure 47. Both total input energy flux and energy frictional dissipation flux were plotted and are shown in Figure 48. Both are also shown in Table 6.

One may observe from Figure 47 that the major energy inputs are from the northern and southern entrances. More important, however, is the fact that energy was still flowing in from the north more than 2 hours after the energy outflow had begun in the south and more than 5 hours after outflow began from the other five entrances. Three of the latter are south of grid row N-24, which was used for the volume flow study discussed earlier. The combined effect of the earlier outflow from the south and the continued inflow from the north tends to produce the net volume flow to the south across row N-24.

Inspecting Table 6 and Figure 48 one may make the following observations:

a) Energy advected into and out of system (E_I) is, at any one time, usually four times the energy dissipated by bottom friction at the same time;
$< |E_I/E_D| > = 3.9$.

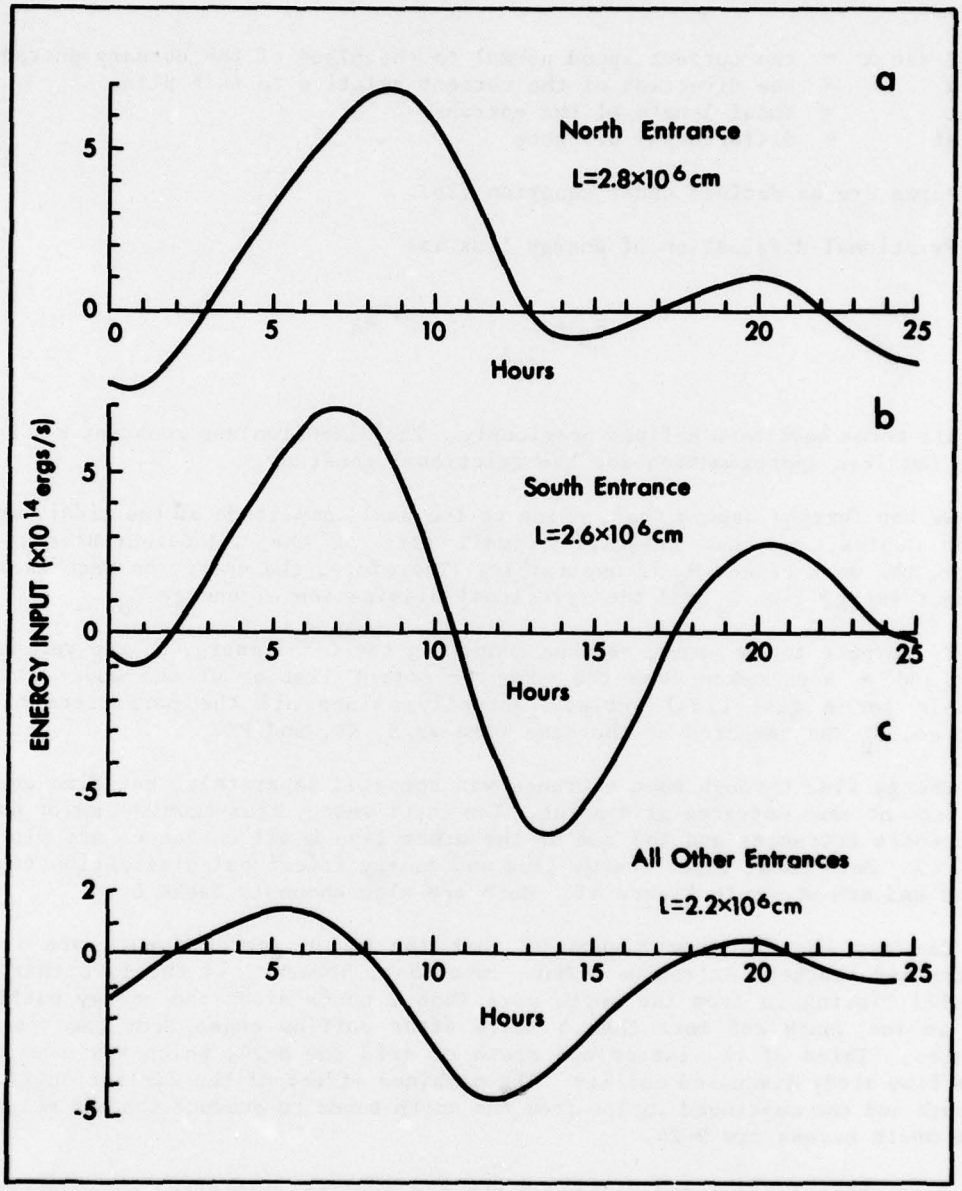

Figure 47. Energy input rate from both main and all other entrances.

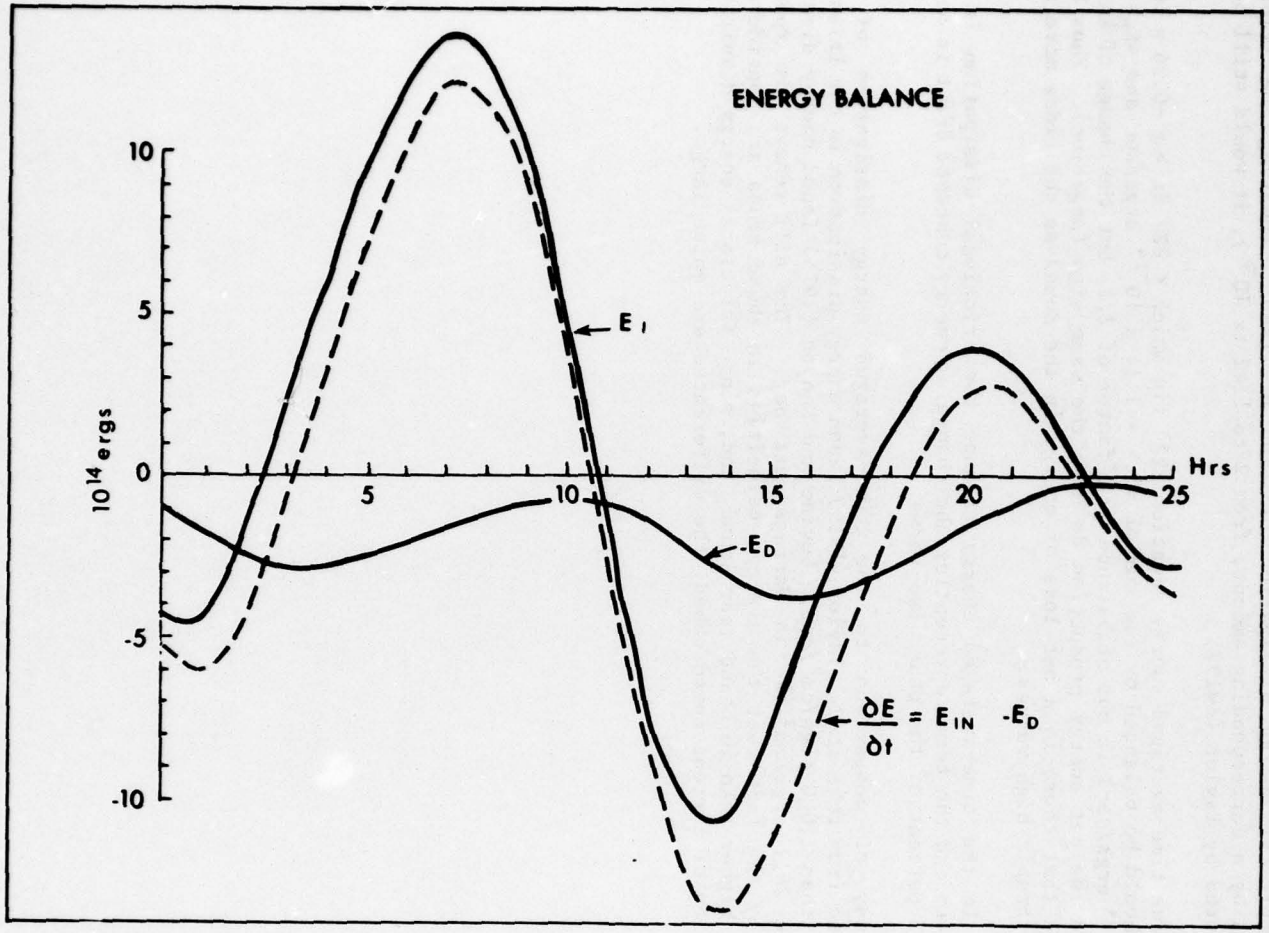

Figure 48. The balance between the change of energy content $\partial E/\partial t$, the advective energy flux E_I, and the energy dissipation in Chandeleur-Breton Sounds as a function of time.

b) The left- and right-hand sides of the instantaneous energy equation (25) are out of balance by more than a factor of two only 4 of the 25 hours in the tidal cycle studied. On the average, the change of energy content (left side) is out of balance with the right side (net energy production) by a factor of 1.4. This is rather good agreement considering the crude finite-difference calculation of $\Delta E/\Delta t$ and the empirical energy dissipation function utilized. Lowering the friction coefficient by a corresponding amount, from 2 to 1.42 ($\times 10^{-3}$), it would still be in the range used by Taylor (1919).

c) The time-averaged energy equation (27) (in which $\langle \partial E/\partial t \rangle = -0.36 \times 10^{-14}$ ergs/sec should be balanced by the sum of $\langle E_I \rangle = 1.14 \times 10^{-14}$ ergs/sec and $\langle E_D \rangle = -1.90 \times 10^{-14}$ ergs/sec) is out of balance by a factor of 2.1, but the change of energy content and the net energy production do have the same sign (negative). Thus both sides agree that there is a net loss of energy in the Sound as the tides move away from their tropic high values.

d) In the time-averaged energy balance the frictional dissipation is the dominant term and the term representing the change of energy content $\partial E/\partial t$ is on the order of 25 percent of the other two terms.

By way of comparison to the time-averaged energy dissipation of 6.1 ergs/cm^2/sec from this study, Taylor (1919) found energy dissipation in the Irish Sea to be more than 1,000 ergs/cm^2/sec. Levine and Kenyon (1975) found energy dissipation to be 26.1 ergs/cm^2/sec in Narragansett Bay. The differences are readily explained by the fact that the average velocities in these areas are considerably different, higher than in Chandeleur Sound, and, since frictional energy dissipation is a function of current speed cubed, the differences are quite large.

CONCLUSIONS

Conclusions that may be drawn from this study of the Chandeleur-Breton Sounds estuary relative to the initial objectives may be grouped in two major categories, i.e., the numerical model and the estuary.

The Numerical Model

The study has shown, by comparison of the model output with observed field data and through a number of tests and comparisons designed to verify the application of the basic theory and assumptions, the numerical scheme itself, and finally its computational accuracy, that the model will generate representative output with an accuracy on the order of 10-15 percent of true values.

The model will provide, at any incremental time step, the fields for surface elevation, current speed and direction, and volume flow.

The model can be operated in modes that consider bottom friction, surface wind friction, and Coriolis and convective inertia term effects. The wind capability of the model also allows the wind to be run for the full length of a model run, or started and/or stopped at any designated time during the run. The latter provides information on response to impulse winds.

Finally, it was shown that the model was programmed in such a way that, by the use of subroutines and single-digit and variable numerical input control cards, the model is suited to easy modification and use by any investigator for application to studies of any similarly adaptable area.

The Chandeleur-Breton Sound

The study showed that the hydrodynamic system is generated primarily by two long waves, one entering from the northern entrance, between Chandeleur Island and the St. Bernard delta lobe, and the other entering from the southeast, around both sides of Breton Island.

The study showed that these waves could be simulated very well by Kelvin waves. The resultant interference pattern reasonably simulated the standing wave pattern that was suggested by the numerical model.

It may be concluded, therefore, that the resultant pattern and description of the estuary are as follows:

1. Two tidal systems enter the estuary, one from the north and one from the

south, and the interference pattern results in a convergence zone somewhat north of the mid-latitude of the estuary.

2. Tides at the northern entrances lead those of the southern end of the estuary by about 1 hour. In order to simulate this with Kelvin waves, the wave from the north had to lag the southern wave by 2 hours.

3. Tidal ranges are greatest in the northwestern part of the estuary. For average tides the range is about 60 cm, whereas for tropic tides the range is about 90 cm. Ranges in the northern part of the estuary are 10-15 cm greater than in the south. This last agrees with the 70-cm range found by Kjerfve (1973) in Caminada Bay, just west of the Mississippi River delta.

4. Slopes in the estuary are on the order of 2×10^{-6} for average tides and 3.5×10^{-6} for wind-induced periods. Both figures agree with similar values found by Kjerfve (1973) in Caminada Bay.

5. Currents average about 10-15 cm/sec, and maximums are about 40-50 cm/sec, in the narrow, shallow entrances through the Chandeleur Island chain. Basically, the flow patterns come in from the northern and southern entrances, drive to the convergence zone, and the residual low-speed currents turn west toward the mainland coast. As the tides turn, the opposite effect is not true. The currents begin to diverge from the zone, but within a few hours after high tide the major flow through the Sound is all to the south.

6. There is a net volume flow past the mid line of the estuary. This flow exists under average and tropic tidal conditions but is dominated by response to wind, i.e., as the wind direction increasingly opposes the direction of flow, the net volume flow will decrease. A directly opposing wind of sufficient strength (heading 040°) will reverse the net flow to the north.

7. Energy balance studies have shown that this is indeed a relatively low energy estuary. The frictional dissipation, when compared to that in other areas, is quite low, as a result of the very low average current speeds in the estuary.

The energy partition is such that there is on the average about six times more potential energy in the system than kinetic. The instantaneous energy balance equation is dominated by the advective energy flux through the entrances to the Sound, and only about 25 percent of the energy entering the system is dissipated by bottom friction inside the Sound. On the other hand, the time-averaged energy balance equation is dominated by the energy dissipation term. The unsteady energy content term $\langle \partial E/\partial t \rangle$ is on the order of 25 percent of the advective and dissipative terms.

REFERENCES

Abbott, M., and G. Marshall, 1970, A numerical model of a wide shallow estuary. Internat. Assoc. for Hydraul. Res., C7-1-7.

Barrett, B. B., 1971, Cooperative Gulf of Mexico estuarine inventory and study, Louisiana--Phase II, hydrology. Louisiana Wild Life and Fisheries Commission, New Orleans, 191 pp.

Blanton, J., 1969, Energy dissipation in a tidal estuary. J. Geophys. Res., 74(23):5460-5466.

Bramble, J. (ed.), 1966, Numerical solutions of differential equations. New York (Academic Press).

Dahlquist, G., 1954, Convergence and stability for a hyperbolic difference equation with analytic initial values. Math. Scand., 2:91-102.

Dronkers, J., 1964, Tidal computations in rivers and coastal waters. New York (American Elsevier)..

Dyer, K. R., and K. Ramamoorthy, 1969, Salinity and water circulation in the Vellar Estuary. Limnol. Oceanog., 14(1):4-15.

Forsythe, G., and W. Wasow, 1960, Finite-difference methods for partial differential equations. New York (Wiley and Sons).

Garrett, C., 1975, Tides in gulfs. Deep-Sea Res., 22:23-35.

Gunaratnam, D., and F. Perkins, 1970, Numerical solution of unsteady flow in open channels. Mass. Inst. Tech. Dept. of Civil Engr., Hydrodynamics Rept. 127.

Hacker, S., W. Pike, and B. Wilkins, Jr., 1971, Analysis of the energy, mass, and momentum transfer in the Louisiana coastal marsh region. Louisiana State Univ., Coastal Studies Bull. 6, pp. 109-153.

Heiskanen, W., 1921, Uber der Einfluss der Gezeiten auf dei sakulare. Acceleration des Mondes, Ann. Acad. Sci. Fennicae, A18, pp. 1-84.

Ippen,A., 1966, Estuary and coastline hydronamics. New York (McGraw-Hill).

Jeffreys, H., 1920, Tidal friction in shallow seas. Phil. Trans. Roy. Soc. London, A, CCXXI:239-264.

Kjerfve, B., 1973, Dynamics of the water surface in a bar-built estuary. Unpublished Ph.D. dissertation, Louisiana State Univ., Baton Rouge.

Leendertse, J., 1967, Aspects of a computational model for long-period water wave propagation. Rand Corp. Memo RM-5294-PR.

Levine, E. R., and K. E. Kenyon, 1975, The tidal energetics of Narragansett Bay. J. Geophys. Res., 80(12):1683-1688.

Masch,F., 1970, Mathematical simulation of a two-dimensional horizontal convective-dispersion in well mixed estuaries. Internat. Assoc. for Hydraul. Res., C32-1-9.

McAlister, W. B., M. Rattray, Jr., and C. A. Barnes, 1959, The dynamics of a fjord estuary: Silver Bay, Alaska. Univ. of Washington, Dept. of Oceanography Tech. Rept. 62, 70 pp.

McLellan, H. J., 1958, Energy considerations in the Bay of Fundy system. J. Fish. Res. Bd. of Canada, 15(2):115-134.

Miller, G. R., 1966, The flux of tidal energy out of the deep oceans. J. Geophys. Res., 171(10):2485-2489.

Mungall, J., and J. Matthews, 1970, A variable-boundary numerical tidal model. Univ. of Alaska, College of Marine Science, Rept. R70-4.

Murray, S. P., 1972, Observations on wind, tidal and density driven circulation in the vicinity of the Mississippi River delta. In (D. Swift, D. Duane, and O. Pilkey, eds.) Shelf Sediment Transport. Stroudsberg, Pennsylvania (Dowden, Hutchinson, and Ross) pp. 127-142.

Murray, S. P., W. G. Smith, and C. J. Sonu, 1970, Oceanographic observations and theoretical analysis of oil slicks during the Chevron spill, March 1970. Louisiana State Univ., Coastal Studies Inst. Tech. Rept. 87, 106 pp.

Pritchard, D. W., 1952, Salinity distribution and circulation in the Chesapeake Bay estuarine system. J. Marine Res., 11:106-123.

Pritchard, D. W., 1956, The dynamic structure of a coastal plain estuary. J. Marine Res., 15:33-42.

Reid, R., and B. Bodine, 1968, Numerical model for storm surges in Galveston Bay. J. Waterways and Harbors Div., Proc. Am. Soc. Civil Engrs., WWI, 5805.

Sobey,R., 1970, Finite-difference schemes compared for wave-deformation characteristics in mathematical modeling of two-dimensional long-wave propagation. U.S. Army Corps of Engrs., Coastal Engr. Res. Center, Fort Belvoir, Va., Tech. Memo. 32.

Stock,G. G., and J. H. Filloux, 1975, Direct gravitational driving and tidal energy balance in elongated gulfs. Phys. Oceanog., Am. Meteorol. Soc., 5(2):376-379.

Street, R. O., 1917, Dissipation of energy in the tides in connection with the acceleration of the moon's mean motion. Proc. Roy. Soc. London, A, 93:348-359.

Taylor, G. I., 1919, Tidal friction in the Irish Sea. Phil. Trans. Roy. Soc. London, A, CCXX:1-35.

U.S. Coast and Geodetic Survey, ESSA, 1968, Tide tables, high and low water predictions east coast North and South America, including Greenland. U.S. Government Printing Office.

Van der Houwen, P., 1968, Finite difference methods for solving partial differential equations. Mathematisch Centrum Tracts, Vol. 19-23, Vol. 20. Amsterdam.

von Rosenberg, D., 1969, Methods for the numerical analysis of partial differential equations. New York (American Elsevier).

Wu, Jin, 1969, Wind stress and surface roughness at air sea interface. J. Geophys. Res., 74(2):444-455.

Youkey, J., 1968, Programming and application of the hydrodynamical numerical method to Da Nang Bay. Fleet Numerical Weather Central Tech. Note 42, Monterey, California.

Unclassified Distribution List
Reports of Contract N00014-75-C-0192,
Project NR 388 002

Office of Naval Research
Geography Programs
Code 462
Arlington, Virginia 22217

Defense Documentation Center
Cameron Station
Alexandria, Virginia 22314

Director, Naval Research Lab
Attn: Technical Information Officer
Washington, D.C. 20375

Director
Office of Naval Research Branch Office
1030 East Green Street
Pasadena, California 91101

Director
Office of Naval Research Branch Office
536 South Clark Street
Chicago, Illinois 60605

Director
Office of Naval Research Branch Office
495 Summer Street
Boston, Massachusetts 02210

Commanding Officer
Office of Naval Research Branch Office
Box 39
FPO New York 09510

Chief of Naval Research
Asst. for Marine Corps Matters
Code 100M
Office of Naval Research
Arlington, Virginia 22217

Office of Naval Research
Operational Applications Div.
Code 200 Arlington, Virginia 22217

Office of Naval Research
Scientific Liaison Officer
Scripps Inst. of Oceanography
La Jolla, California 92038

Director, Naval Research Lab
Attn. Library, Code 2628
Washington, D.C. 20375

Commander
Naval Oceanographic Office
Attn. Library, Code 1600
Washington, D.C. 20374

Naval Oceanographic Office
Code 3001
Washington, D.C. 20374

Chief of Naval Operations
OP 987P1
Department of the Navy
Washington, D.C. 20350

Oceanographer of the Navy
Hoffman II Building
200 Stovall Street
Alexandria, Virginia 22322

Naval Academy Library
U.S. Naval Academy
Annapolis, Maryland 21402

Commanding Officer
Naval Coastal Systems Laboratory
Panama City, Florida 32401

Librarian
Naval Intelligence Support Center
4301 Suitland Road
Washington, D.C. 20390

Office of Naval Research
Code 480
National Space Technology Lab
Bay St. Louis, MS 39520

Commanding Officer
Naval Civil Engineering Lab
Port Hueneme, California 93041

Officer in Charge
Environmental Prediction Research Facility
Naval Post Graduate School
Monterey, California 93940

Dr. Warren C. Thompson
Dept. of Meteorology and Oceanography
U.S. Naval Post Graduate School
Monterey, California 93940

Director
Amphibious Warfare Board
U.S. Atlantic Fleet
Naval Amphibious Base
Norfolk, Little Creek, Va. 23520

Commander, Amphibious Force
U.S. Pacific Fleet
Force Meteorologist
COMPHIBPAC CODE 25 5
San Diego, California 92155

Commanding General
Marine Corps Development and Educational Command
Quantico, Virginia 22134

Dr. A. L. Slafkosky
Scientific Advisor
Commandant of the Marine Corps
Code MC-RD-1
Washington, D.C. 20380

Defense Intelligence Agency
Central Reference Division
Code RDS-3
Washington, D.C. 20301

Director
Coastal Engineering Res. Center
U.S. Army Corps of Engineers
Kingman Building
Fort Belvoir, Virginia 22060

Chief, Wave Dynamics Division
USAE-WES
P.O. Box 631
Vicksburg, Miss. 39180

Commandant
U.S. Coast Guard
Attn: GECV/61
Washington, D.C. 20591

Office of Research and Development
c/o DS/62
U.S. Coast Guard
Washington, D.C. 20591

National Oceanographic Data Center c/o D764
Environmental Data Services
NOAA
Washington, D.C. 20235

Central Intelligence Agency
Attn: OCR/DD-Publications
Washington, D.C. 20205

Dr. Donald Swift
Marine Geology and Geophysics Laboratory
AOML - NOAA
15 Rickenbacker Causeway
Miami, Florida 33149

Dr. Hsiang Wang
Dept. of Civil Engineering
Dupont Hall
University of Delaware
Newark, Delaware 19711

Ministerialdirektor
Dr. F. Wever
Rue/FO
Bundesministerium der Verteidigung
Hardthoehe
D-5300 Bonn, West Germany

Oberregierungsrat
Dr. Ullrich
Rue/FO
Bundesministerium der Verteidigung
Hardthoehe
D-5300 Bonn, West Germany

Dr. Yoshimi Goda
Director, Wave Research Div.
Port and Harbor Research Inst.
Ministry of Transportation
1-1 Nagase, 3 Chome
Yokosuka, 239 Japan

Mr. Tage Strarup
Defence Research Establishment
Osterbrogades Kaserne
DK-2100 Kobenhavn O, Denmark

Prof. Dr. Rer. Nat. H. G. Gierloff-Emden
Institut F. Geographie
Universitaet Muenchen
Luisenstrasse 37/III
D-800 Muenchen 2, West Germany

Prof. Dr. Eugen Seibold
Geol-Palaeontolog. Institut
Universitaet Kiel
Olshausenstrasse 4-60
D-2300 Kiel, West Germany

Dr. R. Koester
Geo.-Palaeontolog. Institut
Universitaet Kiel
Olshausenstrasse 40-60
D-2300 Kiel, West Germany

Prof. Dr. Fuehrboeter
Lehrstuhl F. Hydromechanik U. Kuestenwasserbau
Technische Hochschule Braunschweig
Beethovenstrasse 51A
D-3300 Braunschweig
West Germany

Prof. Dr. Walter Hansen
Direktor D. Instituts f. Meereskunde
Universitaet Hamburg
Heimhuderstrasse 71
D-2000 Hamburg 13,
West Germany

Prof. Dr. Klaus Hasselmann
Institut F. Geophysik
Universitaet Hamburg
Schuleterstrasse 22
0-2000 Hamburg 13, West Germany

Prof. Dr. Nils Jerlov
Institute for Physical Oceanography
Kobenhavns Universitet
Haraldsgade 6
DK-2200 Kobenhavn, Denmark

Mr. William T. Whelan
Telecommunication Ent. Inc.
Box 88
Burtonsville, MD 20730

Dr. H. J. Schoemaker
Waterloopkundig Laboratorium Te Delft
61 Raam, Delft, Netherlands

Ir. M. W. Van Batenberg
Physisch Laboratorium TNO
Oude Waalsdorper Weg 63, Den Haag
Netherlands

Dr. J. Ernest Breeding, Jr.
Dept. of Oceanography
Florida State University
Tallahassee, Florida 32306

Dr. John C. Kraft
Dept. of Geology
University of Delaware
Newark, Delaware 19711

Dr. Dag Nummedal
Dept. of Geology
University of South Carolina
Columbia, South Carolina 29208

ONR Scientific Liaison Group
American Embassy
Room A-407
APO San Francisco, CA 96503

Dr. Choule J. Sonu
Tetra Tech, Inc.
630 North Rosemead Blvd.
Pasadena, California 91107

Dr. Richard A. Davis, Jr.
Department of Geology
University of South Florida
Tampa, Florida 33620

Dr. William T. Fox
Department of Geology
Williams College
Williamstown, Mass. 01267

Dr. John Southard
Dept. of Earth and Planetary Sciences
MIT
Cambridge, Massachusetts 02139

Dr. John T. Kuo
Henry Krumb School of Mines
Seeley W. Mudd Building
Columbia University
New York, New York 10027

Dr. Edward B. Thornton
Department of Oceanography
Naval Postgraduate School
Monterey, California 93940

Prof. C. A. M. King
Department of Geography
University of Nottingham
Nottingham, England

Dr. Douglas L. Inman
Scripps Institute of Oceanography
La Jolla, California 92037

Prof. Toshiyuki Shigemura
Civil Engineering Dept.
National Defense Academy
1-10-20 Hashirimizu
Yokosuka 239, Japan

Prof. Yuji Iwagaki
Civil Engineering Dept.
Kyoto University
9 Shimogamo Zenbucho, Sakyo-Ku
Kyoto, Japan

Prof. Kiyoshi Horikawa
Dept. of Civil Engineering
University of Tokyo
7-3-1, Hongo, Bunkyo-Ku
Tokyo 113, Japan

Dr. William W. Wood
Department of Geosciences
Purdue University
Lafayette, Indiana 47907

Dr. Alan W. Niedoroda
Director, Coastal Research Center
University of Massachusetts
Amherst, Mass. 01002

Dr. Benno M. Brenninkmeyer, S.J.
Dept. of Geology & Geophysics
Boston College
Chestnut Hill, Mass. 02167

Dr. Omar Shemdin
JPL-CALTECH
Mail Stop 183-501
4800 Oak Grove Drive
Pasadena, California 91103

Dr. Lester A. Gerhardt
Rennsselaer Polytechnic Inst.
Troy, New York 12181

Mr. Fred Thomson
Environmental Research Inst.
P.O. Box 618
Ann Arbor, Michigan 48107

Dr. Thomas K. Peucker
Simon Fraser University
Department of Geography
Burnaby 2, B.C., Canada

Dr. Robert Dolan
Department of Environmental Sciences
University of Virginia
Charlottesville, VA 22903

Revised 12-12-77

Unclassified
Security Classification

DOCUMENT CONTROL DATA - R & D

(Security classification of title, body of abstract and indexing annotation must be entered when the overall report is classified)

1. ORIGINATING ACTIVITY *(Corporate author)*
Coastal Studies Institute
Louisiana State University
Baton Rouge, Louisiana 70803

2a. REPORT SECURITY CLASSIFICATION
Unclassified

2b. GROUP
Unclassified

3. REPORT TITLE
A NUMERICAL STUDY OF CURRENTS, WATER SURFACE ELEVATIONS, AND ENERGY DISSIPATION IN CHANDELEUR-BRETON SOUND, LOUISIANA

4. DESCRIPTIVE NOTES *(Type of report and inclusive dates)*

5. AUTHOR(S) *(First name, middle initial, last name)*
William E. Hart

6. REPORT DATE
Feb[illegible]78

7a. TOTAL NO. OF PAGES
97 167

7b. NO. OF REFS
36

8a. CONTRACT OR GRANT NO.
N00014-75-C-0192

8b. PROJECT NO.
NR 388 002

8c.

8d.

9a. ORIGINATOR'S REPORT NUMBER(S)
TR-254

9b. OTHER REPORT NO(S) *(Any other numbers that may be assigned this report)*
Technical Report [illegible]

10. DISTRIBUTION STATEMENT
Approved for public release; distribution unlimited.

11. SUPPLEMENTARY NOTES
WUNR 388 002

12. SPONSORING MILITARY ACTIVITY
Geography Programs
Office of Naval Research
Arlington, Virginia 22217

13. ABSTRACT

Numerical methods in the form of a digital computer model were used to simulate and study the tide- and wind-induced circulation in Chandeleur-Breton Sounds, which form a bar-built estuary southeast of New Orleans, Louisiana. The model output agreed very well with current observations taken over a 6-month period at 15 widely spaced stations in and around the estuary. The responses of the model estuary to average, tropic, and equatorial tides were studied in detail. It was found that the estuary exhibits low current speeds, on the order of 10-20 cm/sec, except in some of the shallow entrances through the Chandeleur Island chain, where speed reaches 50-60 cm/sec for short periods. Surface elevations were found to have an average tide range of 60 cm at the northwestern end of the estuary and to increase in range to 90 cm during tropic tides. The range in the southern part of the estuary was about 15 cm less at all times. It was also shown that the estuary responds directly to an applied wind force and that the expected set-up of the surface is in the downwind direction. The current field is only slightly affected by representative local winds (order of 10 percent). The input to the estuary comes primarily from its northern and southern entrances. These entering tidal wave forms were simulated by two Kelvin waves, which had a resultant form that was found to be in close agreement with the computer model. Furthermore, it was shown that total energy in the estuary is relatively low and that kinetic energy is typically only one-sixth of the potential energy during the tidal cycle. Only about 25 percent of the energy advected into the Sound is dissipated by bottom friction, but the time-averaged energy balance is dominated by the dissipation term. The unsteady energy content term $\langle \partial E/\partial t \rangle$ is about 25 percent of the advective and dissipative terms in the time (tidal) average. (U)

DD FORM 1 NOV 65 1473 (PAGE 1)
S/N 0101-807-6811

Unclassified
Security Classification

A-31408

086 700

14. KEY WORDS	LINK A		LINK B		LINK C	
	ROLE	WT	ROLE	WT	ROLE	WT
Digital computer model						
Tide-induced circulation						
Wind-induced circulation						
Chandeleur-Breton Sounds, Louisiana						